University of Stavanger

Faculty of Science and Technology

MASTER'S THESIS

Study program/ Specialization: **MSc in Petroleum Engineering**	Spring semester, 2012 **Restricted access**
Writer: **Gulnar Yerkinkyzy**	…… (Writer's signature)

Faculty supervisor: **Prof. Dr. Dimitrios G. Hatzignatiou (UiS &IRIS)**

External supervisors: **Diego Rafael Cepeda (STATOIL)**

Frode Velsand Blindheim (STATOIL)

Title of thesis:

Late Life Field Material Balance Analysis – Statfjord Fm.

Credits (ECTS): **30**

Key words: Statfjord Formation Material Balance History matching Non-linear regression Production forecast	Pages: 75…… + enclosure: 13…… Stavanger, June 2012

ACKNOWLEDGEMENTS

I am deeply indebted and thankful to my professor, Dimitrios Hatzignatiou, for his detailed and constructive comments, valuable suggestions, and for his continuous support throughout my thesis. In spite of having tight schedule, he provided me with the help and guidance I needed to successfully complete this project.

I warmly thank Egil Stangeland for offering me an exciting project at Statfjord PETEK and extensive discussions around my work.

I am grateful to my supervisor, Diego Rafael, who assisted with valuable suggestions.

During this thesis, I have collaborated with many colleagues for whom I have great regards. I would like to extend my gratitude to Marius Heide, Siv Kari Lien, Arne Egil and Hilde Breivik.

Finally, I gratefully thank my friend Rauan Zhamangarin and my family for support and encouragement.

ABSTRACT

Recently, it has become apparent that the prediction of the Statfjord reservoir potential determined from the ECLIPSE simulator differs from the actual formation performance, i.e. simulated fluid production results are too optimistic, especially for the gas phase. Since the validity of the Statfjord ECLIPSE model is considered questionable, the alternative approach of material balance is employed to evaluate the possibility of using simplified models (MBAL) to assess the dynamic reservoir performance.

It is well established that the material balance methodology is a zero dimensional model much simpler compared to reservoir simulation one (e.g. ECLIPSE model). Despite the simplicity of the material balance technique, it can develop a consistent understanding of the reservoir. It is believed that for the model in order to reproduce the actual reservoir behavior the reservoir understanding plays important role rather than the degree of complexity with which it was constructed.

Prior to modeling the Statfjord formation, a quality review was done to the entire production/injection history, pressure depletion behavior and drainage strategy in order to broaden the knowledge regarding the reason of the experienced simulation/actual data mismatch.

A sensitivity analysis based on the history matching procedure was conducted in terms of the matching variables choice, such as fluid migration and aquifer influence, and the uncertainty surrounding them. In the history matching process, a combination of the analytical non-linear regression and manual history matching methods were used to mimic the actual average reservoir behavior. Following the history matching procedure, the STOIIP and aquifer influx determined from MBAL were crosschecked with the ECLIPSE simulator's results. The comparison indicated that the MBAL and ECLIPSE values for these two variables were very close.

Once a representative MBAL model was established, the average reservoir pressure and gas production were forecasted until the field's abandonment pressure. The MBAL gas production forecast was lower to the one obtained from the ECLIPSE reservoir simulator. The comparison of the average reservoir pressure depletion between ECLIPSE and MBAL yielded acceptable results.

Summarizing, this thesis presents the application of the MBAL tool for the Statfjord formation to quantify the remaining reserves and reservoir pressure depletion performance.

TABLE OF CONTENTS

LIST OF FIGURES

LIST OF TABLES

1. INTRODUCTION

Statfjord, the largest producing oil field in the Norwegian Continental Shelf, is currently in the late life production phase. Therefore, it is crucial to review the field in order to examine its remaining potential and design strategies that produce the remaining reserves in an optimal way. Recent analysis conducted by the field's operator (RDP, 2011) indicates that the oil and gas recovery factors in the Statfjord field are approximately 66 % and 57 %, respectively.

A simulation model for the Statfjord field was built to assist with the reservoir optimization and management. It is undoubtedly true that the production forecasting plays a vital role in reservoir optimization and management studies, especially when it turns to gas forecasting which also includes long-term market sales contract. Existing contractual obligations lead to the need of establishing accurate gas prediction forecasts. History matching, a complex procedure involving different disciplines, is a fundamental basement for making accurate forecasts. Unfortunately, the current numerical simulation model, particularly for the Statfjord formation, is not able to make accurate fluids production predictions with the discrepancy between actual and predicted gas cumulative production data to be enormous (0.4 GSm^3). In other words, the model is optimistic in establishing the true reservoir potential.

Consequently, a clear understanding of the reservoir performance is required in terms of drainage mechanisms and production data. Moreover, the accuracy of the historical data, for instance, initial reservoir properties, needs to be evaluated since it creates large uncertainties when estimating gas reserves.

A classical approach using material balance was chosen to overcome this problem. This is primarily due to its simplified nature and ability to narrow down the uncertainty associated with the initial fluid properties, especially in a mature field. As shown in Fig. 1.1, having provided the PVT, pressure profile and production/injection data two unknowns, namely N and $W_{e,}$ can be determined for use in the ECLIPSE simulator; in other words, no geological terms are involved, so that the reservoir is treated as zero-dimensional tank. However, the drawback of the material balance comes in the prediction procedure, as a key example is uniform future average pressure decline. This suggests subdividing the reservoir into several tanks in order to reflect the observed field geology.

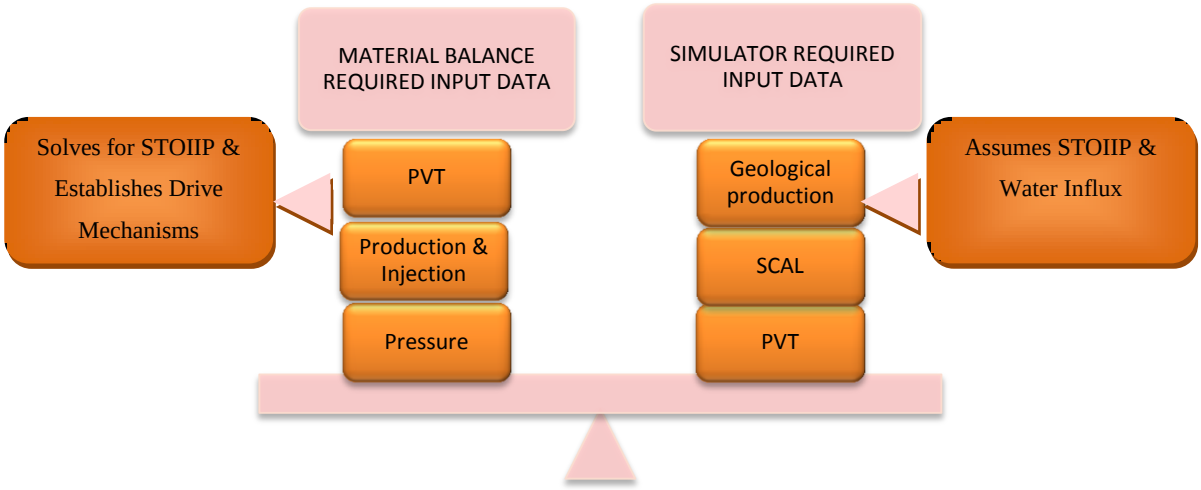

Figure 1.1 - Contrast between material balance and numerical simulation approaches.

The major aim of this work is to model the Statfjord formation using the material balance technique in the MBAL tool and establish the production forecast. Prior to examining the STOIIP and aquifer parameters via MBAL, a quality review of reservoir performance will be assessed with regards to historical drainage strategy and geology.

1.1 Literature Review

A considerable number of literature studies have been reviewed as part of this work and in the following three main areas:

- Papers which present and discuss the Statfjord formation;
- References introducing and applying the material balance modeling techniques;
- Research papers presenting history matching procedures along their– challenges and pitfalls.

The first group of papers aims to enable the full understanding of the Statfjord formation including field geology, formation characteristics, fluids production history. For instance, Aadland et al. (1994) discussed the long-term field development perspectives including the application of WAG and other EOR methods, while a detailed work was done related to the updip water injection (Hegre et al., 1994). In that paper Hegre et al. (1994) demonstrated that updip water injection enhances the field performance; the author also investigated the effects of gas trapping on the fluids and concluded that the field performance can be optimized via the upflank water injection.

Boge et al.(2005) reported on a depressurization drainage method by illustrating all the stages of the new drainage strategy.

The second group of papers addressed how to apply the material balance concept in order to validate the understanding of physics of reservoir performance and reviewed the material balance's strength and weaknesses. Since the first formulation (early 1930th) of the material balance technique by Schilthuis (1936), more advanced and complex models were developed using digital computers to allow a better performance. Miranda et al. (1975) described the milestones of material balance equation and proposed to use the cumulative reservoir withdrawals instead of original fluid in place.

Bui et al. (2006) used the material balance analysis to determine the mature Samarang field's reservoir compartmentalization. A workflow for material balance analysis was proposed and the effects of the relative permeability curves on the history match effectiveness were investigated.

Another similar paper (Mazloom et al., 2007) compared the material balance prognosis results from both single- and multi-tank models against a fine grid simulation model, and concluded that the single tank overestimates recovery factor. The authors also concluded that the single-tank model was unable to capture the reservoir heterogeneities for the condensate field which they investigated, whereas the multi-tank model results were in an acceptable range when compared with the simulation results.

Moreover, several studies have been performed on fluids migration examining the transmissibility parameter. For example, Vera et al. (2009) analyzed an uncertain transmissibility parameter using single- and multi-tank models and summarized that the multi-tank material balance technique was an effective method for examining fluids migration.

Some other authors (Amudo et al., 2011; Esor et al., 2004) addressed the application and methodology of the MBAL tool on establishing connected hydrocarbon volume in place and drive mechanisms.

Garcia et al. (2007) proposed the methodology to assess the most significant parameter that affects material balance computation. His work showed that OOIP estimation is very sensitive to reservoir pressure and PVT data.

The third group of papers pinpoints the challenges and errors of both ECLIPSE and MBAL simulators in history matching procedure. For example, Baker et al. (2006) provides a workflow for determining history matched variables in ECLIPSE simulator, while DeSorcy (1979) estimates the accuracy of each variable in the material balance equation. Galas (1994) investigated an automated history matching technique in material balance method by evaluating non-linear regression function and summarized that the limits of matching parameters should not be neglected.

This thesis is organized as follows:

The second chapter gives a brief overview of the geology of the Statfjord field. Mainly Statfjord formation is described with regard to reservoir structure, properties, and drainage strategies. Ultimately, the numerical simulation model is introduced and described briefly.

In the third chapter a case study is presented to look into why the simulation model cannot reproduce the actual field behavior. Various hypotheses are evaluated in an attempt to provide reasonable explanation for this problem.

The material balance methodology for building a model is described in the fourth chapter by establishing the required workflow.

The next chapter, chapter five, deals with the history matching procedure in the MBAL tool and the uncertainties in the input data. A discussion of the production forecast is addressed at the end of the chapter.

Finally, conclusions reached from the results obtained in this work and future recommendations are summarized in the last chapter.

2. STATFJORD RESERVOIR DESCRIPTION

This part will review the geology of the Statfjord field and is mainly based on The Statfjord Reservoir Development Plan. The study will focus on the Statfjord Fm. reservoir. Therefore, the Statfjord Fm. will be described in more details with respect to reservoir structure, properties, and drainage strategies. At the end of the chapter will give a general overview to simulation model in order to have an understanding of the output of further results.

2.1 Field Overview

The Statfjord Field was discovered in 1973 and started production in 1979. It produces from three platforms, Statfjord A (1979), Statfjord B (1982) and Statfjord C (1985).

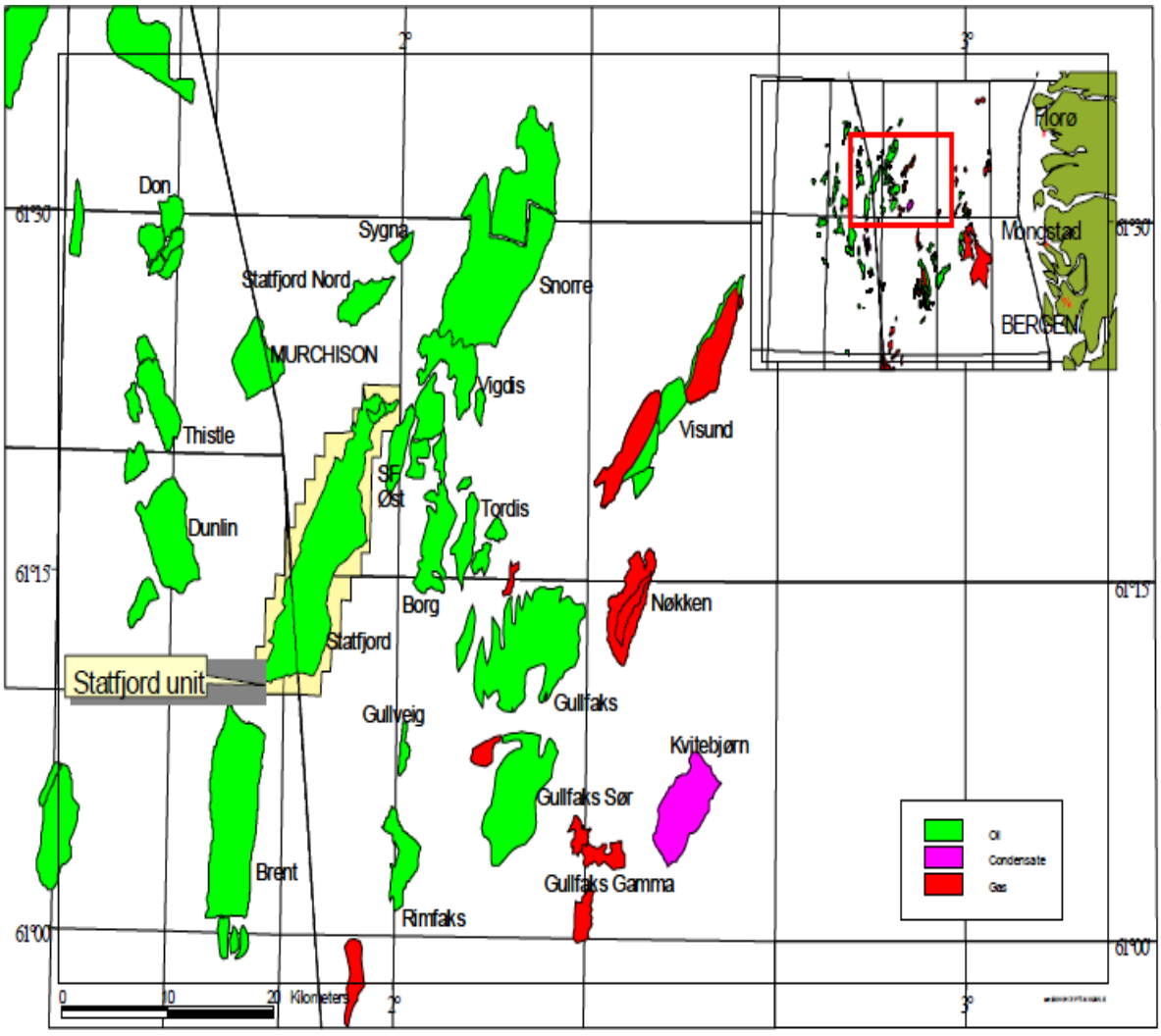

Figure 2.1 - Statfjord Unit and Tampen area (STRDP, 2005).

The production is from three reservoirs, the Brent group, the Statfjord formation and Cook formation. In 2005 the Statfjord Late Life (SFLL) project was sanctioned to include depressurization of the Statfjord Field (Brent Gp. and Statfjord Fm.) in order to liberate gas from the remaining oil. The original plan was to start the depressurization in October 2007. However, during 2006 it was found beneficial to prolong the pressure maintenance in the Brent Gp. by one year. Based on the updated plan, water and gas injection was stopped in 2007 in the upper Statfjord Fm. In the period August (Statfjord A and Statfjord C) to November 2008 (Statfjord B) water and gas injection was stopped in Brent Gp. and the lower Statfjord Fm.

2.2 Geological Field Description

The Statfjord Field (oil zone) covers an area of about 26 x 5 km^2, and is located on the western margin of the North Sea Rift System, on the crest of a SW – NE trending tilted fault block, and on the footwall of one of the major faults on the western side of the North Viking Graben (Fig. 2.1).

The field can be divided in a relatively uniform Main Field fault block (with a dip of approximately 6-7 degrees), intersected by steep normal cross-faults (trending NW – SE) and an East Flank gravitational collapse zone, heavily deformed by rotational block slides along the main fault scarp (Fig. 2.2).

The Main Field reservoirs consist of sandstones ranging in age from late Triassic to mid Jurassic. Reworked mid - upper Jurassic reservoir sandstones are found in the east flank. Based on production experience it was indicated that there is a limited connection throughout the fault F11.

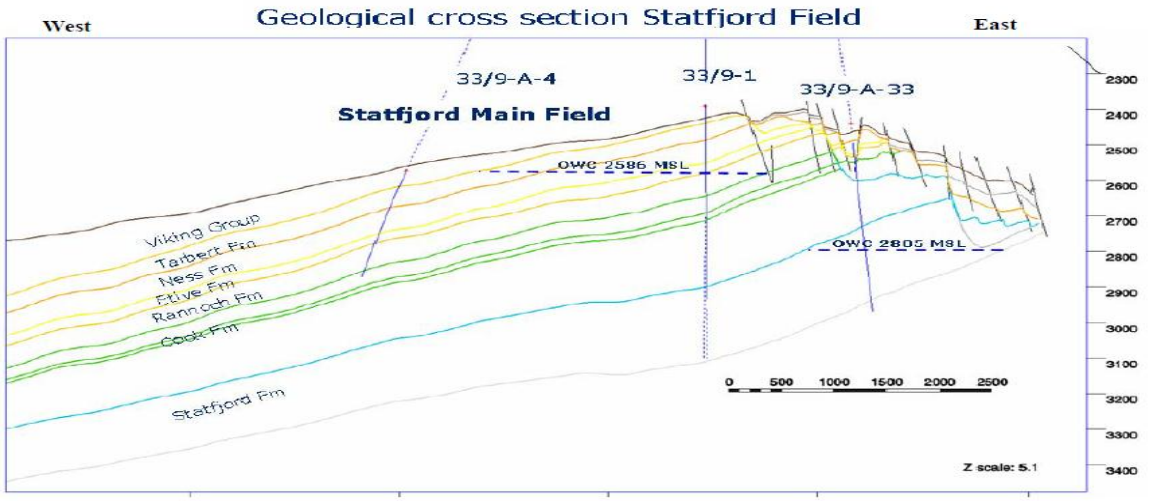

Figure 2.2 - Statfjord field with geological cross section (STRDP, 2007).

2.2.1 Reservoir Zones

The Statfjord Main Field consists of the following 5 main reservoir levels (Fig. 2.3):

- Lower Statfjord Fm, comprising the Raude Mbr.;
- Upper Statfjord Fm, comprising the Eiriksson and Nansen Mbrs;
- Cook Fm. of the Dunlin Gp;
- Lower Brent Gp, comprising the Etive, Rannoch and Broom Fms;
- Upper Brent Gp, comprising the Ness and Tarbert Fms.

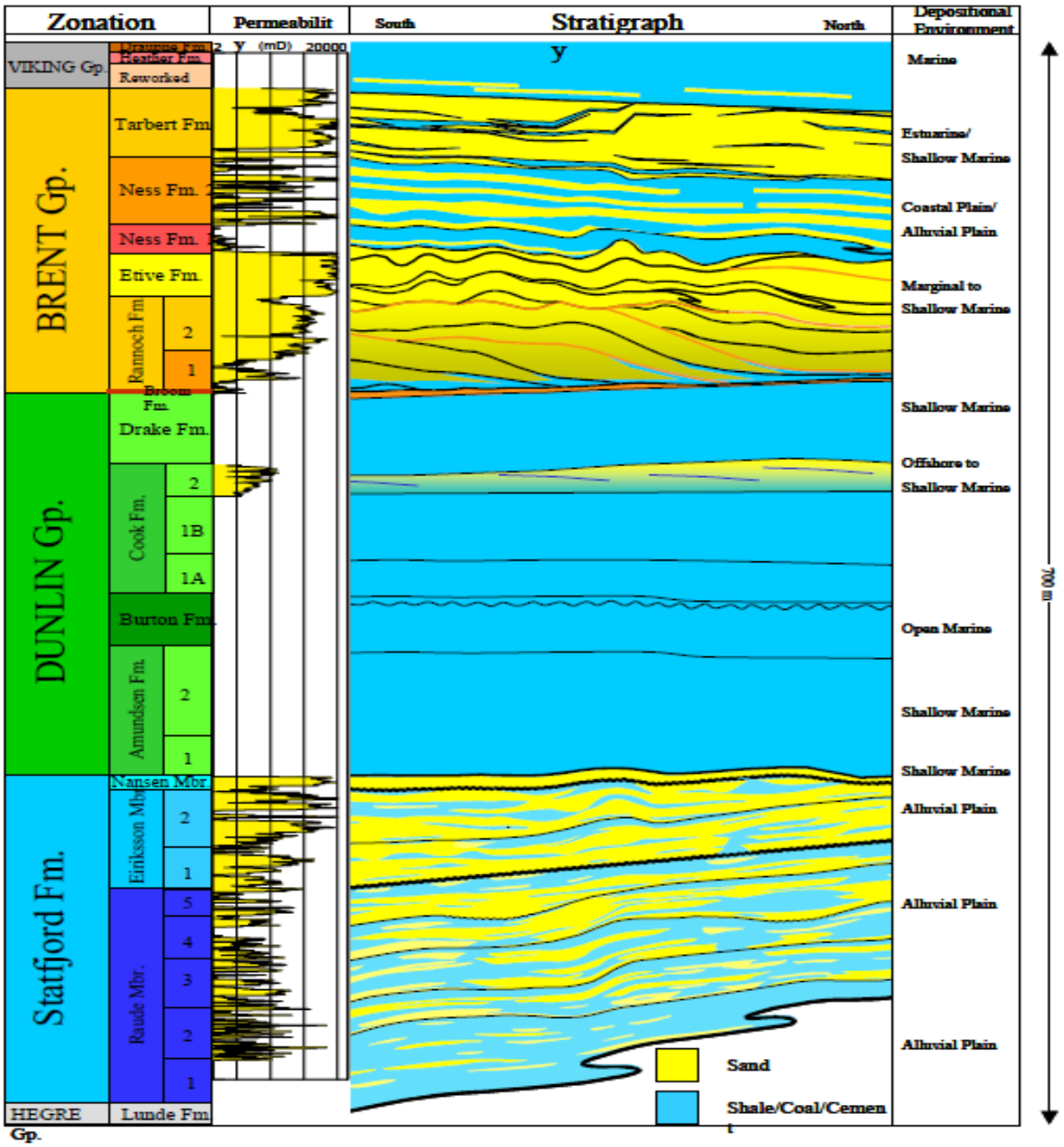

Figure 2.3- Typical stratigraphy and permeability for the reservoir units of the Statfjord field (STRDP, 2005).

The Statfjord formation is a sandstone reservoir of lower Jurassic to upper Triassic age with oil being trapped along the crest of a rotated fault block having a dip of 6-8 degree to the west. The reservoir is subdivided from the top to the base into three units; the Nansen member, the Eiriksson member and the Raude member, and has an improving reservoir quality upwards within each member (Fig. 2.4).

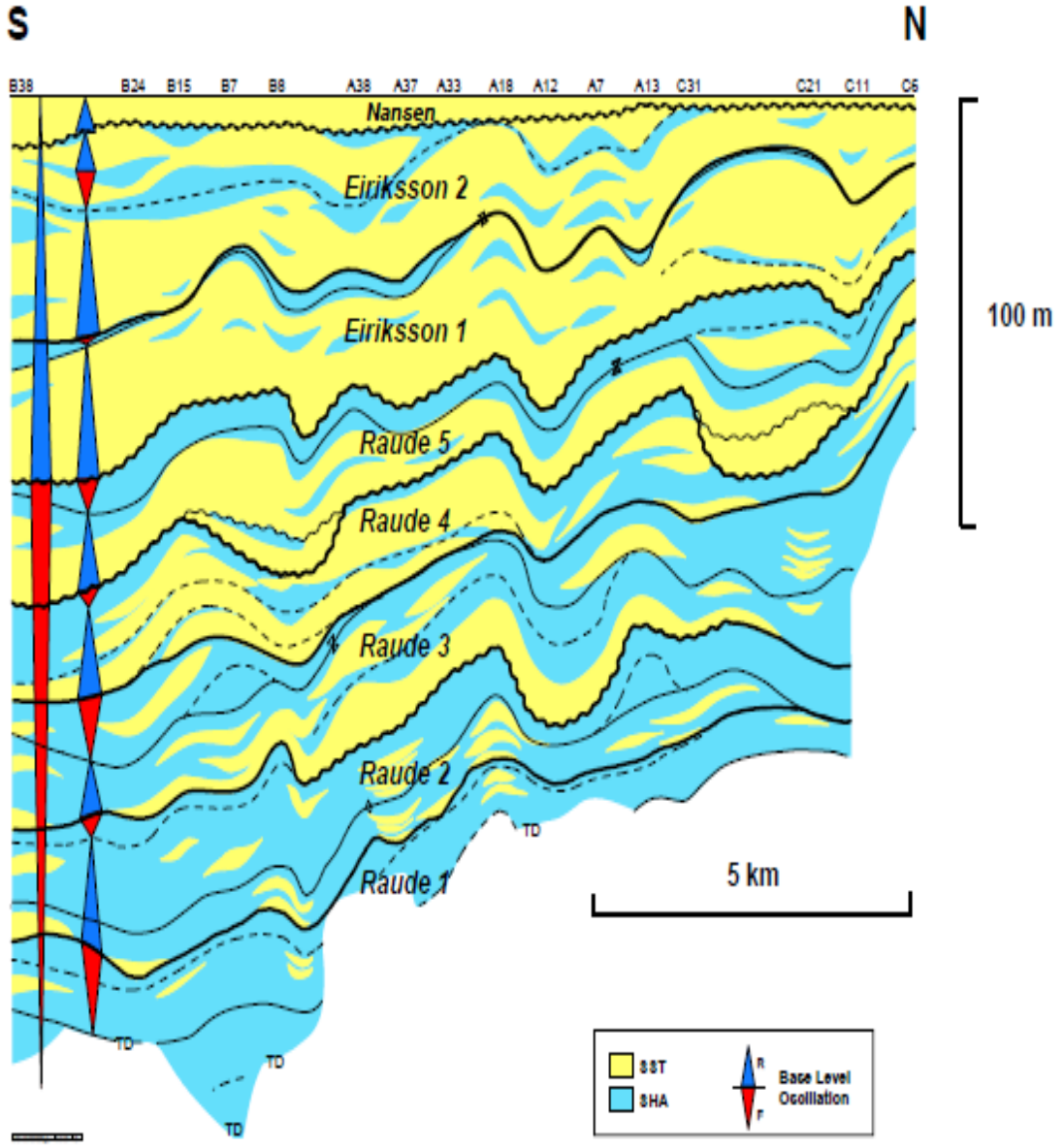

Figure 2.4 - Sequence stratigraphic framework Statfjord Formation (S-N profile) (STRDP, 2005).

Nansen Member

Nansen is composed of shallow marine sandstones; it is 5-15m thick and has excellent reservoir properties. The base Nansen is a transgressive surface of marine erosion (Fig. 2.5).

Eiriksson Member

The Eiriksson member is a 40-60m thick sequence of fluvial style is one of the highly amalgamated channel bodies of wide lateral extension. Eiriksson consists mostly of coastal plain deposits, but shows an upwards trend towards a marine environment. It consists of more than 80 % sandstone (Fig. 2.5).

Raude Member

The lower Raude is generally characterized by lower sand-rich part consisting of laterally amalgamated and vertically amalgamated braided stream deposits, whereas the upper parts of the zones are dominated by floodplain clay sandstones (Fig. 2.5). A field-wide shale layer is found on top of Raude and acts as a barrier between the upper and lower Statfjord (Fig. 2.4). The upper Raude has a high proportion of sandstones and a good productivity, while the lower Raude is dominated by single channel deposits with typically low productivity due to more restricted stratigraphic continuity and limited aquifer support.

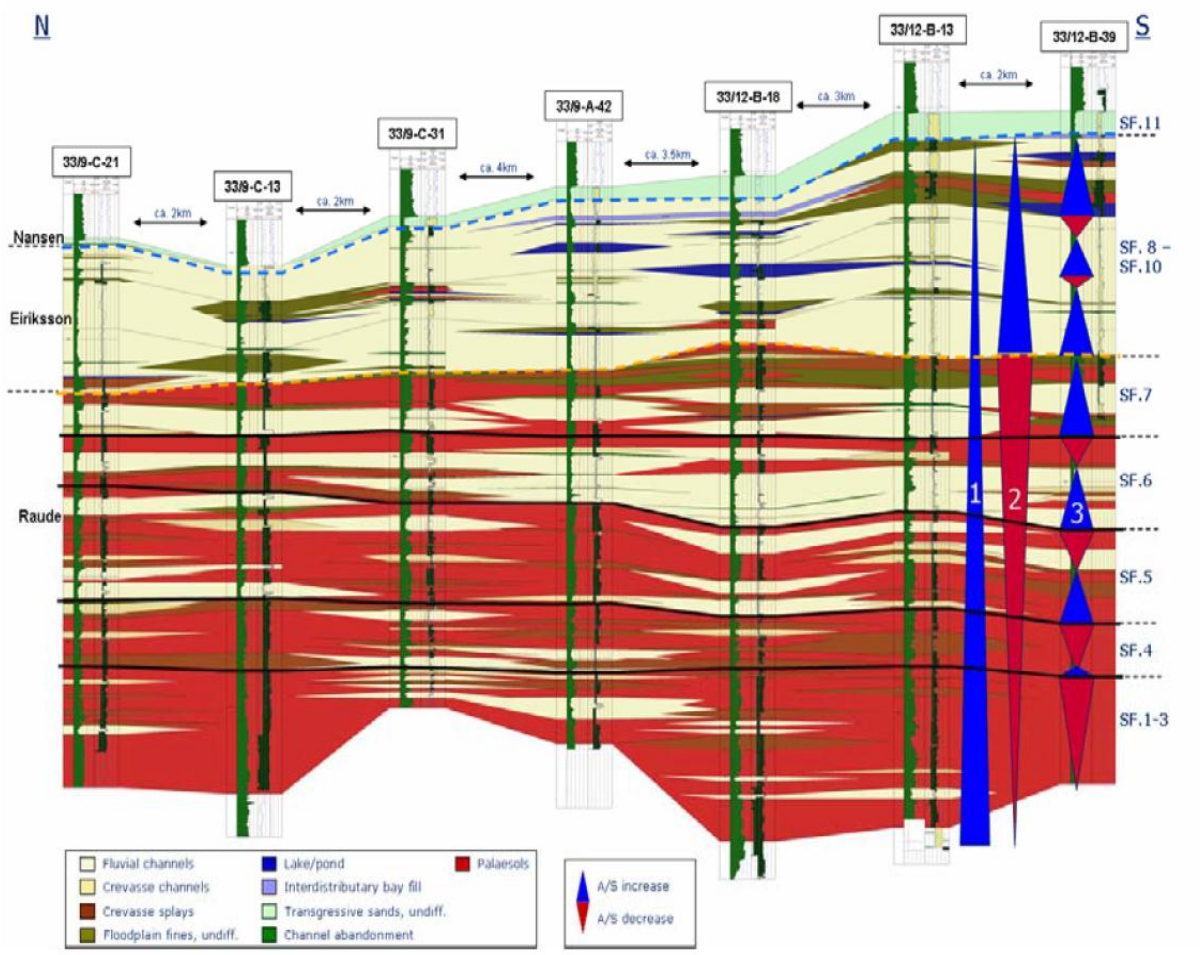

Figure 2.5 - A typical log for the Statfjord Formation (S-N profile) (STRDP, 2007).

Overall, the formation consists of a coarsening-upwards sequence of interbedded sandstones, siltstones and shales. The gross formation average thickness is 125 m. The boundary between the Eiriksson and Raude members is widespread shale acting as a pressure barrier over a significant area of the field (Fig. 2.4).

2.3 Reservoir Description and Initial Conditions

Table 2.1 contains typical average rock properties for the Statfjord reservoir.

Reservoir	Zone	Porosity, %	Connate water saturation, %	Net/gross, %	Horizontal permeability, mD
Statfjord	Nansen	29	11	100	5000
	Eiriksson	25	15	70	1250
	Raude	20	20	40	100

Table 2.1–Statfjord formation reservoir properties (STRDP, 2005).

The initial reservoir conditions for Statfjord are summarized in the Table below.

Statfjord	Datum Depth	2701	m TVD MSL
	Datum Pressure	404.3	Bara
	Datum Temperature	96.7	ºC
	Oil-Water Contact North	2829.9	m TVD MSL
	Oil-Water Contact Central	2814	m TVD MSL
	Oil-Water Contact South	2806.3	m TVD MSL
	Oil Gradient	0.0655	bar/m

Table 2.2 - Statfjord formation initial reservoir conditions (STRDP, 2005).

Reservoir	Bubble Point Pressure, Bar	At Initial Reservoir Conditions				
		Bo m^3/Sm^3	Rs Sm^3/Sm^3	Viscosity mPa*s	Water Compres. $Bars^{-1}$	Rock Compres. $Bars^{-1}$
Statfjord	200	1.48	156.6	0.36	4.79E-05	5E-05

Table 2.3 - Statfjord formation - Black oil data at initial reservoir pressure (STRDP, 2005).

2.4 Recovery Mechanisms and Drainage Strategies

The original reservoir development strategy of the Statfjord field is continuously being optimized, and has been adjusted throughout field life based on existing condition. Different drainage mechanisms have been invoked in the different reservoir units. Due to insufficient pipeline system in the first years, the produced gas was injected into the Statfjord Fm. in an up dip position, while the Brent reservoir was depleted until pressure maintenance by down flank water injection was established in 1981 for the lower Brent and 1982 for the upper Brent (Fig. 2.6).

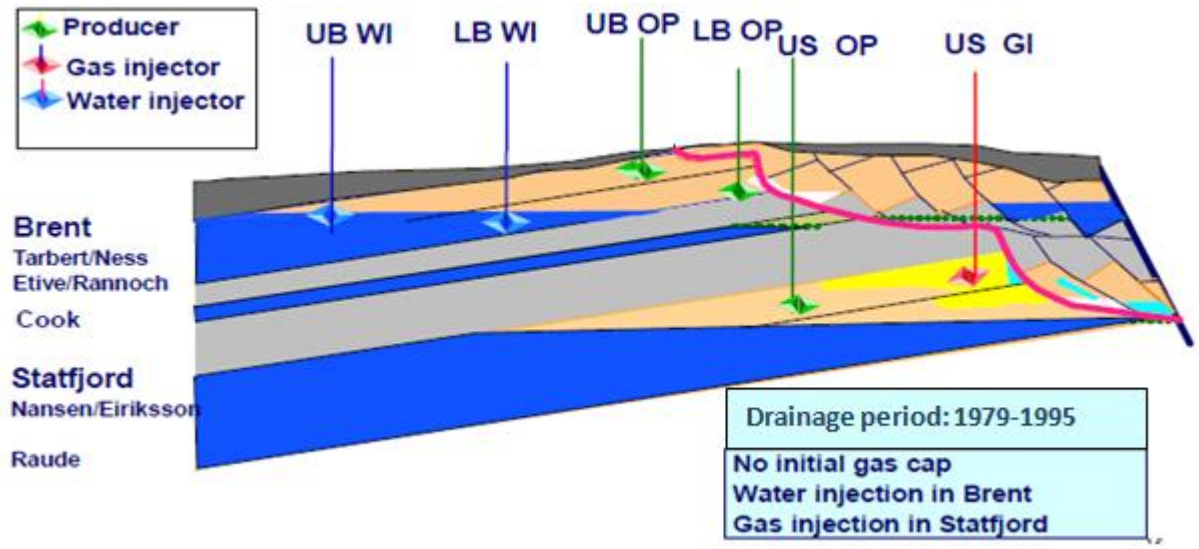

Figure 2.6 - Illustration of the initial drainage strategy on the Statfjord field (STRDP, 2005).

Particularly for the Statfjord formation: the upper and lower parts were initially drained by up-dip miscible gas injection. The oil producers were located down flank (Fig. 2.6). Since 1996 the upper Statfjord gas injection has been supplemented with up-dip water injection, with the objectives being to maintain pressure and to drain the lower parts of the upper Statfjord formation overridden by gas. On top of that, the criterion for choosing water injection was the shortage of gas availability.

In the lower Statfjord, down-dip WAG injection was done. The drainage strategy that is illustrated in Fig. 2.7 had been performed until 2007. Due to limited lateral continuity of the Raude sands, several areas of Raude remain undrained.

The drainage strategy, which is started in 2008, is shown in Fig. 2.8. To extend the production life of the Statfjord field required to change drainage strategy from pressure maintenance to depressurization, in other words, the oil field will be turned into gas field.

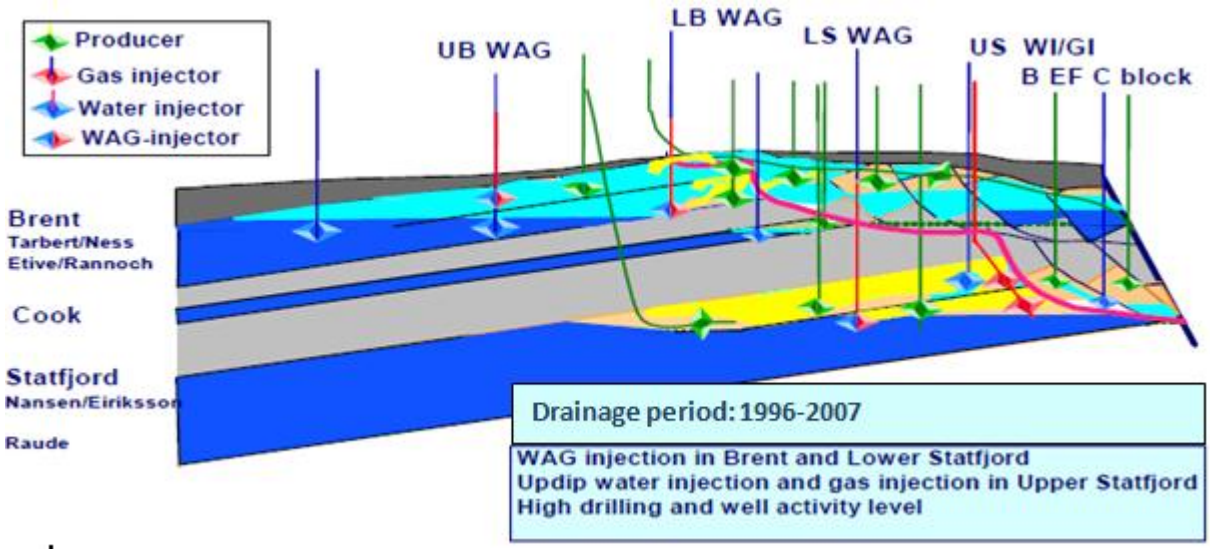

Figure 2.7 - WAG injection in Brent Fm. and up-dip injection in Statfjord Fm. (STRDP, 2005).

This new strategy is called Statfjord Late Life (SFLL). The SFLL has been carried out by producing massive water production which will lead to depletion and consequently the gas will liberate from the oil and move towards the crest where it will be produced. In 2007 pressure depletion was started for upper Statfjord and a year after in October it was started in Brent and lower Statfjord.

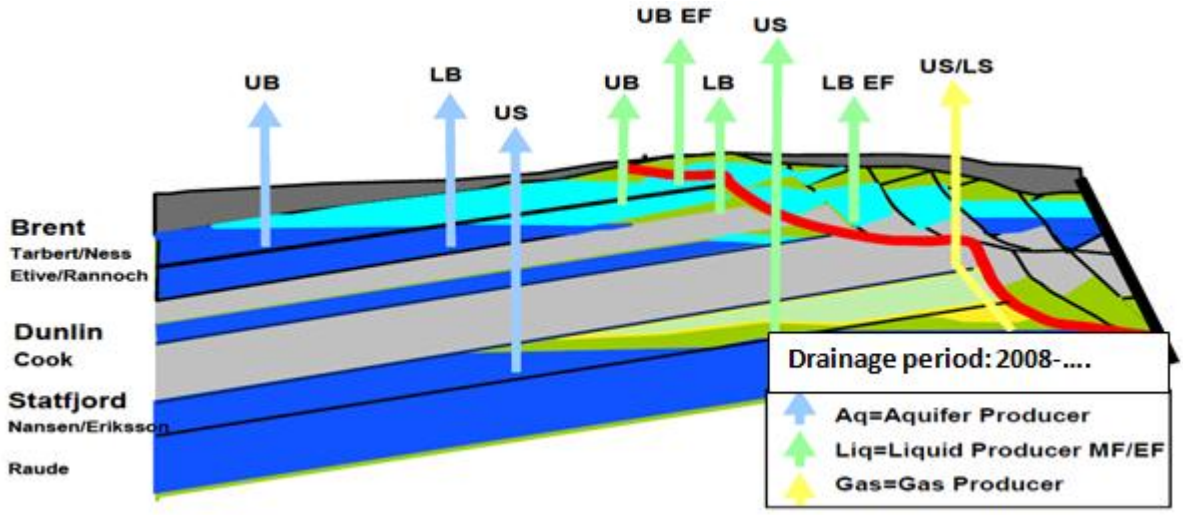

Figure 2.8 - Current SFLL drainage strategy (STRDP, 2007).

Fig. 2.9 demonstrates the main stages of depressurization: as all injectors have been shut down the reservoir pressure falls below the bubble point pressure at the stage of depressurization start up, gas will be released from the remaining oil and migrate towards the

crest. Currently, most of the gas is trapped in the water flooded zone due to large amount of water being injected at the crest during the history. This trapped gas will expand and become mobile as reservoir pressure drops. During the first years of depressurization, the Statfjord Fm. has been providing the majority of the produced gas. The Brent Group will gradually take over as a main gas supplier when the reservoir pressure drops below bubble point pressure and gas is liberated from the oil in Brent.

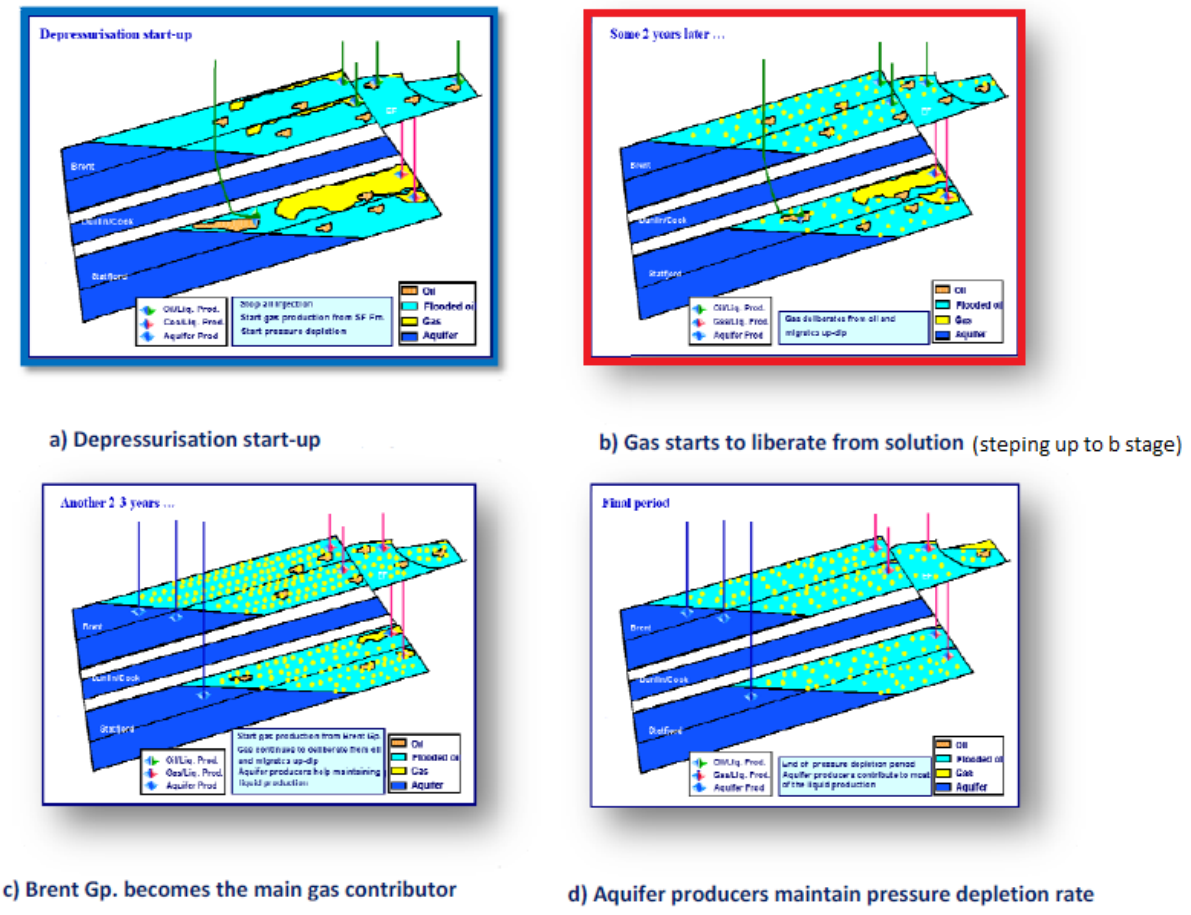

Figure 2.9 - Illustration of the depressurization mechanisms (STRDP, 2005).

2.5 Reserves and Volumes In-situ

By the end of 2011 the cumulative oil production from field was 661 MSm^3 oil, corresponding to a recovery factor of 66 %. The expected remaining oil at the end of 2020 is estimated to be 4.7 MSm^3 and the total expected recovery is to be increased to 66.2 % (Fig. 2.10).

The total rich gas production by the end of 2011 was 102 GSm^3 (Fig. 2.11), of this 87 GSm^3 was exported, the rest used to fuel and flare and injection. So far the gas recovery is 57

%. The total gas production to the end of 2020 is estimated to be 216 GSm^3, of this 102 GSm^3 rich gas are expected to be exported. The gas injection stopped in October 2007 and since then, gas has only been injected for regularity purposes, for instance, when the capacity is reduced at the gas terminal or for enhancing the oil recovery in an isolated fault blocks on the East Flank. Gas injection is ongoing as an IOR method in an isolated Brent block in the SFB area. Figs. 2.10 and 2.11 summarize the oil and gas reserves for each reservoir on the field. Gas injection had been subtracted from both the gas reserves and cumulative net gas production, but fuel and flare had been included.

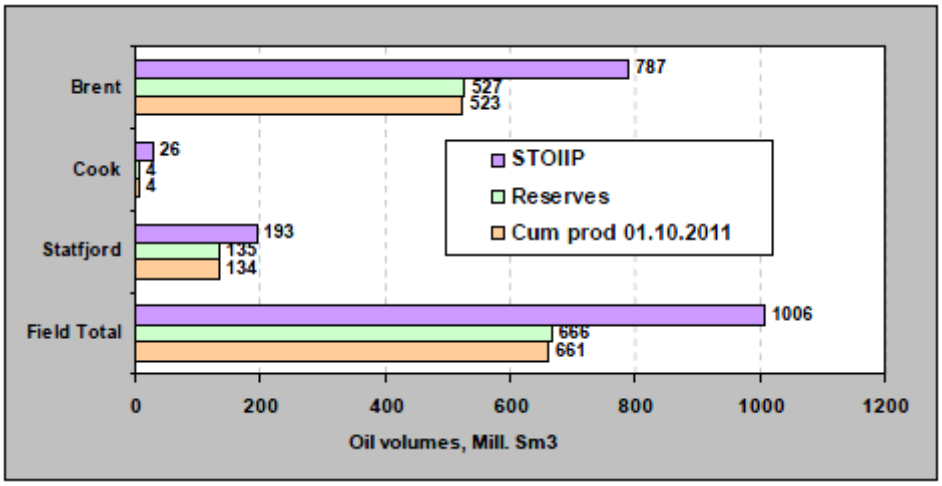

Figure 2.10 - Statfjord field cumulative oil production (STRDP, 2011).

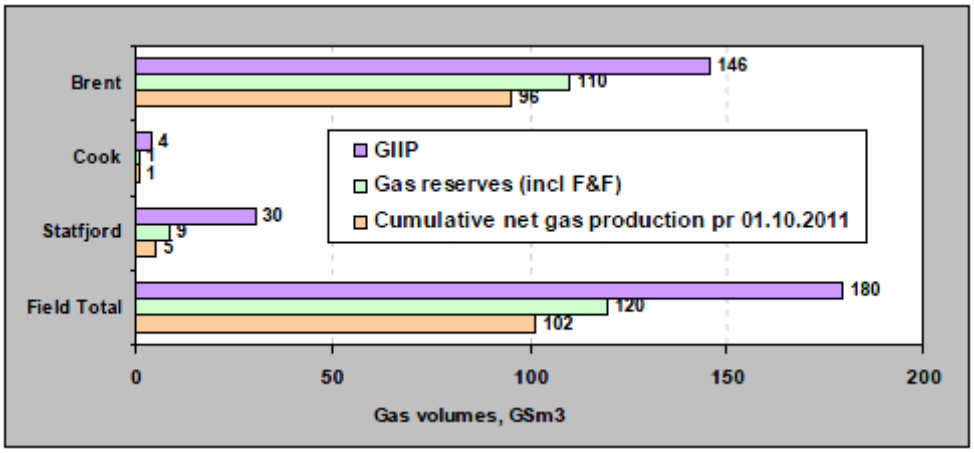

Figure 2.11 - Statfjord Field cumulative net gas production (STRDP, 2011).

2.6 The Reservoir Simulation Model

The Statfjord reservoir FFM2005 model is currently used. The geomodel of Statfjord Fm. was upscaled from the original 96 layers to 46 layers in the reservoir simulation model. The east flank has attached to the formation was primarily presented as a volume for material balance purposes (Table 2.4). A layer overview of both reservoir simulation model FFM2005 and the geomodel are shown below in Table 2.4

A 65 x 262 x 46 simulation grid with 251341 active grid blocks was built based on RMS geomodel. The lateral dimensions were the same as the full field geological grid, except that the vertical dimensions of the simulation grid was doubled. The cell dimensions are 75 x 75 x 3 m with the grid orientation parallel to the OWC to best reprocess the contact movement, and obtain flow perpendicular to grid (Table 2.5).

Lithostratigraphy		Lithostratigraphy Statfjord	Geomodel FFM2005	Dynamic Reservoir Simulation Model FFM2005
Statfjord	Nansen	Nansen	1-4	1-2
	Eiriksson	Eiriksson	5-39	3-19
	Raude	Raude 2	40-88	20-42
		Raude 1	89-96	42-46

Table 2.4 - Reservoir zonation and grid layer in the geomodel and simulation model (STRDP, 2007).

Grid characteristics	
Grid dimension	65 x 262 x 46
Total grid cells	783 380
Active grid cells	251 341
Cell dimensions	75 x 75 x 3

Table 2.5 - Simulation: Grid summary (STRDP, 2007).

Hysteresis is introduced to trap gas in water in upflank water injection.

There are still major challenges:

- Vertical communication within Eiriksson and Raude;
  - ✓ In gas injectors, where the gas was injected simultaneously into Eiriksson and Raude Mbs., the poor Raude properties resulted in excessive gas flowing to upper reservoir.

- The distribution of gas between the upper and lower Statfjord;
- Extension of shale modeled in the geomodel;
  - ✓ Gas ascends to the crest too fast in Eiriksson
- Static model had too tight Raude Mb,thereby isolated in some areas;
  - ✓ The reason is that it was modeled stochastically with shale as background and sand modeled as channels. By increasing permeability the dynamic parameters improved significantly, but still there are areas where a history match has proven difficult to obtain.
- Eclipse had to extrapolate PVT-properties beyond input, as a result slowing down to unacceptable running times.

The historical performance of Eiriksson Mbr. is matched; however the Raude Mbr. is not fully matched and will be a challenge for future modeling. Overall, dynamic reservoir simulation model FFM2005 represents satisfactorily match of historic performance until 2007 and afterwards overestimates the gas production where the reason of mismatch will be addressed in chapter 3.

3. PRODUCTION HISTORY AND DRAINAGE MECHANISMS

A history-matched, full field reservoir model was used to obtain estimates of fluids production versus time. However, it was admitted that the prognosis for gas was over-estimated and to show the enormous discrepancy between two data Fig. 3.1 opposes the prognosis with allocation.

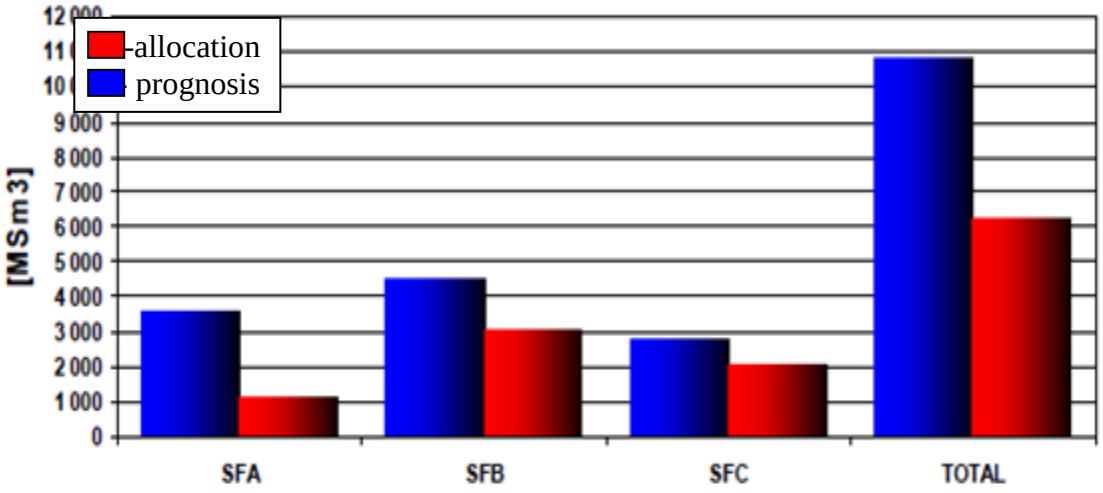

Figure 3.1 - Cumulative gas production and estimated volumes from wells drilled during 2007-2011 (SFRDP, 2011).

Outlining the prediction results (Fig. A.1.1):

- The discrepancy between the actual gas volume is 0.4 GSm^3 and about 4 GSm^3 remains to be produced;
- Approximately 0.9 MSm^3 for oil production;
- Water production is high ‘deliberately’; increased water production will lead to faster pressure decline and faster gas liberation.

This study was initiated due to the deficiency of gas production. Therefore, this chapter provides some possible explanations that may have caused a mismatch between the simulated and actual data.

It is believed that the historical drainage strategy can establish first hint, therefore chapter starts by re-examining the historical drainage process.

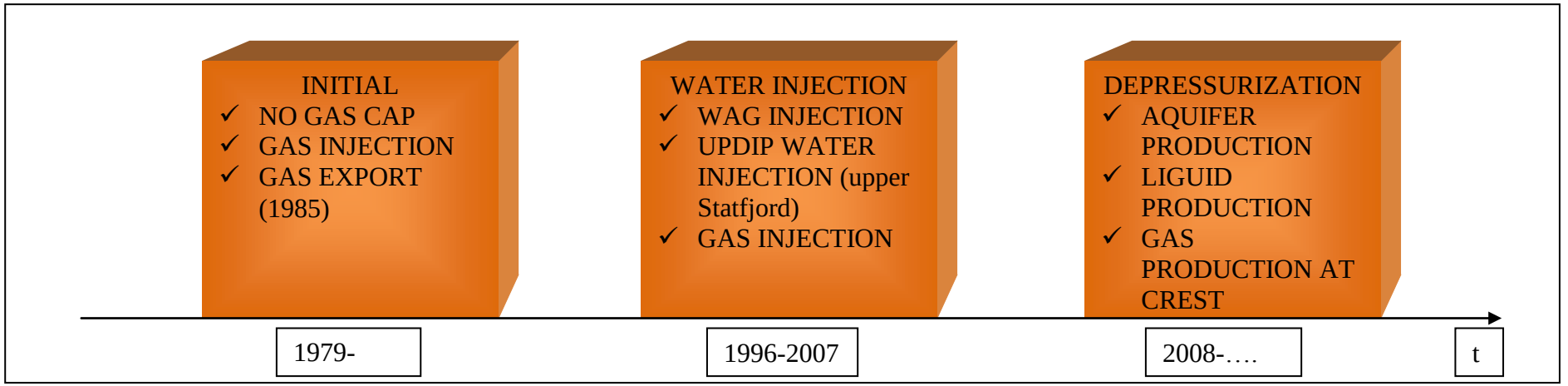

Figure 3.2 – Applied drainage strategy during the production period.

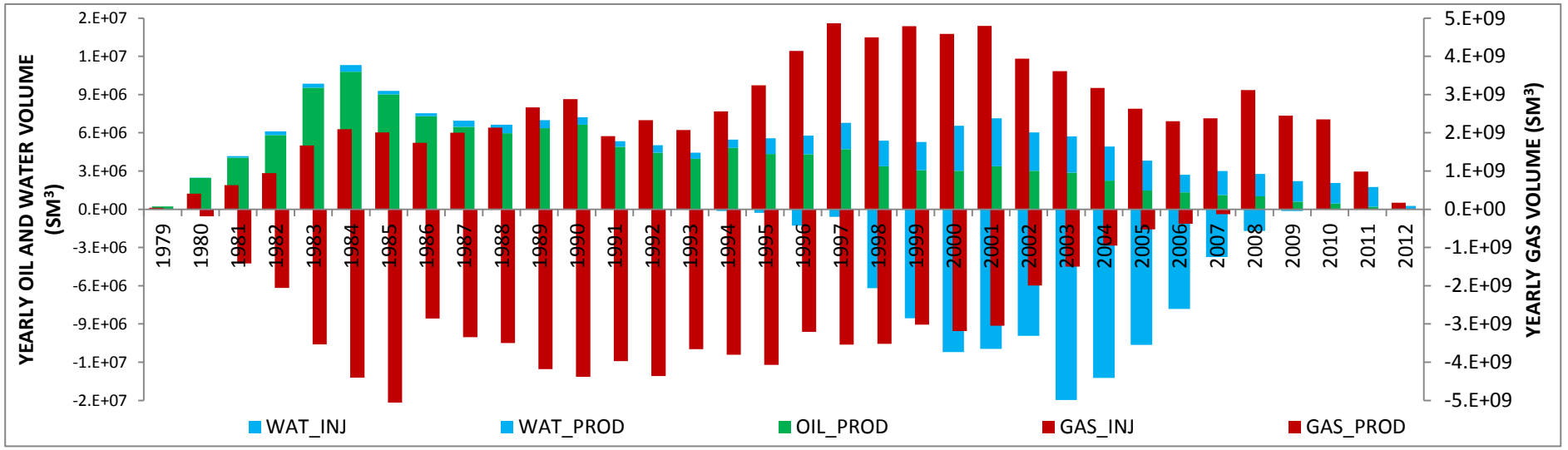

Figure 3.3 – Historical production performance of Statfjord formation (Prosty, 2010).

3.1 Overview of Reservoir Performance

From Fig. 3.2, where the drainage strategy is displayed as a function of time, we can note that three different drainage strategies have applied; consequently, each had an impact on reservoir characteristics and future way of acting.

Fig. 3.3 shows that the peak for oil production was in 1984 whereas for the gas production it lasted over the 5-year period starting from 1997. As it was mentioned in chapter 2, one of the reasons of gas injection was transportation issues, which was solved in September 1985 and caused the reduction of available gas volume for injection (Fig. 3.3).

The following highlight some important aspects concerning the gas phase in the Statfjord formation:

- Injected gas that formed gas cap throughout the formation, which is currently mainly located in the southern part of the fault F11 where only gas has been injected historically in this area (Fig. 3.4);
- There are different gas liquid contacts in the Statfjord area (Fig. A.1.2). This fact will be discussed in details later in this work with respect to the field geology.

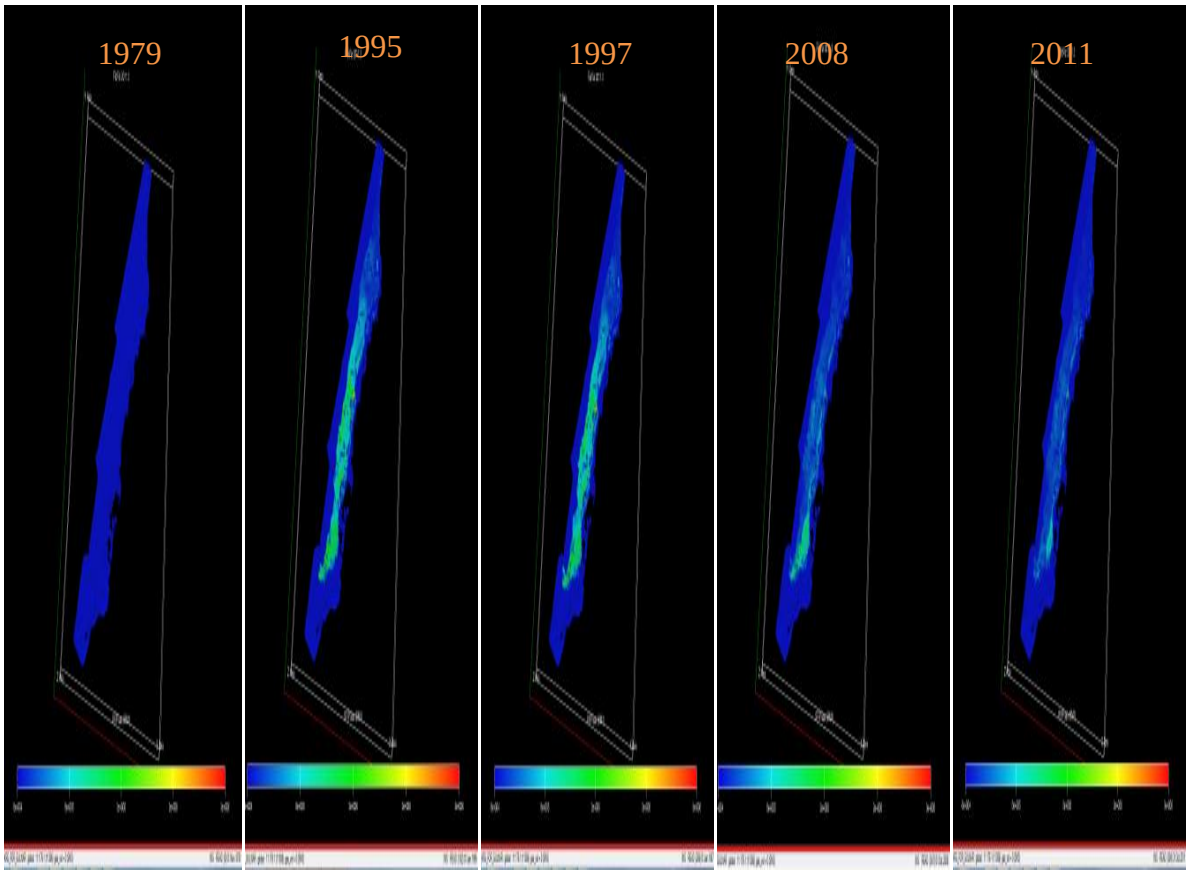

Figure 3.4 - Illustration of GIIP from FLOVIZ.

The Statfjord formation was initially developed based on the gas and water injection to provide pressure support. Although well configuration was designed to ensure good sweep efficiency and to delay breakthrough time, nowadays, well after well dies due to water breakthrough this has a direct impact on the gas production.

Therefore, to extend understanding of injectors and producers' behavior, the overview of wells is done (Figs. 3.5 and 3.6). This will evaluate briefly the potential location of free gas that has been injected in early times of drainage history. Overall, the Statfjord Fm. contributes 52 % of potential gas and gas producers as B-17AT3, B-34and B-23C producing from the gas cap in the south of F11 adds 34 % of total gas production. The main gas producer at SFA is A-18D which has been perforated in the upper Statfjord and brings about 41 % of the potential total gas production at SFA. During 2009, SFA wells experienced massive water breakthrough. In general, it is believed that the SFA area is water flooded by upflank water injection. The three wells, i.e. B-23C, B-17AT3and B-34, donate 55 % of the total gas potential at SFB. SFB wells located in the north of F11 watered out in 2010 and at the same year SFC gas producers water out. Moreover, from SFC the wells as C-12DT2, C-29AT2 and C-40C benefit 48 % of gas potential.

Production performance confirms that the gas locates at the crest as it was described in drainage strategy in chapter 2.

Main highlights from the historical well overview:

- Only gas was injected in the southern of fault F11;
- Gas producers are at the crest and mainly in the upper part;
- Low formation productivity in the lower part of the Statfjord formation.

3.2 Where is the Gas?

Various approaches have been put forward to solve this issue. At the end, it has been concluded that most likely, that the gas might be trapped during the updip water injection, however there are other possibilities:

- Probability of compositional change;
- Introducing barriers such as shale extension into the model;
- Split factor for injectors is wrong.

As discussed in subsection 3.1, the gas was injected as soon as production started, so that there is no doubt that during the miscibility process the composition of original fluid is changed. Unfortunately, ECLIPSE simulator model uses the initial PVT data, hence, the simulator does not take into account the compositional effect.

UPPER STATFJORD

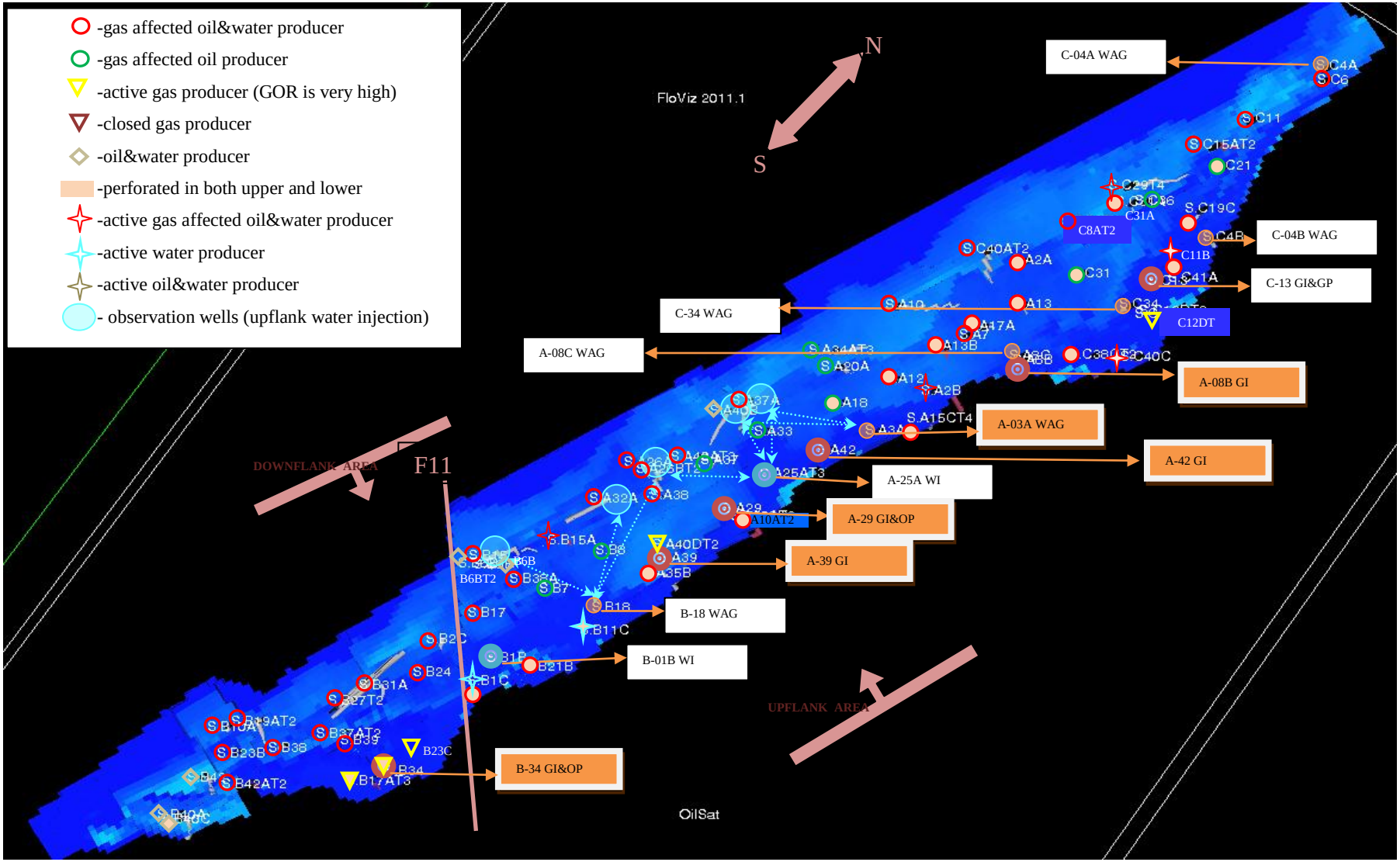

Figure 3.5 - Overview of the upper Statfjord Fm. model (Floviz).

LOWER STATFJORD

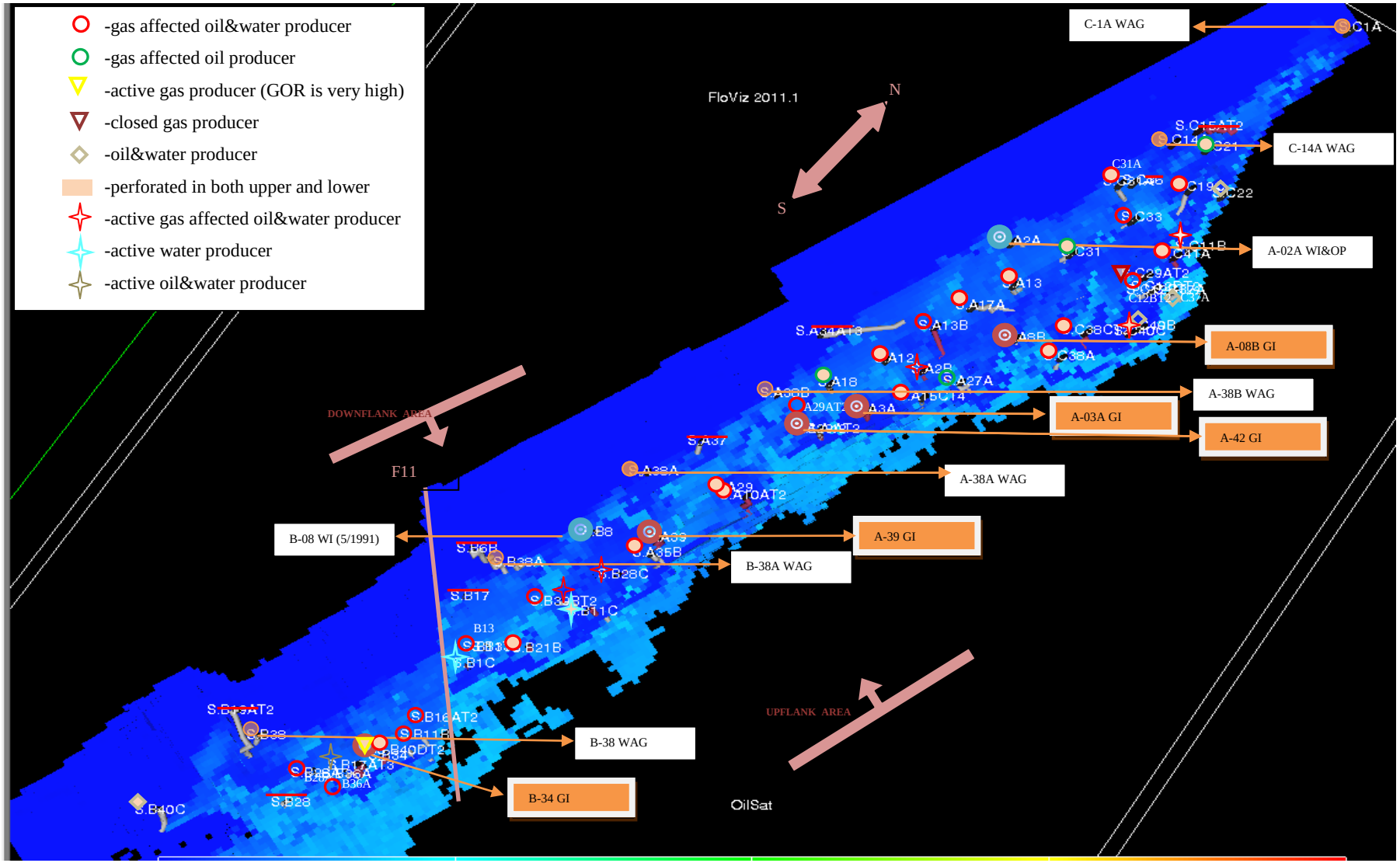

Figure 3.6 - Overview of the lower Statfjord Fm. model (Floviz).

Another reason for the mismatch could be allocation volumes. Some wells drilled in the Statfjord field penetrate through the Brent formation, upper and lower Statfjord formations (Figs. 3.5 and 3.6). From experience, it is said that identifying which formation contributes to production and/or injection could be uncertain. This uncertainty could introduce some errors when the split factor (derived from formation productivity) is used to calculate allocation volumes.

All the listed bullets need to be investigated in the future in order to enhance simulation model quality.

Since the initial task was to analyze the trapped mechanism in the Statfjord formation further studies will be focus on only upflank water injection drainage process.

3.2.1 Performance of Updip Water Injection in Statfjord Formation

The next important key aspect is to observe the upflank water injection performance. For this reason water flowing process will be examined. The analysis carried out responding to the question as how long upflank injected water stayed in the gas zone, the observation is done only for the upper Statfjord due to complexity of the lower Statfjord, in order to observe it 5 downflank production wells and 4 upflank water injection wells were considered (Fig. 3.5).

Well name	WI period	Cumulative Water Injection (MSm^3)	Upper (U) / Lower (L) Statfjord	Classification
A-3A	01/1996-08/2006	16.4	U+L	UPFLANK
A-38A	03/1998-05/2003	4	L	DOWNFLANK
A-2A	04/1998-06/2002	2.9	L	DOWNFLANK
A-25AT3	06/1999-05/2007	16.6	U	UPFLANK
A-8C	12/2000-06/2006	6.3	U	UPFLANK
A-38B	07/2003-08/2008	4.4	L	DOWNFLANK
B-38	09/1994-06/1997	0.48	L	DOWNFLANK
B-38A	11/1997-10/2005	5.9	L	DOWNFLANK
B-18	02/1998-08/2003	8.8	U	UPFLANK
B-1B	05/2000-03/2007	20.2	U	UPFLANK
C-1A	06/1996-02/1997	0.22	L	DOWNFLANK
C-34	12/1999-12/2001	1.6	U	UPFLANK
C-4A	05/2001-01/2003	1.4	U	DOWNFLANK
C-14A	12/2002-08/2008	7.9	L	DOWNFLANK
C-4B	07/2003-11/2004	4.2	U	UPFLANK

Table 3.1 - Water injected wells in the Statfjord Fm. (Well comments, 2011).

	PRODUCTION WELLS				
	B-15	A-32A	A-26A	A-40B	A-37A
Breakthrough time	Nov-99	May-00	Jun-02	Nov-01	Mar-00

Table 3.2 - Sea water timing (Well comments, 2011).

The interaction of the B-18 injection well to production wells as B-15, A-32A and A-26A is shown in Fig. 3.5. Similarly, both A-3A and A-25AT3 injection wells communicated with production wells such as A-40B and A-37A. Moreover, the breakthrough time is shown in Table 3.2. The difference between starting date of the injection (Table 3.1) and breakthrough time indicates when the injected water started to leave the gas zone, we can conclude that required time was at least one year. More details on communication paths between injector and producer are verified by water and gas tracers, can be found in Appendix 1 (Table A.1.1).

Consequently, after one year water started to interact with oil and formation water (Fig. 3.7). Since it is known from chapter 2 that the formation is inclined, hence the gravity will play one of the important roles in the updip water injection process as it is shown in Fig. 3.7. However, the impact of the gravity segregation will not be considered in this study.

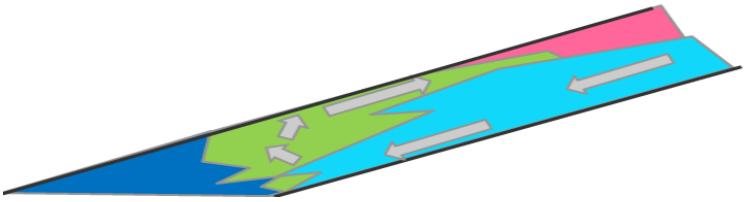

Figure 3.7 - Gravity segregation.

As soon as water is injected into the gas cap it starts to trap the gas. Fig.3.8 illustrates how the flow of upflank water is trapping the gas and entering to original water zone. It is obvious that GOC lift will not cause the gas to be trapped due to the miscibility. As it was mentioned above all the water that has been injected remained in the gas zone for one year.

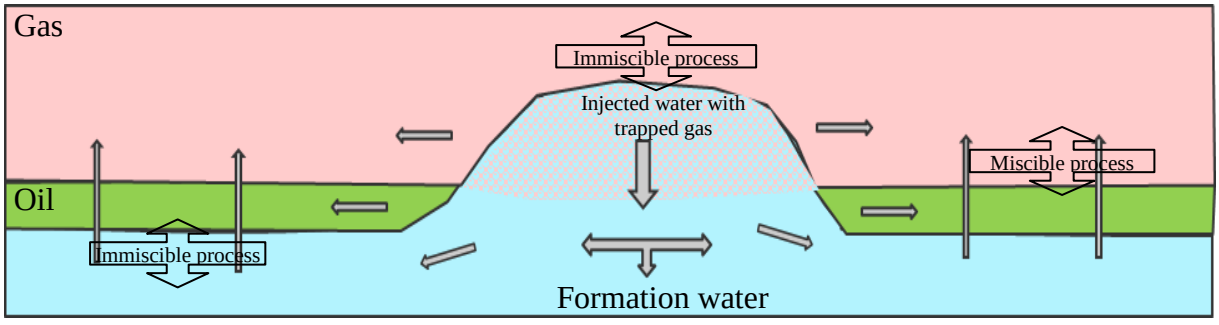

Figure 3.8 - Upflank water flow conceptual cross-section.

When water moves through the gas zone, gas phase is partially pushed aside and partially gas trapped by water. Water, injected after entering the formation, occupies partly additional gas zone and partially moves toward the aquifer. In the next stage when the water injection has been stopped, redistribution of fluids has been taken place. During the redistribution of phases period water has gone to aquifer due to gravity while lifting GOC or GWC. The current fluid contact depth has been changed and is shown in Appendix 1 (Fig. A.1.2).

Combining all the statements, we can conclude that the growth of GOC is not due to trapped gas and the trapping has started immediately after injection and today the liberation of the gas has not been started yet. Furthermore, the prognosis of trapped gas will be discussed using the recent estimation in full field model.

3.2.2 Statfjord Formation: Trapped Gas and Prognosis of Liberation

In a major advance at Statoil, Heide (2011) surveyed the subject and pointed out two main uncertainties in the research, i.e. uncertainty in S_{gi} and Land's constant (K) in the Land's correlation. After conducting a sensitivity analysis the overall response to those uncertainties are:

- A high K value in the Land's correlation will lead to low trapped gas saturation;
- High initial gas saturation (S_{gi}) will result in high trapped gas saturation.

The findings would seem to suggest that total trapped gas volume today is approximately 4-8 GSm^3 and the upper Statfjord contributes 90 % (Fig. 3.9). Interestingly, despite the fact that the water injection stopped the trapped gas volume increased. It can be reasonably explained, first, water injection is still segregating and, second, due to aquifer influx which helps to immobilize the gas at gas water contact. The author reaches the conclusion that higher trapped gas volume nowadays leads to more gas being liberated in the future but it cannot guarantee high gas production in the future because this gas will have low relative permeability. This phenomenon was observed for the lower Statfjord, i.e. the gas production is negative in Table 3.4. In addition, there is one more crucial aspect needs to be highlighted, as trapped gas can be an important history matching parameter for water production as well as for overall prognosis. According to Fig. 3.10, the trapped gas will start releasing approximately in 2015.

The software program to analyze the data was FLOVIZ by filtering critical gas saturation (GASKR<0.01) and as a base case Land's constant K is equal to two. It is believed that the trapped gas has saturation less than 0.01.

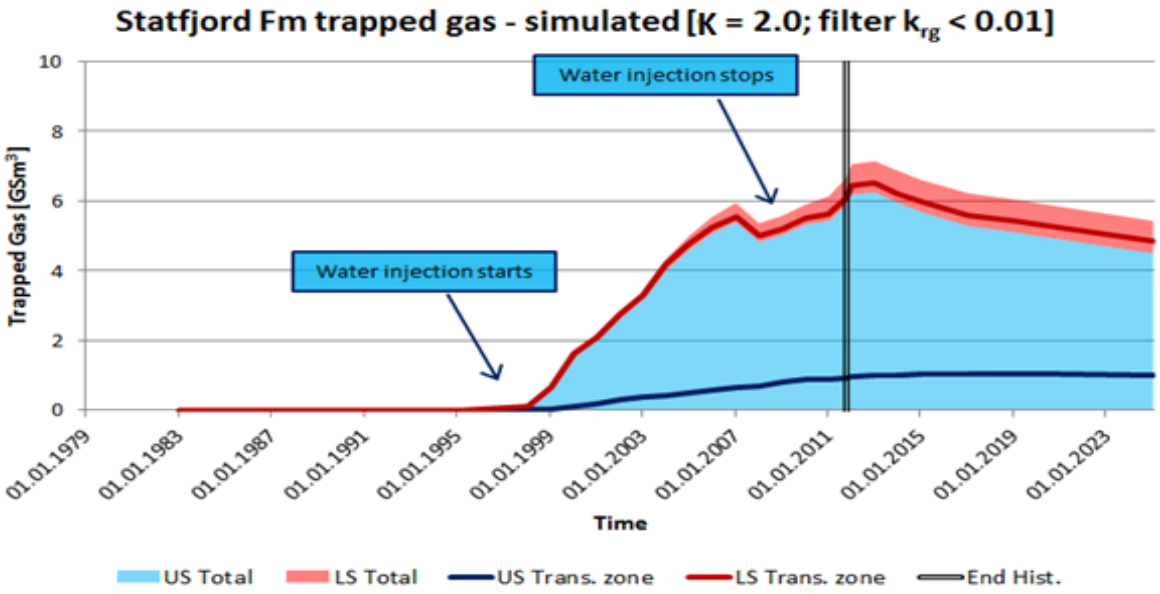

Figure 3.9 - Historical and future trapped gas volumes (Statfjord Fm: trapped gas, 2011).

Time period	Upper (GSm^3)	Lower (GSm^3)	Total (GSm^3)	Transition Zone (GSm^3)
Trapped 2011	5.9	0.8	**6.7**	1.2
Trapped 2021	4.9	0.9	**5.8**	1.4
Trapped 2025	4.5	0.9	**5.4**	1.4

Table 3.3 – Statistical data for trapped gas volume (Statfjord Fm: trapped gas, 2011).

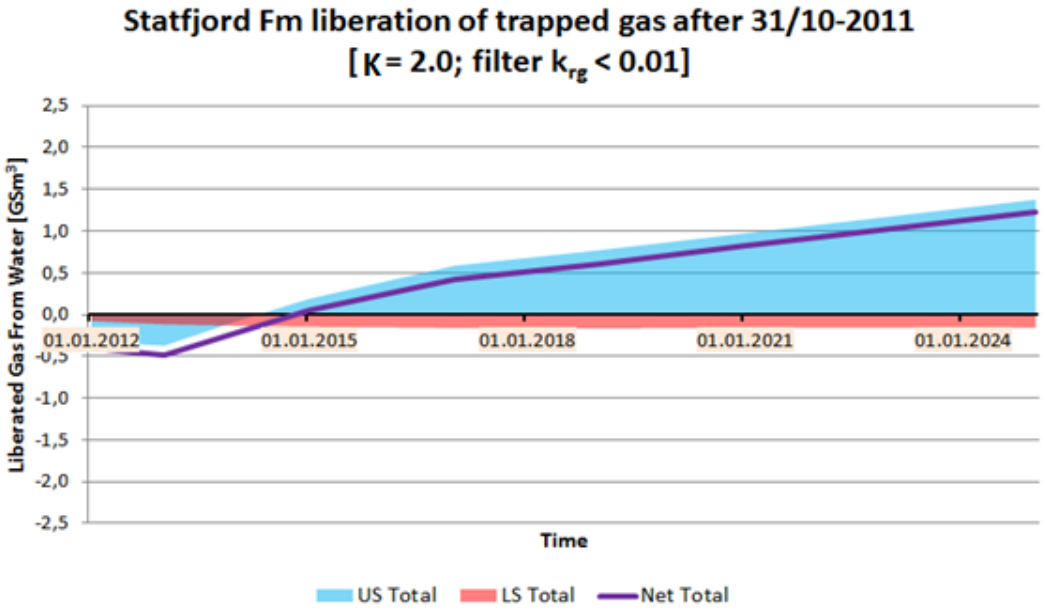

Figure 3.10 - Prognosis for liberation of trapped gas (Statfjord Fm: trapped gas, 2011).

Time period	Upper (GSm^3)	Lower (GSm^3)	Total (GSm^3)
Liberated 2021	1	-0.2	**0.8**
Liberated 2025	1.4	-0.2	**1.2**

Table 3.4 - Prognosis for liberation of trapped gas (Statfjord Fm: trapped gas, 2011).

Fig. 3.11 displays the trapped gas volume as a function of time, four major dates were chosen, in particular the initial production, beginning of updip water injection, end of updip water injection and current day. The most striking phenomenon is trapped gas located mainly in SFA and SFB area, however it needs to take into consideration that through the time it can migrate.

The main weakness in his study is that wells are controlled on the gas rate, in other words, production rate is set and restricted although in future perhaps production index can increase due to liberation. Hence, it is not a good starting point for estimation the volume of trapped gas.

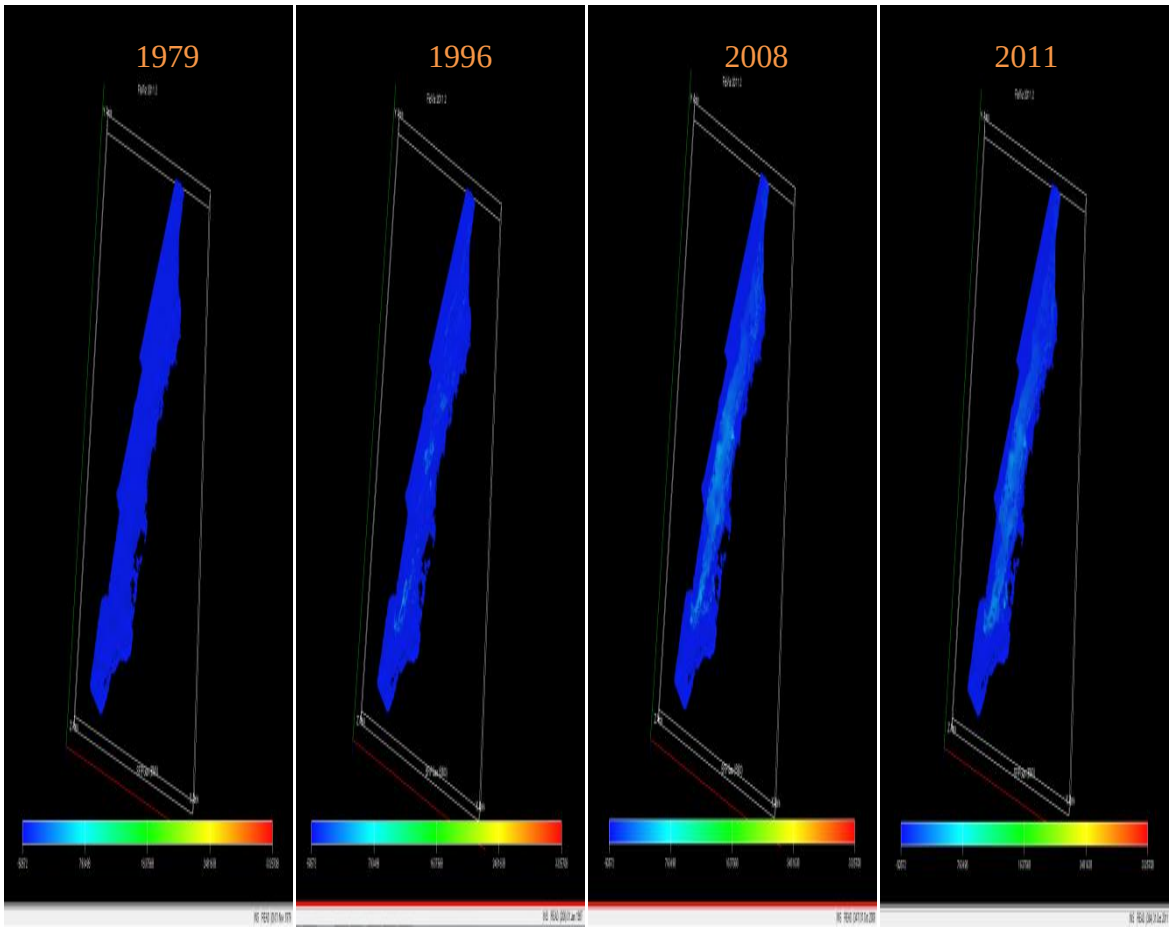

Figure 3.11 - Illustration of trapped gas location from FLOVIZ.

4. STATFJORD FORMATION MATERIAL BALANCE ANALYSIS

There is no doubt; nowadays wide utilized tool in industry is the numerical simulation model. However existed perception cannot eliminate the use of classical analysis as material balance. It helps to gain understanding of dynamic performance, especially at the early stage of field development. Since the simulation prediction for the Statfjord Fm. was off (incorrect), an alternative solution like using MBAL tool was posed due to its simplicity and the rapidity.

The chapter describes the frame in a building the MBAL model, i.e. workflow; input data screening; production, injection and pressure histories will be analyzed and the main uncertain and matching parameters will be defined.

4.1 The Material Balance Evaluation and Methodology

MBAL (MBAL user manual, 2011) is a simplified analytical tool to identify reservoir characteristics using the concept of material balance. Due to its simplified nature; MBAL is governed by several assumptions such as:

- Homogenous reservoir tanks;
- Constant tank temperature;
- Uniform pressure and hydrocarbon saturation distributions in the tank;
- Instantaneous transmission of pressure changes throughout the system.

The main purpose of a material balance study is to identify the remaining reserves, most importantly, gas reserves, and future field performance. Furthermore, secondary objective is to verify and analyze the aquifer size. The detailed workflow is shown in Appendix 2 (Fig. A.2.1). The workflow tests matching parameters within the uncertainty range and it is applicable either for single or multiple tanks.

Fig. 4.1 provides an overview of the tank model which all the calculations are based on. It should be stressed that water injection into gas cap is disregarded in the MBAL application. It is by no means certain that upflank water injection can be applied in MBAL. However, hysteresis function can be chosen in order to count the trapped gas effect.

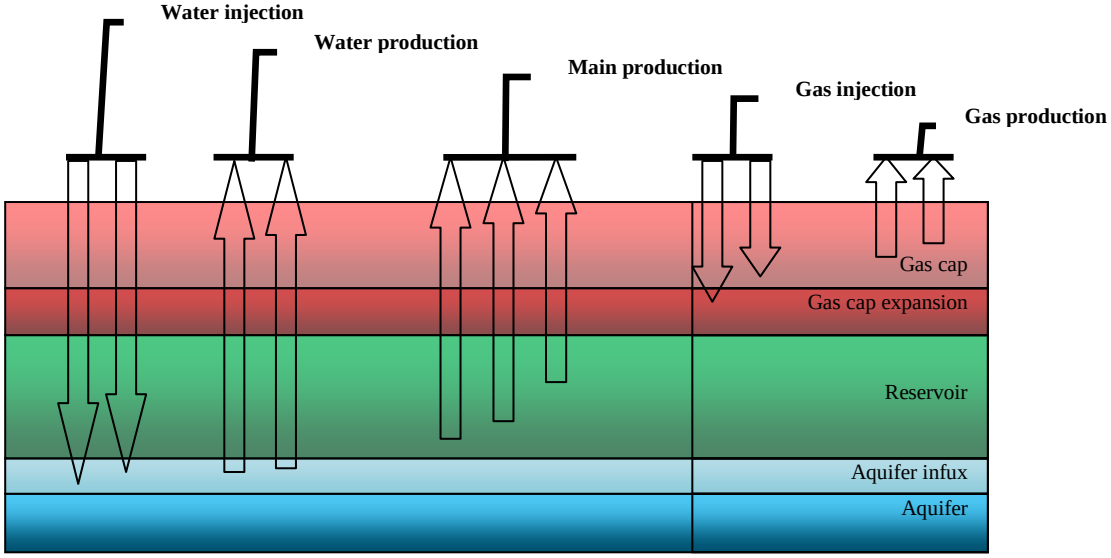

Figure 4.1 – Schematic diagram of a material balance tank model (MBAL user manual, 2011).

4.2 Collection and Verification of Input Data

For building the model different data sources were used such as simulation model, Prosty and 'Reservoir engineering dynamic model and forecast' report.

Bui et al. (2006) proposes the main steps that have to be taken for analyzing the input data. The recommendations are:

- RFT data, static pressure data and fault system are the major data target for identifying the compartments;
- Analysis of production, injection and pressure histories.

The steps proceed very much in the same manner that is reported by Bui et al. (2006). Fig. 4.2 illustrates RFT pressure distribution reported at a datum depth of 2701 m. According to the figure, the most striking aspect is that the RFT data is more scattered in the lower Statfjord formation as compared to the upper Statfjord. Therefore, the formation is divided vertically into two sections and laterally split into two sections due to the fault F11.

Fig. 4.2 reveals an interesting pressure behavior. A fluctuation happened due to injection. The most noticeable feature is three peaks in pressure depletion trend, the same as in injection history during the following periods (Figs. 4.2 and 4.3):

- 09/1984-10/1985;
- 01/1989-05/1991;
- 04/2002-02/2004.

In addition, Fig.4.2 provides a clue about transmissibility being the factor for determination of total fluid migration from one tank to others.

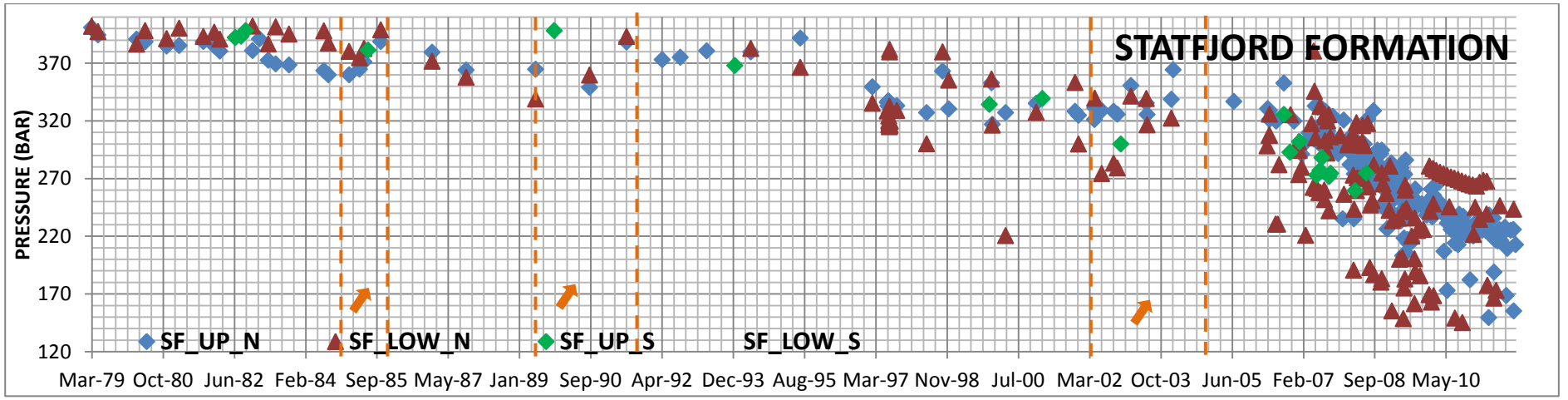

Figure 4.2 - Pressure data for Statfjord model (RFT spreadsheet).

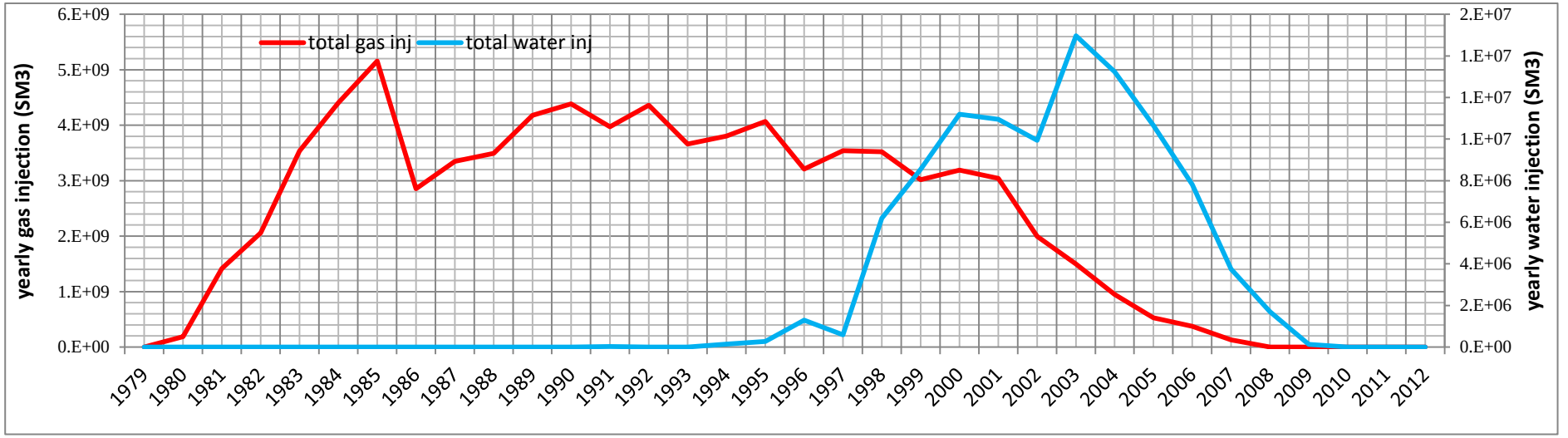

Figure 4.3 - Historical yearly gas and water injection volumes in the Statfjord Fm.

At the same time communication throughout the regions were examined using the FLUXNUM property in the simulation model. Regions were introduced to allow controlling the communication over faults. There are several conclusions concerning the upper and lower parts of the Statfjord formation following the analysis of the RFT measurements (Fig. 4.4):

- Regions 1 and 3 have good Eiriksson-Raude communication, whereas in region 2 the communication is restricted;

- Regions 4 and 6 have limited interaction, but a well B-38 in the south of region 6 has shown good vertical communication, consequently, region 7 was introduced to provide pressure equilibrium.

It was observed that Nansen Mbr. has no lateral barrier and through the fault F11 the communication is limited.

According to all the findings, it was decided to construct a multi tank model (4 tanks; see Fig. 4.4) in order to capture the formation heterogeneity, however a single tank model will be built to make a rough estimate of all uncertain parameters. More details on pressure distribution for each tank with neighboring tanks are given in the Appendix 2 (Fig. A.2.2).

The interaction of the tanks can be also analyzed with respect to the drainage performance. For example, water was injected in the northern part of fault F11, whereas only gas was injected in the southern region; however the amount of trapped gas increased during the updip water injection period which will be an evidence of having the communication between the northern and southern part of the Statfjord formation. More details on the drainage performance of each platform can be found in Appendix 2 (Fig. A.2.3).

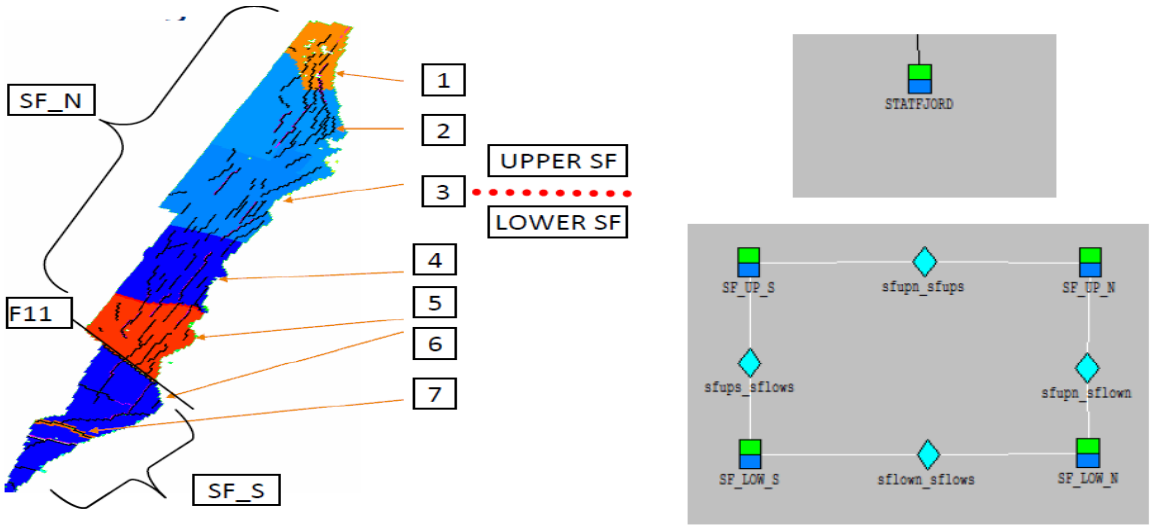

Figure 4.4 - FLUXNUM regions used in the Statfjord Fm. simulation model (The Statfjord field FFM2005 study, 2007).

4.2.1 General Input Data Screening

Dake (2001) in his work explained the concept of material balance based on rock compaction, pressure drop across the reservoir and cumulative water influx. Therefore, reservoir rock and fluid properties are crucial variables in material balance calculations.

PVT data

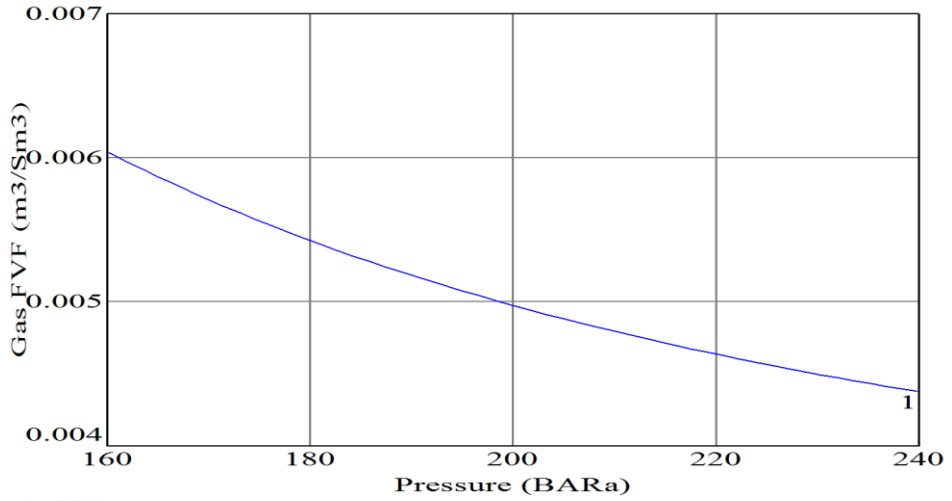

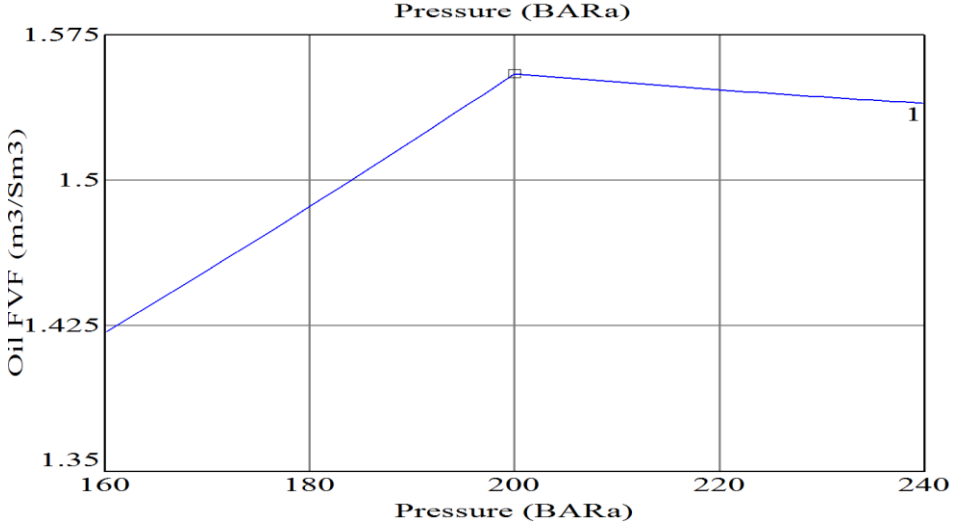

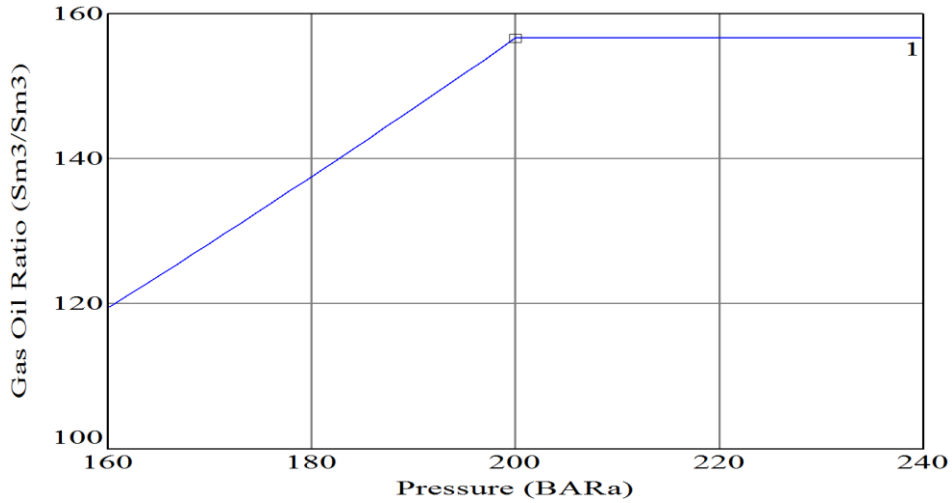

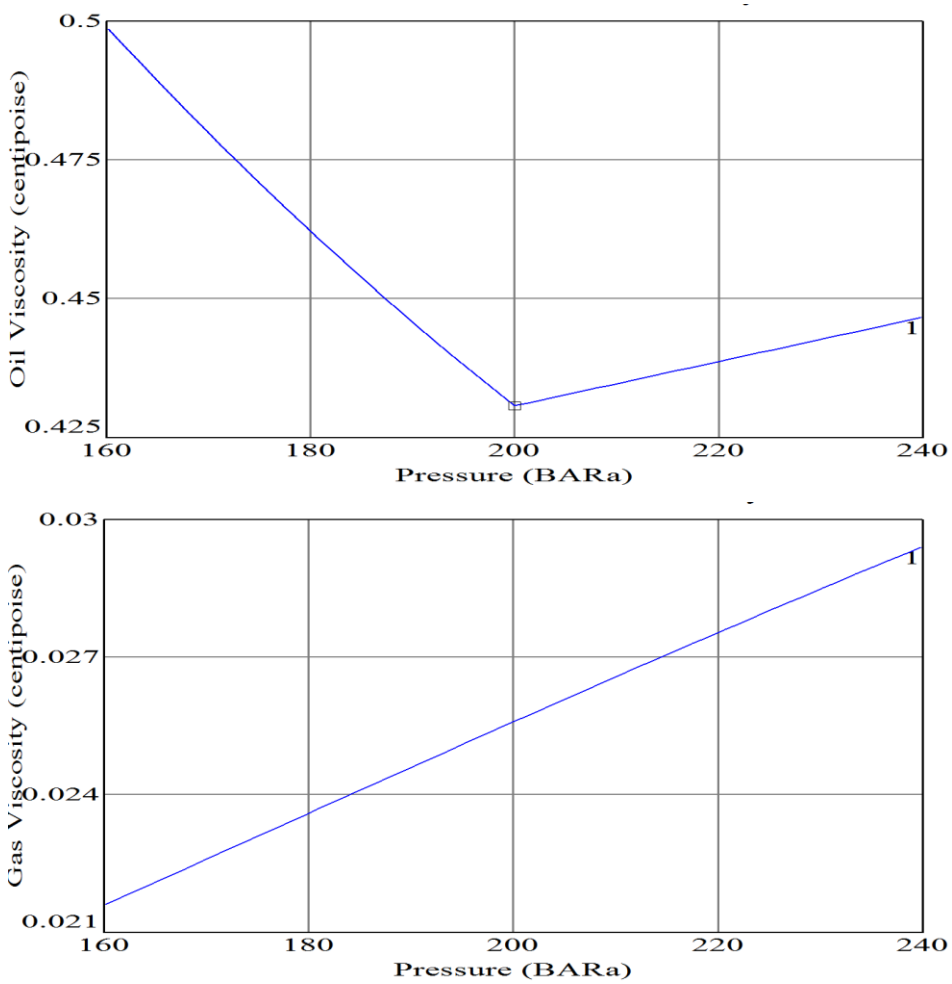

Figure 4.5 – The summary of PVT parameters in the MBAL model.

The PVT data was retrieved from the simulation model. Remark: PVT data should be matched only at bubble point in the MBAL tool (Fig. 4.5).

Reservoir fluid volume in place.

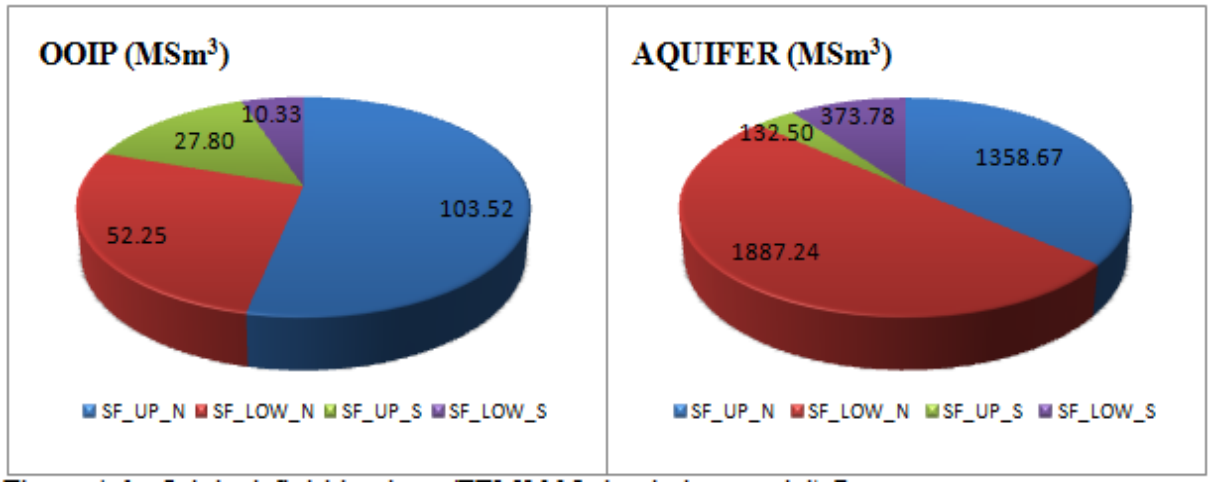

Figure 4.6 - Original fluid in place (FFM2005 simulation model).

For the first run the reservoir fluid volumes are duplicated from the simulation model (Fig. 4.6).

Bui et al. (2006) states that MBAL :(a) may not decrease uncertainty range in the STOIIP estimation; and (b) is only able to assure that the hydrocarbon volumes and aquifer strength combination agrees (functions) correctly.

Relative permeability curves

Relative permeability data is used only for prediction calculation. In the model the relative permeability curve was duplicated from the simulation model as an initial estimate (Fig. 4.7). Relative permeability was widely investigated (Bui et al., 2006) and proposed to use the relative permeability linked to the observed production data. More details on this topic can be found in chapter 5.

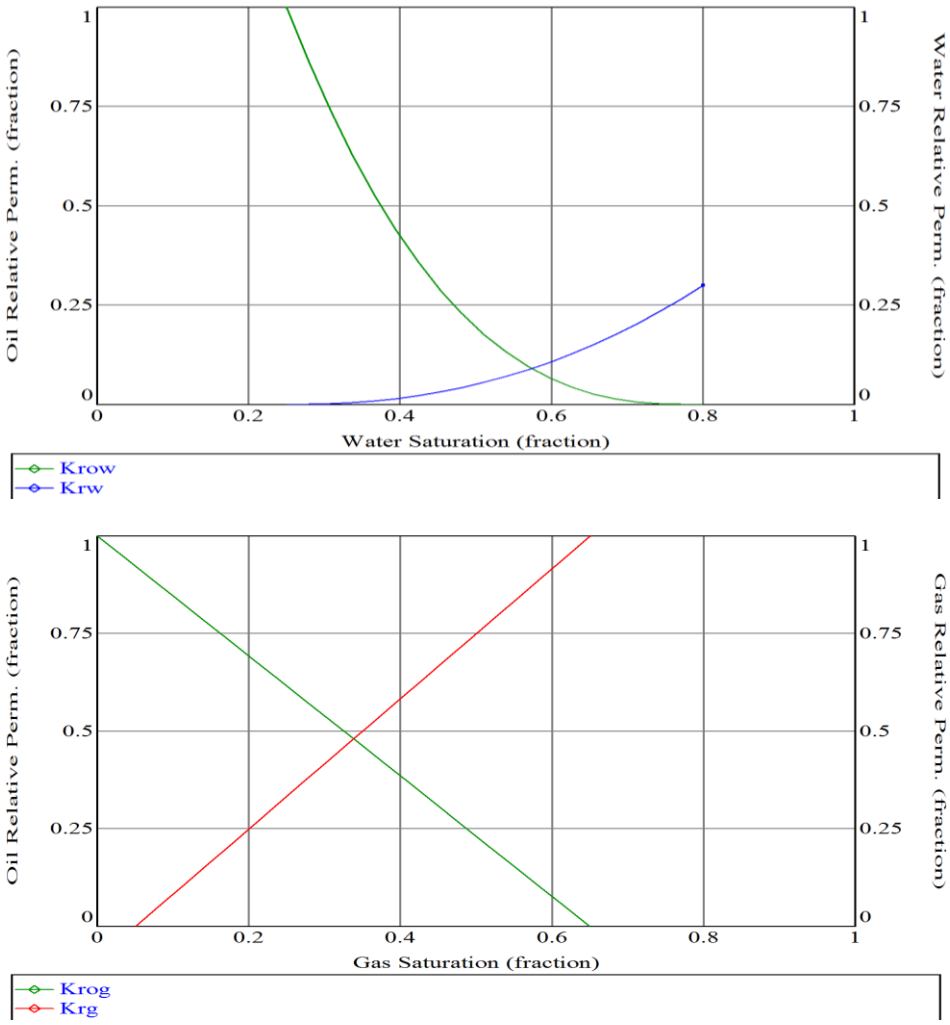

Figure 4.7 - Relative permeability curves.

Transmissibility

Fluid migration from one tank to another is governed by the transmissibility parameter. The following equation is used in the MBAL tool to model inter-tank fluids communication:

$$Q_t = T * \sum_i \frac{K_{ri}}{\mu_i} * \Delta P \quad (4.1)$$

where:

$$Q_t = Q_o + Q_g + Q_w \quad (4.2)$$

Q_t is the total downhole flow rate,

T is the transmissibility constant,

k_{ri} is the relative permeability,

μ_i is the viscosity of phase i,

and ΔP is the pressure difference between the two tanks.

It can be seen that transmissibility is affected by relative permeability data as well, in other words both of them have mutual relation.

Aquifer system

Due to inevitable (unavoidable) uncertainties in the aquifer characteristics, it was proposed to apply the simulation data as a starting point.

	SFC	SFA	SFBN	SFBS	SUM
UPPER	36.78	717.37	604.51	132.50	1491.17
LOWER	184.51	750.26	952.47	373.78	2261.02
SUM	221.30	1467.63	1556.98	506.28	3752.19

Table 4.1 - Aquifer volumes (MSm^3) as history matched in the FFM2005 Statfjord Fm reservoir simulation model (Reservoir engineering dynamic model and forecast, 2007)

The final total aquifer size connected to the Statfjord formation reservoir was 3.75 GSm^3, which is around 13.1 times larger than HCPV of the reservoir. Throughout time the aquifer volume has changed during the history matching effort by adjusting cross sectional area which is connected to the reservoir. Other properties were set constant:

- As high side permeability was fixed at 1000 mD, the average permeability is believed to be in the order of 20 to 400 mD;
- The porosity is equal to 25 percent.

Aquifer influx model	Assumption	Equation	Characteristics
Pot aquifer	$\partial t = 0$ V_A=const	$W_e=(c_w+c_f)W_{Ai}(p_i-p)$	Only applicable to small aquifer ΔP transmitted immediately
Schilthuis steady state	Steady-state flow regime	$\frac{dW_e}{dt} = C(p_i - p)$	ΔP transmitted immediately
Hurst steady state	Steady-state flow regime	$\frac{dW_e}{dt} = C\sum_0^t (\frac{\Delta p}{\ln at})\Delta t$	Pressure diffusivity was introduced Discretization of boundary pressure
Hurst-van Everdingen-Dake	Unsteady state	$W_e(t) = C\sum_0^{n-1} U\Delta p W_d\, \alpha(t_n - t_j)R_d$	
Fetchovich steady state	$\frac{dW_e}{dt} \propto \Delta p$ Approximated method	$\frac{dW_e}{dt} = J(p_a - p_r)$	Pressure diffusivity was introduced Doesn't require superposition principle
Fetchovich semi-steady state		$W_e(t) = \frac{W_i}{p_i}(p_i - p_r)\exp(-\frac{Jp_i}{W_{ei}})$	
Hurst-van Everdingen modified	Water influx rate for each time step	$W_e(t_n) = \sum_0^{n-1} \frac{U}{\alpha}\frac{\Delta p}{(t_i - t_{i+1})}\int W_D\, dt$ $U = V_{aq} * (c_f + c_w)$ $\alpha = \frac{k}{\emptyset * \mu_w(c_f + c_w)L_{aq}^2}$	Pressure diffusivity and Laplace transformation were introduced
Carter-Tracy	Approximation to diffusivity eq. solution	$W_{en} = W_{e(n-1)} + (t_{Dn} - t_{D(n-1)}) * (\frac{B\Delta p_n - W_{e(n-1)}p'_{Dn}}{p_{Dn} - t_{D(n-1)}p'_{Dn}})$	Pressure diffusivity was introduced Constant water influx rates over each finite time Doesn't require superposition principle

Table 4.2 - Aquifer model features (MBAL User manual, 2011).

Several aquifer models have been developed in the MBAL tool. After analyzing their practical application, the best fit (suit) aquifer model was 'Hurst-van Everdingen-modified' due to the quality of solving the hydraulic diffusivity equation (Table 4.2). In Marques et al. (2007) analysis of aquifer model, fundamental theory, and equations have been overviewed.

4.3 MBAL Model Results

A systematic procedure was carried out with combination of single- and multi-tank models. Furthermore, the result from both models will be presented and examined. The models were run based on pure ECLIPSE simulator data. Two sets of graphs are illustrated in Figs. 4.8 and 4.9.The first set of graphs represents analytical method where the oil production calculation is based on input average reservoir pressure, water production, gas production, and water/gas injection data. While MBAL simulation method does the reverse calculation: the average tank pressure is computed with respect to input rates. In analytical method (Fig. 4.8), three lines with different colors are displayed. Red line represents when cumulative production is calculated as a function of aquifer influx and transmissibility, green line when only transmissibility data is taken into account and purple one when calculation is done without transmissibility data but considering the aquifer influx. If green line (production without aquifer) is drown on the left hand side of historical data (⊠), it will assure the validity of PVT data otherwise it needs to be checked.

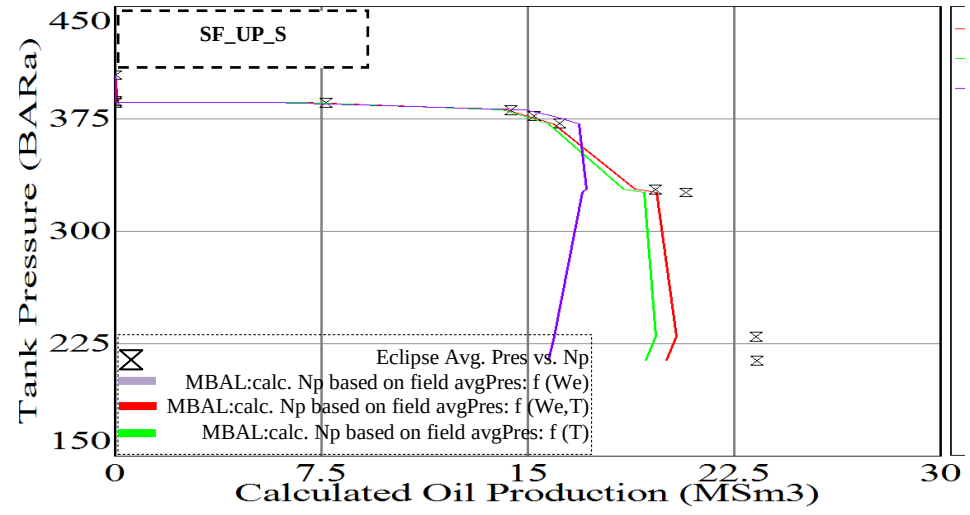

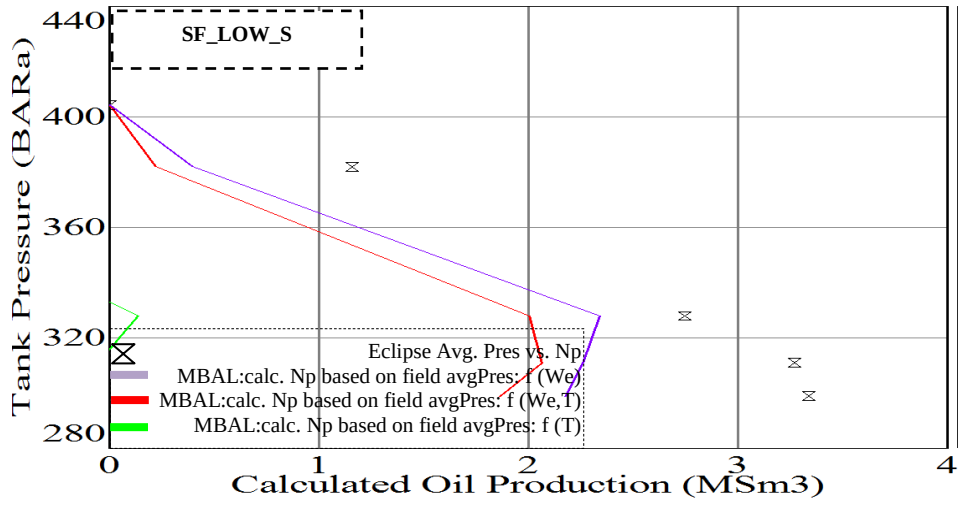

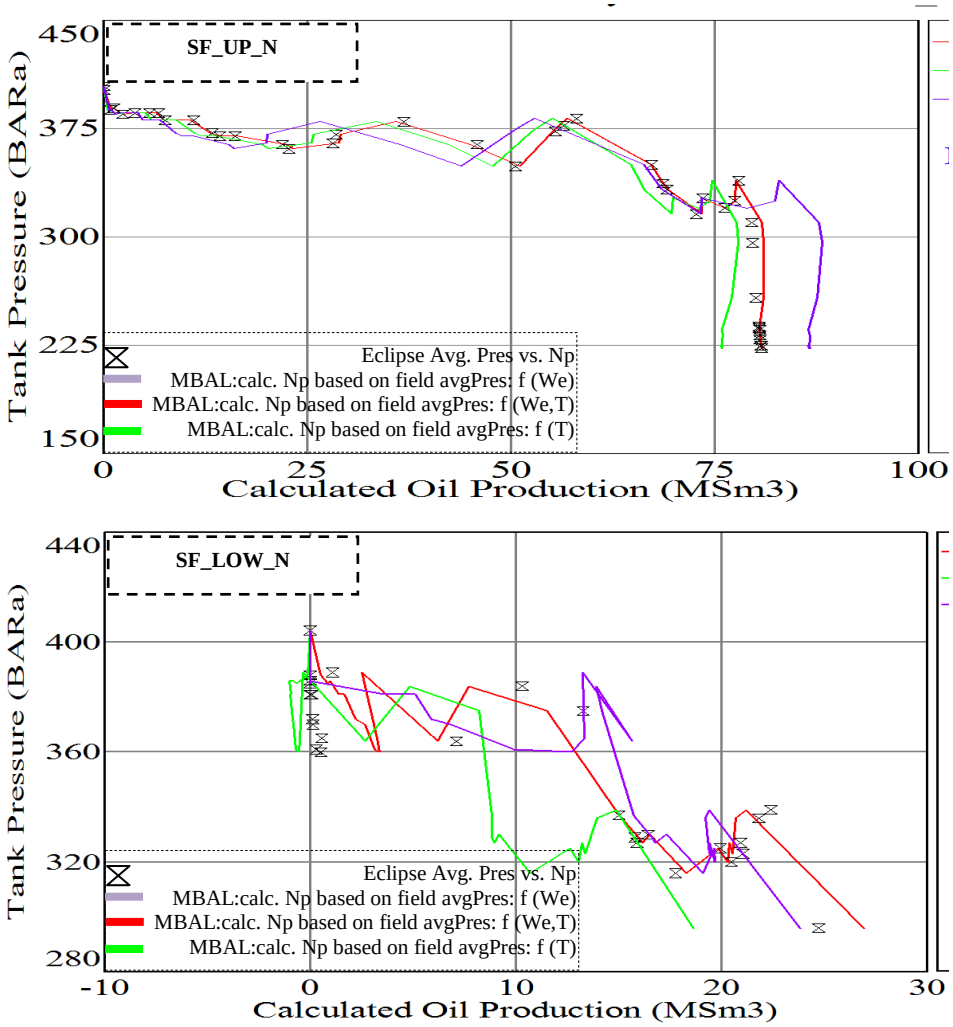

Figure 4.8 - Analytical method for a four tank-model.

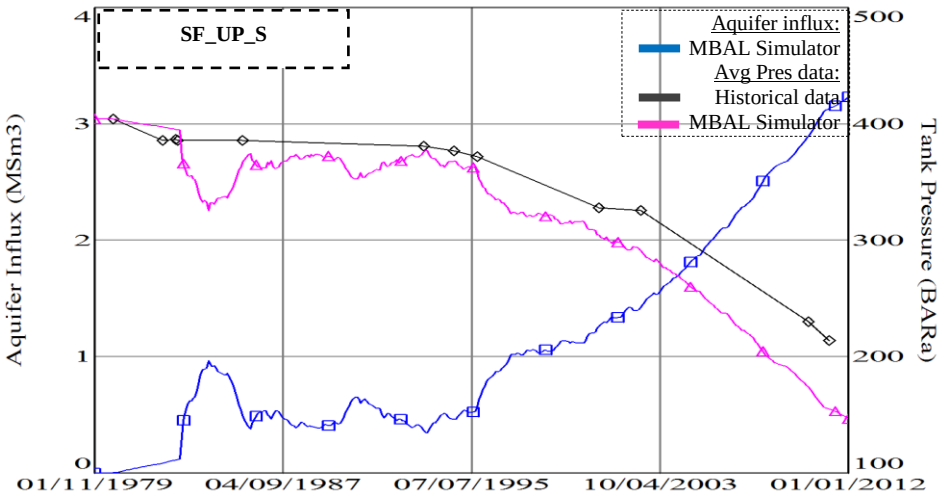

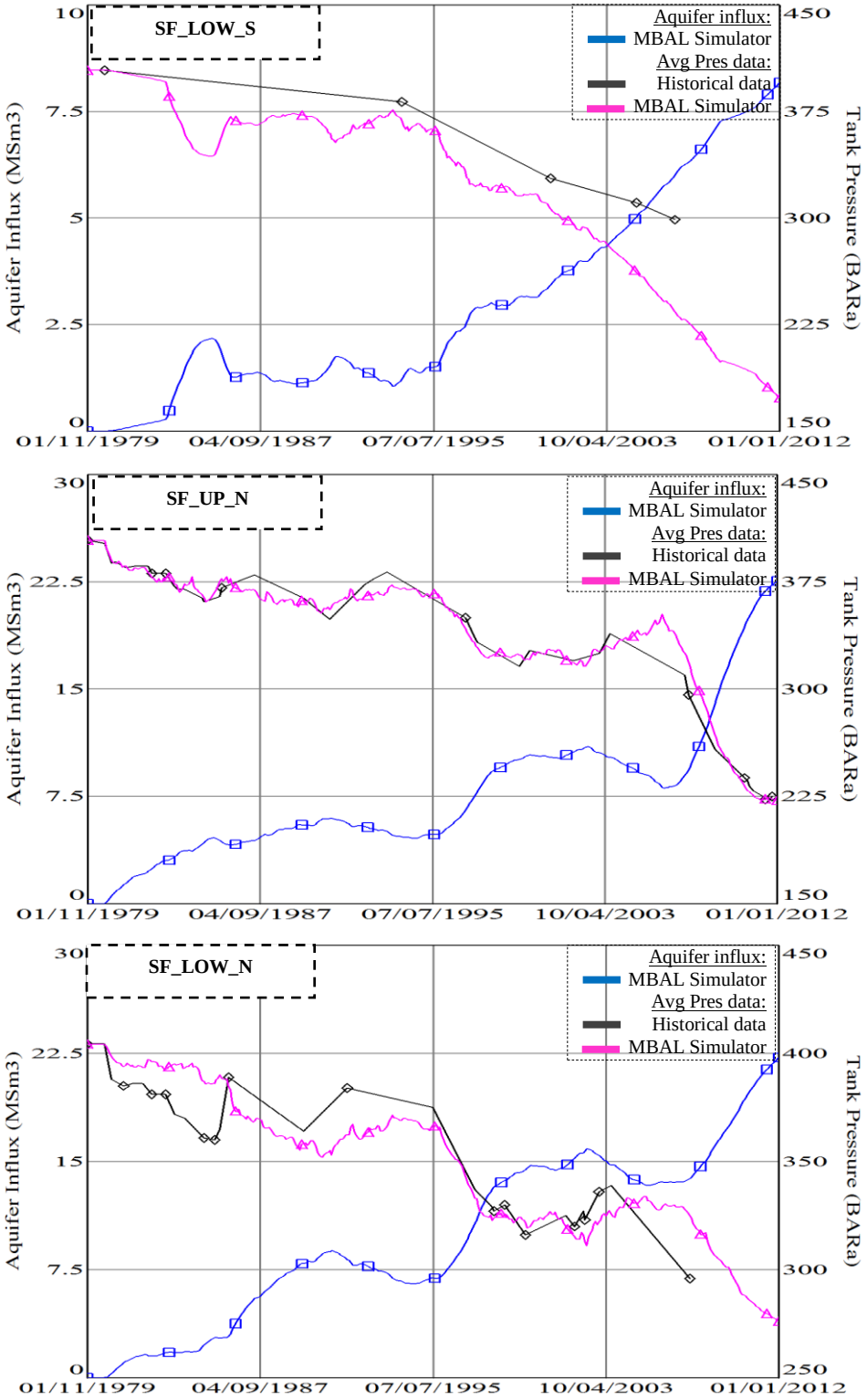

Figure 4.9 - Production simulation method.

Overall, there is no a large discrepancy between calculated and field data in the single tank model (Fig. A.2.4), but the calculated and observed data points do not lie on top of each other (do not coincide), therefore non-linear regression is applied, and the result will be discussed in the next chapter. It is interesting to note that STOIIP turned out to be 1.4 MSm^3 higher than

the one obtain in the simulation work. Although, in multi-tank model the STOIIP is estimated to be similar to the ECLIPSE simulation data, the details will be discussed in chapter 5.

Concerning the four tanks model, the calculation based on pure ECLIPSE model is off; apart from one tank namely SF_UP_N (Figs. 4.8 and 4.9). In general, production for the SF_UP_S and SF_LOW_S is underestimated while that of SF_LOW_N is overestimated (Fig. 4.8). Similarly, the production simulation's plots in Fig. 4.9 show that the calculated trend behaves the same way as in the analytical method. In this method water influx is shown over the time. The plots indicate that the matching process has to be performed.

5. FIELD HISTORY MATCHING AND PERFORMANCE PREDICTION

The findings from the previous chapter show that the MBAL model does not reproduce the field behavior (performance). To overcome this problem, the strategy for history matching procedure is designed and the most uncertain matching parameters are selected.

This chapter covers the main steps for the history matching procedure followed and the analysis conducted for the prediction process.

5.1 History Matching Strategy for MBAL

There is no unique strategy for performing the history match. Nevertheless, MBAL software offers a set of systematic instructions for performing this activity (Fig. A.2.1).

5.1.1 Determination of the Matching Parameters

The initial approach was to use the simulator input data and afterwards to match the MBAL results with the observed data by altering the most uncertain variables. The reason behind the building of a single-tank model was to reduce the number of uncertainties; in fact, the number was shortened by discarding the transmissibility parameters. This gives an opportunity to estimate approximately the aquifer system parameters and afterwards to apply them in the multi-tank model construction.

The MBAL non-linear regression option can be used to optimize several parameters in one realization. However, caution needs to be taken because optimizing all uncertain parameters may give unrealistic results. Even uncertain parameters have their own degree of uncertainty, and for this reason it is crucial to determine a best set of variables.

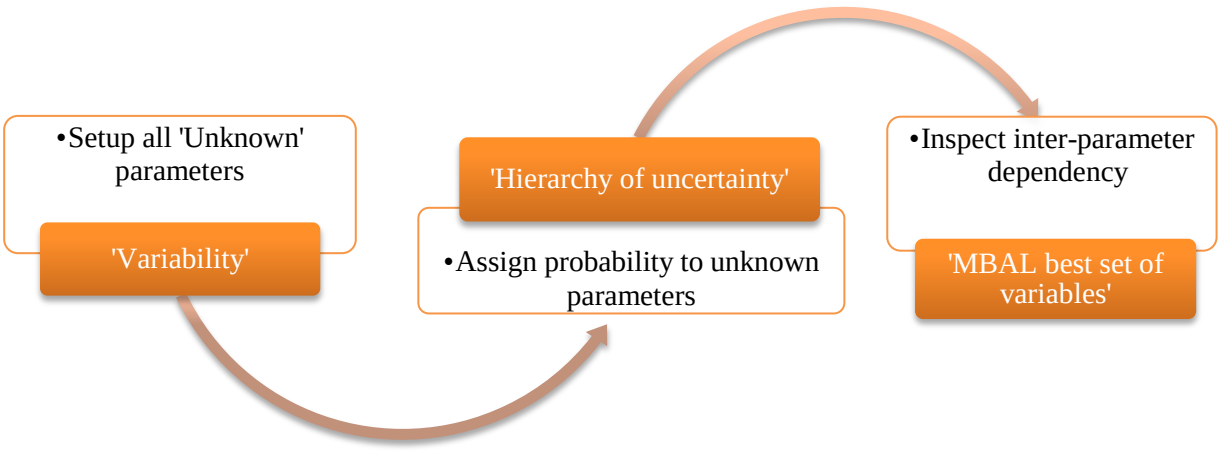

Figure 5.1 - Workflow in determining matching parameters.

As illustrated in Fig. 5.1, the determination of 'MBAL best set of variables' consists of three stages and the outcomes of each step are:

- Variability - establish all uncertain parameters;
- Hierarchy of uncertainty – consult with expert in order to assign the probability to each variable;
- MBAL best set of variables – examine inter-parameter dependency using related equation.

$$N_p[B_o + (R_p - R_s)B_g] + W_p B_w = N[(B_o - B_{oi}) + (R_{si} - R_s)B_g] + mNB_{oi}\left(\frac{B_g}{B_{gi}} - 1\right) + \frac{(1+m)NB_{oi}(c_w S_w + c_f)\Delta p}{1 - S_{wc}} + W_e B_w$$

Figure 5.2 - Potential unknown parameters(Dake, 2001).

The same steps were taken to identify the best set variables for the Statfjord MBAL model. Having established the potential unknowns (Fig. 5.2), the next step is to fulfill the concept of the 'hierarchy of uncertainty', i.e. ranking the uncertain data by questioning ourselves as which data is the most or least reliable.

DeSorcy (1979) evaluated the expected accuracy of parameters in Table 5.1. Having consulted with experts and estimated the uncertainty associated with parameters from the Statfjord formation (Table 5.1), the result of choosing the most uncertain parameters was following: (Fig. 5.3):

- ✓ Transmissibility (T);
- ✓ Relative permeability (k_r);
- ✓ Aquifer volume (V_{aq});
- ✓ Aquifer permeability (k_{aq}).

Data	Typical Source	Approximate range of expected accuracy (%)
Production data: • Oil • Gas • Water	 Measured Measured Measured or estimated	 **±1-3*** **±1-3*** **±2-10***
Temperature	Measured or estimated from correlation	**±2-10***
Pressure	Measured	±1-4 for reservoir of high k/μ **±5-10 for reservoir of medium k/μ*** ±10-20 for reservoir of low k/μ
Fluid analysis data: • Gas solubility, formation volume factor, bubble point pressure	Laboratory analysis of fluid samples Correlations	**±5-10*** ±10-30
Interstitial water saturation	Papillary pressure data Oil base cores Saturation logs Correlations	±5-15 ±5-15 ±10-25 **±25-60***
Rock compressibility	Measured or estimated from correlations	±5-10 for consolidated fm. ±10-20 for friable fm. **±20-50 for unconsolidated fm***

***Data reflects the Statfjord formation.**

Table 5.1 – Source and accuracy of data used in material balance calculation (DeSorcy, 1979).

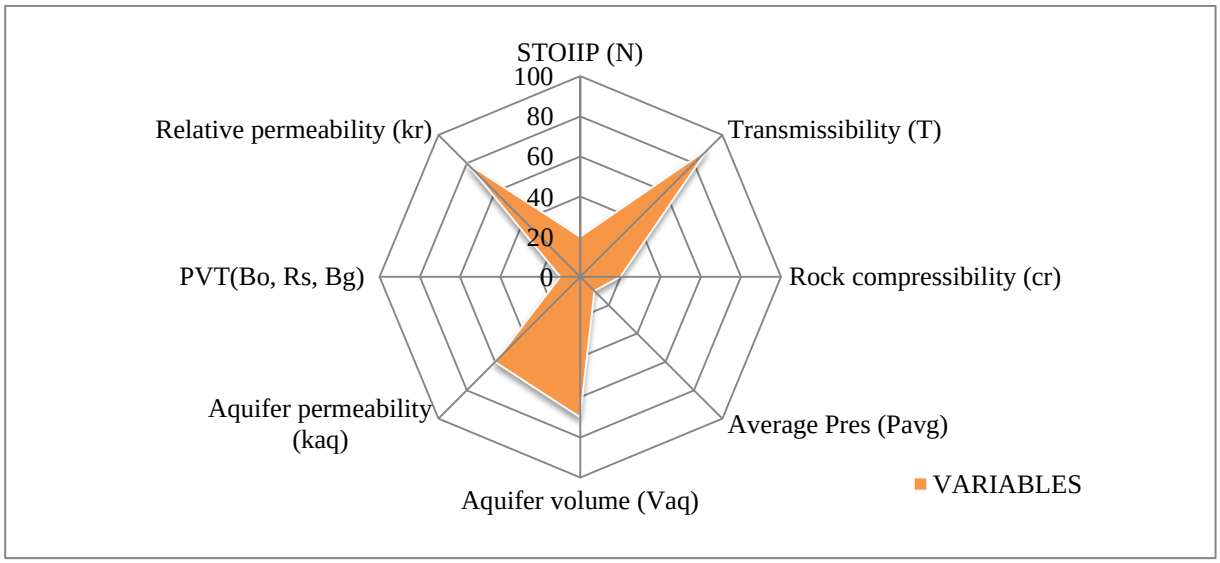

Figure 5.3- Hierarchy of uncertainty.

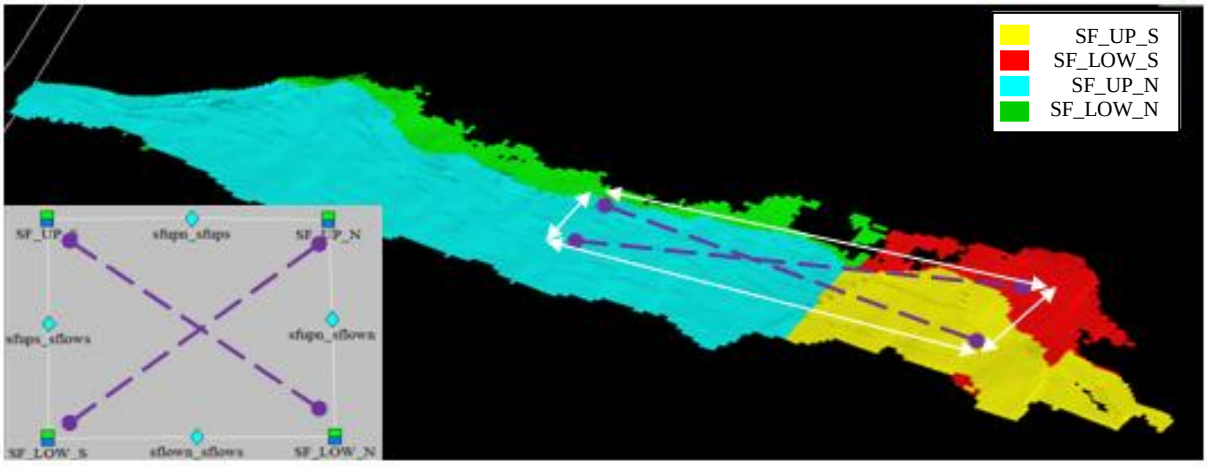

Figure 5.4 – Illustration of MBAL tanks in the eclipse simulation model.

First, the inter-tank transmissibility will be adjusted and next the aquifer parameters will be tuned unless the matched model will be generated. The reason for the transmissibility parameter being the most uncertain is that the MBAL model has some limitations; for example, fluids flow migration is limited to only the two neighboring tanks in both directions. However, it cannot skip one tank and go in direction of purple line as shown in Fig. 5.4, i.e. the flow moves tank by tank along white arrows and the flow cannot be cross-flowed.

A study by Torony and Saleri (1988) on the effect of matching variables is summarized in Table 5.2. For example, pore volume variation leads to change pressure with time while relative permeability change affects matching saturation variations in time and space. In the study the fluid property was excluded due to accuracy of the data. Two parameters were chosen as the matching parameters for the MBAL model which is indicated in Table 5.2, consequently, aquifer volume impacts on pressure match procedure, while relative permeability influences on saturation match procedure in production forecasting. The equations with the matching variable are worth studying in order to examine inter-parameter dependency (see Chapter 4 for the equations of matching variables)

Parameter	Pressure match	Saturation match
Pore volume	$\Delta p/\Delta t$	*
Permeability thickness	$\Delta p/\Delta x$	$\Delta S/\Delta x$
Relative permeability	Not used	$\Delta S/\Delta x \& \Delta S/\Delta t$
Rock compressibility	*	Not used
Bubble point pressure	$\Delta p/\Delta t$*	*

*Avoid changing if possible.

Table 5.2 - Influence of key history matching parameters (Torony and Saleri, 1988).

Another difficulty with the history match procedure is that all altered parameters must attain values with physical meaning; in other words, altered parameters need to be within the range of values representing the Statfjord formation. For this reason, the workflow should include a feedback from the field geologist after each realization in the MBAL tool.

5.1.2 Manual vs. Automatic History Matching

As it was mentioned above, the MBAL can speed up the matching process via non-linear regression, which offers the best-fit value for a given reservoir parameter. The question then arises as how the best-fit value is calculated and secondly, whether to use the best-fit estimates or not, (i.e., if the 'best-fit' closely approach the correct result).

Regarding the concern of the best-fit computation technique, the aquifer parameter regression is considered below as an illustration:

1) First, the reservoir (tank) pressure (P_i^{cal})is calculated for each time step given the aquifer configuration parameters,

2) The estimated value is then compared against measured data P_i^{abs}

$$\chi^2 = \sum_{i=1}^{n} \frac{\left(P_i^{abs} - P_i^{cal}\right)^2}{\sigma_i^2} \quad (5.1)$$

3) After each iteration matching parameters, (i.e. the set of matching variables that was selected by user to be changed) are altered to lower down χ^2 and continued until a minimumis found

Turning to the second question, many attempts have been made (Marquardt, 1963; Tehrani, 1985) with the purpose of estimation the reliability of the 'best-fit' function and concluded that a small standard deviation is an indication how accurate and reliable the 'best-fit' option.

During the history match procedure the first run was based on pure non-linear regression option by selecting all matching parameters and the matching parameters lied out of the geological range (TablesA.2.1 and A.2.2). The recent study by Tavassoli et al. (2004) commented that a perfect history matched model with incorrect geological features might lead to bad forecast. Consequently, the main target will be to populate the model manually by capturing geological characteristics after that as a quality check to run the regression for each set of matching parameters separately (i.e. selecting only transmissibilities for all tanks, then aquifer volume, etc.,) to see how the values will change and do some sensitivity scenarios to assess the quality and degree of representativeness of the model. For that reason, a lot of attention paid to the geology and the reservoir itself in this work.

5.1.3 Manually History Matched Statfjord Model

According to geology, the transmissibility between the tanks was ranked as shown in Fig. 5.5 and the MBAL model was constructed according to this transmissibility ranking information. Note: corresponding transmissibility numbers are used in the MBAL model.

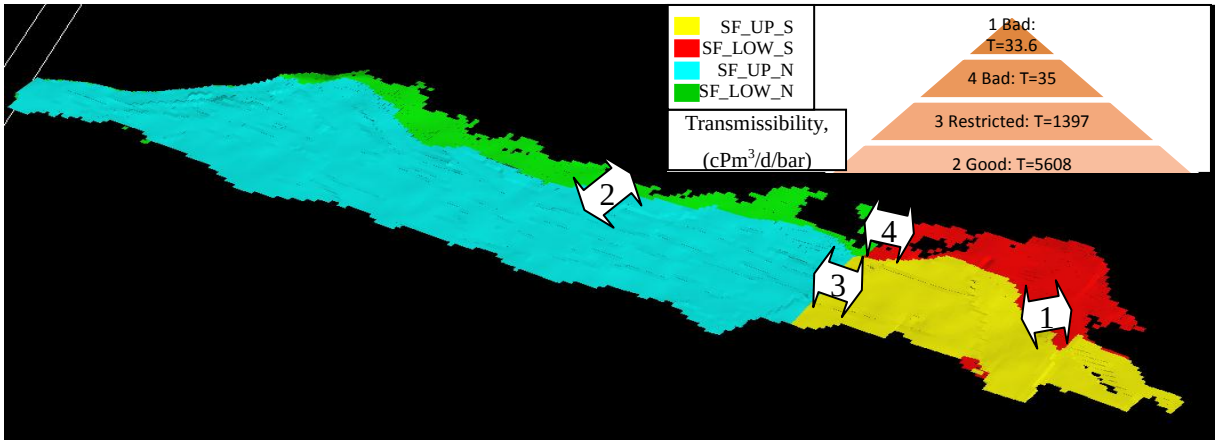

Figure 5.5 - Illustration of transmissibility values for the multi-tank MBAL model.

Before getting a reasonable matched model, many realizations have been run. During the history matching, STOIIP and aquifer influx data between the ECLIPSE simulator and MBAL was reconciled (Table 5.3).

Parameter	Model	SF_UP_N	SF_LOW_N	SF_UP_S	SF_LOW_S
Aquifer size (Mm^3)	ECLIPSE	1358.67	1887.24	132.50	373.78
	MBAL	1359	1886	133.5	387
STOIIP (MSm^3)	ECLIPSE	103.52	52.25	27.80	10.33
	MBAL	103.5	52	27.75	10.31

Table 5.3 - Comparison of MBAL and ECLIPSE simulator STOIIP and aquifer volumes.

Fig. 5.6 presents MBAL analytical (left four figures) and MBAL simulation (right four figures) matching plots. MBAL analytical results obtained by calculating cumulative oil production based on given average tank pressure, injection and production data excluding the oil phase. The details of the computation for two methods are given in subchapter 4.3. After matching manually, non-linear regression method was applied for each type of matching variable separately; as a result, it improved the matching quality and lied within the geological range. Two tanks' trends, namely SF_UP_S and SF_LOW_S, do not coincide with the observed data. A possible explanation can be that the observed data points are few and a trendline connects two points by using linear extrapolation.

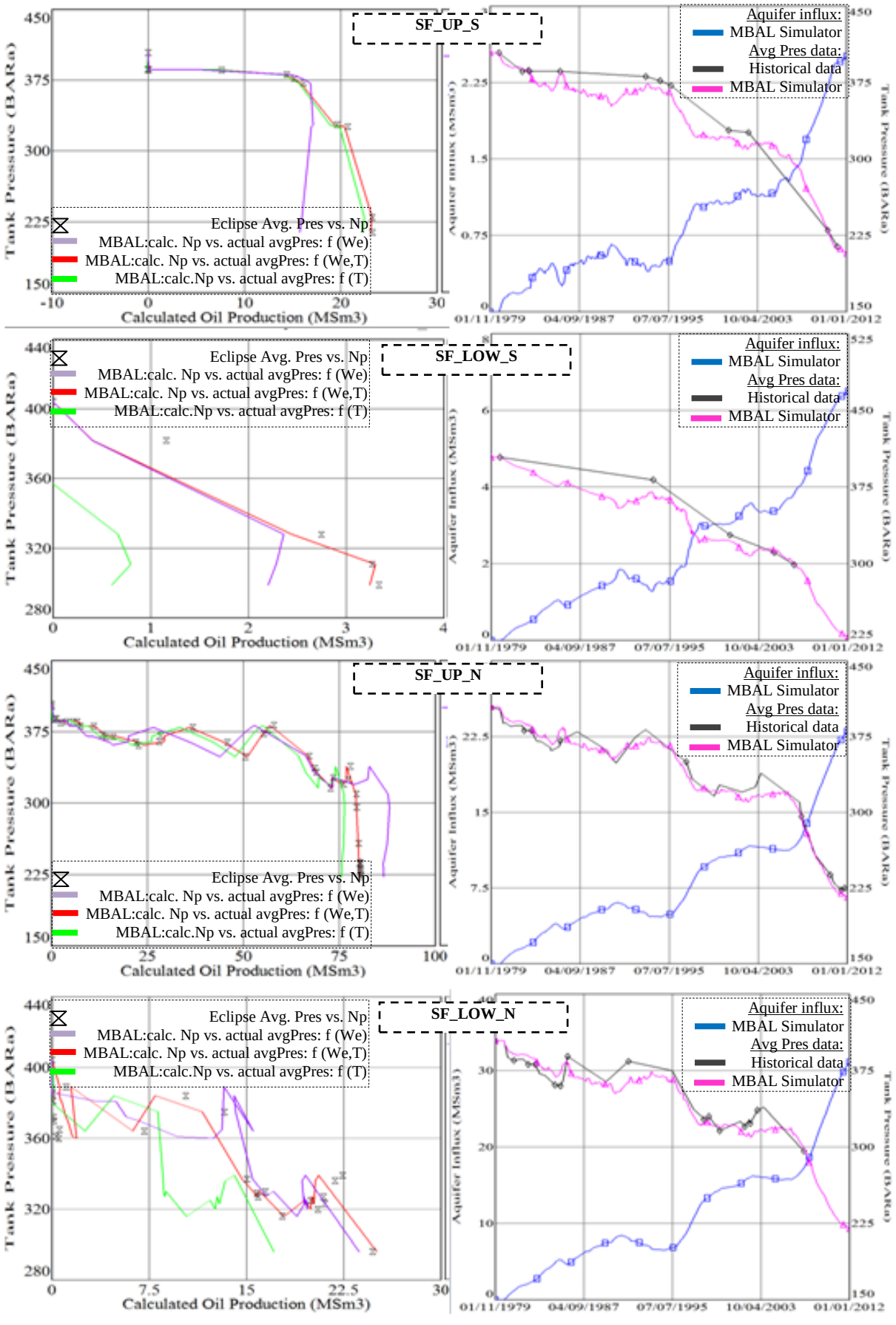

Figure 5.6 - History matched model: MBAL analytical and MBAL simulation plots.

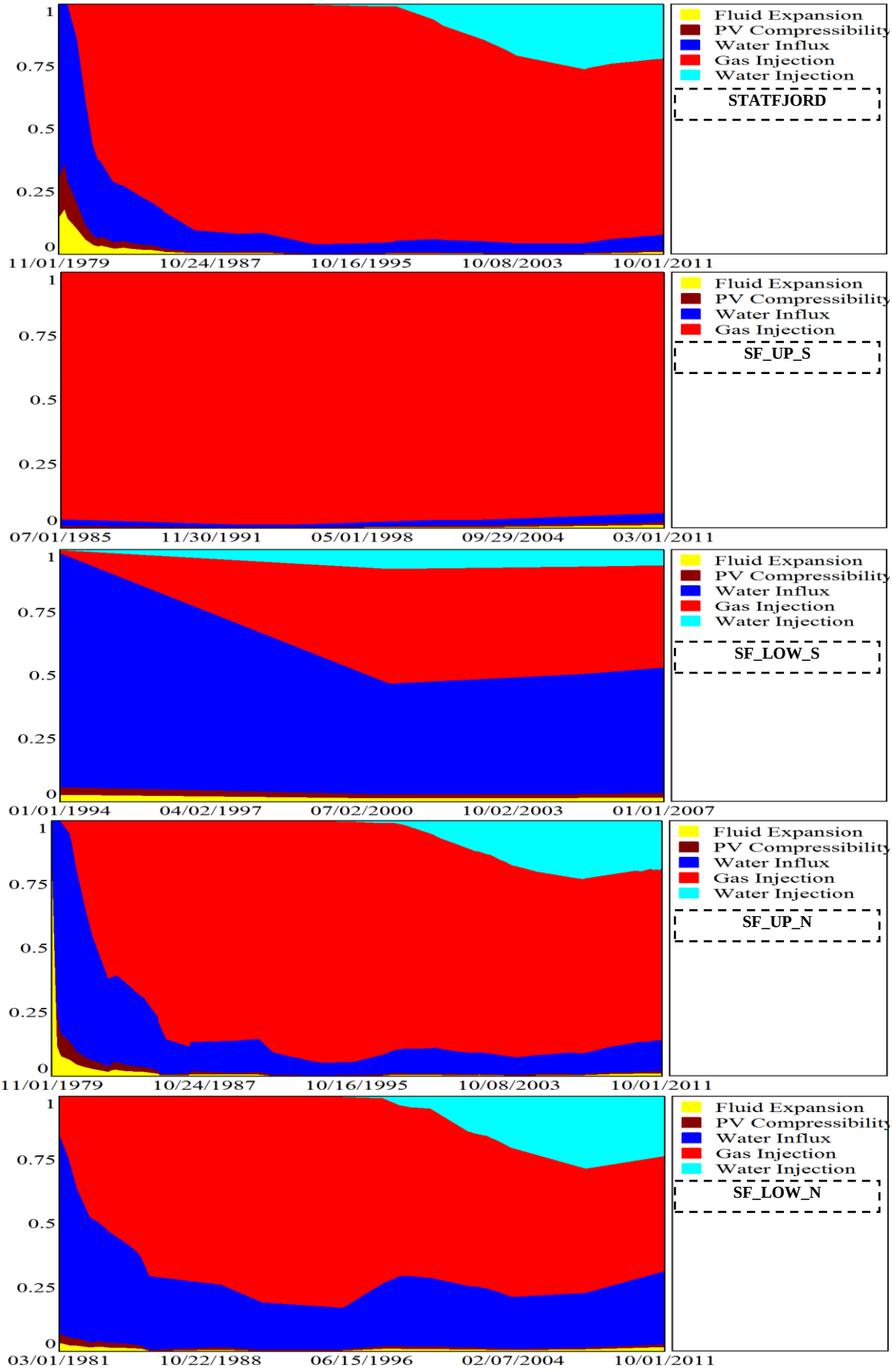

Figure 5.7 – Reservoir energy map – Drive mechanisms vs. time.

	SF_UP_S	SF_LOW_S	SF_UP_N	SF_LOW_N
PORV (MRm^3)	485.3	1182.2	925	1836
Aquifer volume (MSm^3)	133.5	387	1359	1886
Production start date	11/1982	6/1990	11/1979	10/1981
Cumulative volume of produced oil/PORV (MSm^3/MRm^3)	0.05	0.003	0.09	0.01
Cumulative volume of produced gas/PORV (MSm^3/MRm^3)	31.9	1.2	57.7	8.5
Cumulative volume of produced water/PORV (MSm^3/MRm^3)	0.02	0.002	0.02	0.005
Time duration of gas injection	12/1982-6/2007	10/1993-4/2002	6/1980-10/2007	11/1980-5/2004
Cumulative volume of injected gas/PORV (MSm^3/MRm^3)	28.3	0.71	59.1	5.8
Water injection duration	-	9/1994-6/1997	1/1996-2/2009	5/1991-7/2008
Cumulative volume of injected water/PORV (MSm^3/MRm^3)	-	0.00041	0.8151	0.01387

Table 5.4 – The main highlights from the field history (Prosty, 2010).

MBAL tool offers to assess the drive mechanisms of the formation. Overall, Fig. 5.7 reflects the historical drive mechanism. The comparison is made between two data such as MBAL calculated and field data. According to Fig. 5.7, the most striking feature is no water injection applied in SF_UP_S tank, in fact, as field history reveals water was never injected into that area and a second enormous quantity of gas was injected (Table 5.4) which can be confirmed from the MBAL energy map as well. Similar to injection behavior, the second large amount of gas was produced from this tank. Significant water and gas volumes were injected into and produced from SF_UP_N, which also can be observed from Table 5.4. The least amount of gas was injected into the tank SF_LOW_S, similarly, the same pattern can be established from the field data. Moreover, the productivity of SF_LOW_S tank was the lowest among four tanks. Water influx is more noticeable in the lower parts, especially, in SF_LOW_S is more dominant. Taken as a whole all the tanks reflects the actual field data which sustains (validates) the model representativeness.

Overall, the history matching (Fig. 5.6) can be considered good enough for doing the sensitivity analysis and to run prediction despite a point-to-point match was not established. More concentration was given on the latest data because it is a starting point for forecast.

5.2 Sensitivity Analysis

As outlined in chapter 4 the single tank was built in order to estimate aquifer parameters such as aquifer volume and permeability. According to the single-tank result, the multi-tank model was built to capture the Statfjord formation geology. Sensitivity analysis on aquifer parameter was not captured since it has a certain impact on the model.

Overall, six different scenarios is run to see the impact of each parameter, pressure behavior of each scenario is compared with base case model and at the end the most sensible parameter will be determined and described starting from the most affected parameter, the observation are given in the Table 5.5.

In fact, the model is affected by transmissibility parameter. The model was run without transmissibility as a separate tank with given aquifer parameters in order to see the strength of each tank. As a result, two tanks SF_UP_N and SF_LOW_N have large potential energy. Large two transmissibilities (Fig. 5.5) that were linked with these tanks were reduced 4 times, consequently, as it was expected two low potential tanks (SF_UP_S and SF_LOW_S) were underestimated whereas SF_LOW_N tank's result was overestimated. Low strength tanks' transmissibilities (Fig. 5.5) does not affect to the computation's result. Another interesting fact, that if the all transmissibility constants are changed to the same magnitude, the results will not be affected.

The next concern is related to interdependency of two parameters, namely, aquifer influx (W_e) and transmissibility constant (T) parameters. From the equation of 'Hurst-van Everdingen modified' model pressure change is proportional to aquifer influx volume (Table 4.2) while from eq. 4.1 two variables as delta P and transmissibility constant are inversely proportional. However, two variables cannot be correlated because it depends on the tank strength. Therefore, we cannot correlate the transmissibility constant with the aquifer influx. It is undoubtedly true that two variables have an influence (link) to each other.

The following parameter to consider is aquifer permeability. Generally speaking, it has no impact on the model when the permeability was raised, but when it is halved, the calculated trend was lower than actual trend, except SF_LOW_S tank. For detailed review on this topic, see Table 5.5.

Scenarios	**SF_UP_S**	**SF_LOW_S**	**SF_UP_N**	**SF_LOW_N**
TRANSMISSIBILITY*2	- No change - Cum. aquifer influx trend identical	- No change - Cum. aquifer influx trend identical	- No change - Cum. aquifer influx trend identical	- No change - Cum. aquifer influx trend identical
TRANSMISSIBILITY/2	- No change - Cum. aquifer influx trend identical	- No change - Cum. aquifer influx trend identical	- No change - Cum. aquifer influx trend identical	- No change - Cum. aquifer influx trend identical
LARGE TRANS: SFUPN^SFLOWN/4 SFUPN^SFUPS/4	- Underestimation (2004-2012) - Cum. aquifer influx trend identical	- Underestimation (2004-2012) - Cum. aquifer influx trend identical	- No change - Cum. aquifer influx trend identical	- Overestimation (2004-2012) - Cum. aquifer influx trend identical
SMALL TRANS: SFUPS^SFLOWS*4 SFLOWS^SFLOWN*4	- No change - Cum. aquifer influx trend identical	- No change - Cum. aquifer influx trend identical	- No change - Cum. aquifer influx trend identical	- No change - Cum. aquifer influx trend identical
PERMEABILITY OF AQUIFER*2	- No change - Cum. aquifer influx trend identical	- No change - Cum. aquifer influx trend identical	- No change - Cum. aquifer influx trend identical	- No change - Cum. aquifer influx trend identical
PERMEABILITY OF AQUIFER/2	Underestimation (2007-2012) - Cum. aquifer influx decreased slightly	- No change - Cum. aquifer influx trend identical	Underestimation (2005-2012) - Cum. aquifer influx decreased slightly	Underestimation (2007-2012) - Cum. aquifer influx decreased slightly

Table 5.5 - Observations from sensitivity analysis.

5.3 Model Calibration: History and Prediction

In the prediction set up section two options are available in the MBAL tool:

- Profile from production schedule (no wells);
- Production profile using well models.

In the first mode the targets are set by the user, i.e. production profile has to be established whereas for the second the prediction is based on individual well performance which is introduced into the system.

In our model the wells have not been introduced and target rates with respect of each region are retrieved from the simulation model.

The methodology of sensitivity analysis is to implement two scenarios on the prediction profiles:

- Rate cut-off: the target rates from the simulation model;
- Date cut-off: keeping in mind the last future cumulative values and accelerate the production activity.

At the end, the cumulative gas production until an abandonment reservoir pressure will be examined and compared with ECLIPSE simulation prediction data.

5.3.1 Relative Permeability Data

Prior to run the prediction the relative permeability data needs to be examined since fluid behavior is governed by relative permeability curve. It can be done by matching f_w and f_g , so that a set of Corey function parameters should be able to recreate the fractional flows observed in the history. A set sequence of computation is shown in Fig. 5.8.

It was recommended (MBAL User manual, 2011) that the late WC data needs to be excluded since it does not represent the original fractional flow. The reason behind is that the late data usually is affected by water breakthroughs and other EOR methods. However, the data points from the history were too scattered in order to be regressed. As a result, the relative permeability data, normalized at reservoir scale in the ECLIPSE simulation model, is used. Plots of the fractional flow versus saturation for each tank are given in Fig. A.2.6.Three features are plotted in the graph:

- Water breakthrough- green line;
- Data points, where the calculation is linked to the history production and PVT data;
- Theoretical curve, where the calculation is based on the PVT and relative permeability input data, blue solid line.

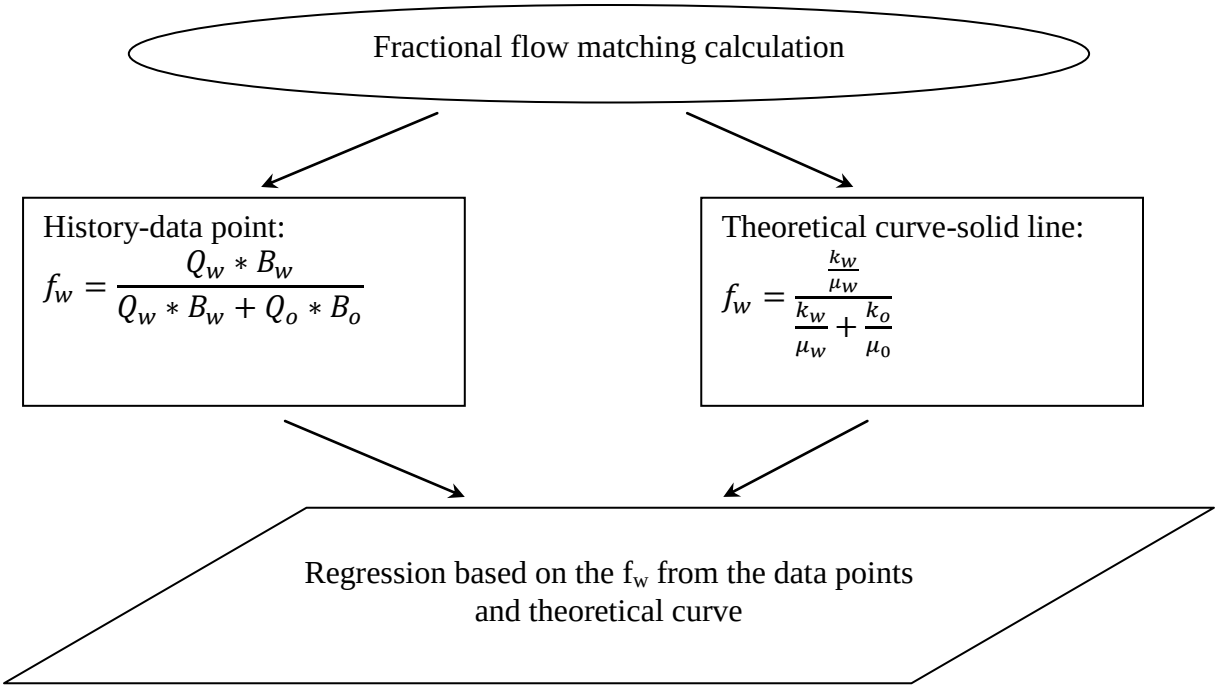

Figure 5.8 - Water fractional flow matching procedure (MBAL user manual, 2011).

Similarly, Bui et al. (2006) advocates that the relative permeability data needs to be conditioned to the field production data. Two graphs, such as the relative permeability from core data and conditioned to the production history, revealed substantial different trend. Therefore, the applicability of this method is questionable.

5.3.2 Prediction Results

The prognosis is run until December 2030. As it was mentioned the rates are retrieved from the ECLIPSE simulation model to see the response from the reservoir pressure. Moreover, the similarities and differences of simulation and material balance prognosis will be examined thereafter.

MBAL data will be considered up to abandonment pressure, at which an amount of production is insufficient economically to continue the operation.

Fig. 5.9 displays the historical and future pressure behavior for four tanks.

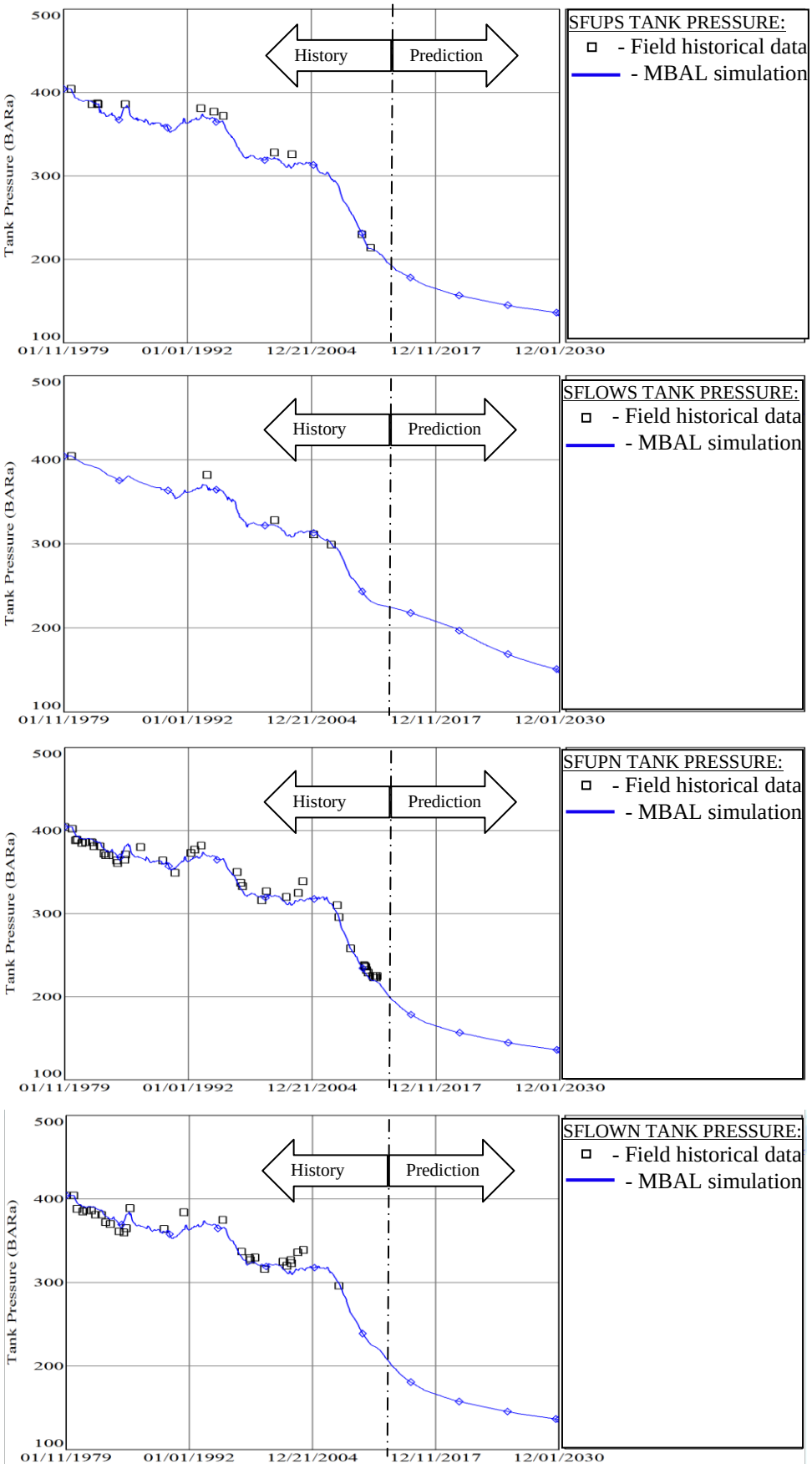

Figure 5.9 - Historical and future reservoir pressure profiles.

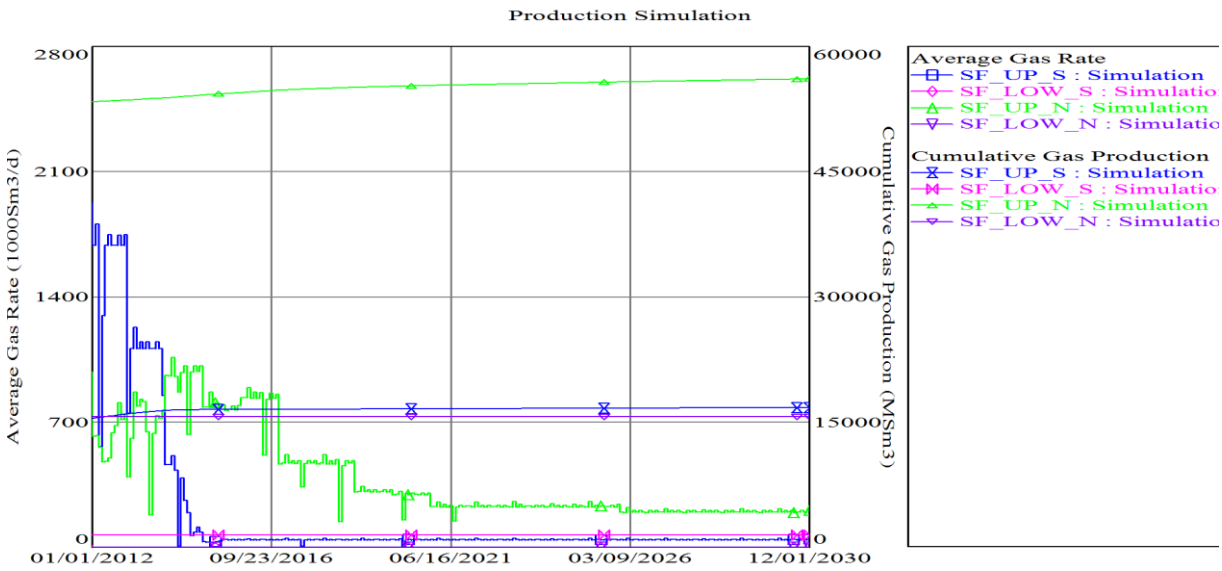

Figure 5.10 - Rate cut-off: gas prognosis.

The raised question was whether or not the MBAL determine the formation future behavior, particularly for the gas production, with regard to material balance concept. Thus, further analysis is addressed only to the gas phase.

Future prognosis is done only for the upper part of the formation due to low inflow performance of the lower formation.

	SF_UP_S	SF_LOW_S	SF_UP_N	SF_LOW_N
Abandonment Pressure(Bar)	152.4	161	145.2	165.8

Table 5.6 – Abandonment reservoir pressure (ECLIPSE simulator, 2012).

Parameters	Model	SF_UP_S	SF_LOW_S	SF_UP_N	SF_LOW_N
Abandonment date	ECLIPSE_2030	1/12/2030	1/2/2012	1/12/2030	1/2/2012
	MBAL_2030	1/12/2021	1/2/2012	1/4/2025	1/2/2012
	MBAL_2020	1/11/2015	1/2/2012	1/3/2017	1/2/2012
Cumulative oil (MSm^3)	ECLIPSE_2030	23.72	3.67	81.29	25.56
	MBAL_2030	23.64	3.67	81.26	25.56
	MBAL_2020	23.57	3.67	81.22	25.56
Cumulative gas (MSm^3)	ECLIPSE_2030	16770	1475.28	56141	15644.8
	MBAL_2030	16627.8	1475.28	55716.8	15644.8
	MBAL_2020	16689	1475.28	55617.4	15644.8

Table 5.7 – Comparison of cumulative gas production for the ECLIPSE and MBAL.

Table 5.7 compares the data on gas cumulative production and reveals that the MBAL total future gas production is reduced compared to ECLIPSE simulator because the average reservoir behavior was different for the MBAL model and cumulative volume is taken until abandonment pressure value. According to ECLIPSE simulator, forecast of the remaining produced gas amount is 4 GSm^3, while MBAL calculates as 3.4 GSm^3, so the total amount of future gas production is reduced to 0.6 GSm^3. The details on the average pressure depletion are discussed in subchapter 5.4.

MBAL tool predicted that the gas phase is in the south of fault F11 similar to ECLIPSE simulator. The overview of initial and forecasted saturation data (Table 5.7, MBAL_2030) is illustrated in Fig. 5.11. As it was mentioned previously, there was no gas cap, and then it was created due to gas injection. The most of the oil phase has been extracted for all tanks. The saturation distribution looked alike for the MBAL_2020 model where the production performance accelerated. The most watered out regions are the lower part of Statfjord Fm. and north part of F11.

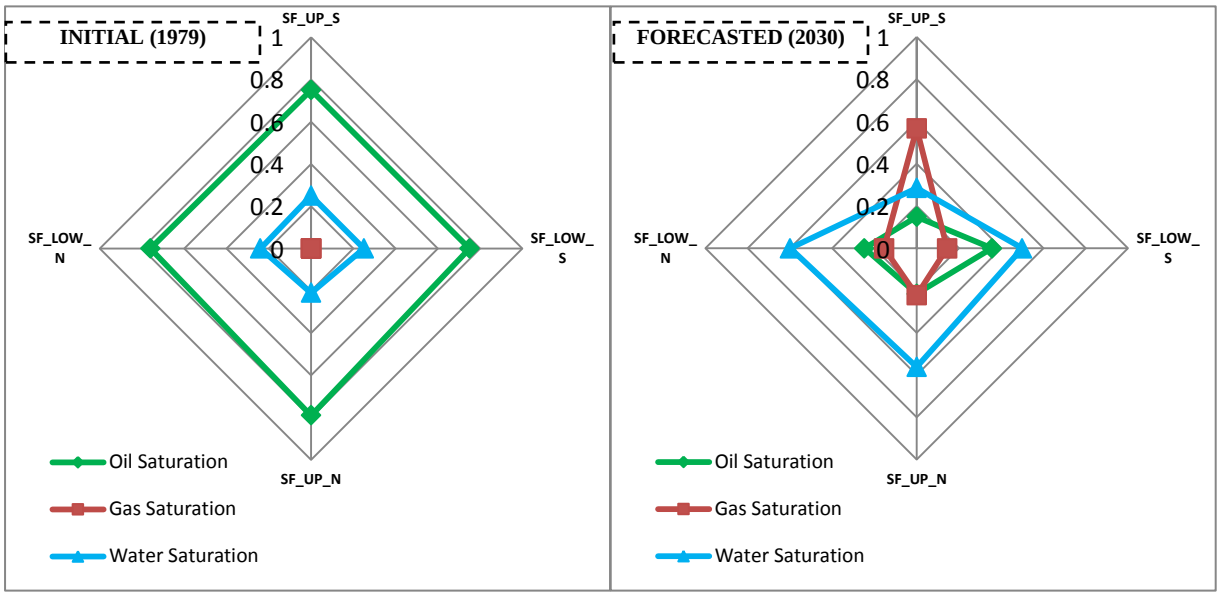

Figure 5.11 – Saturation distribution for MBAL_2030.

The conclusion can be underlined from the production prediction result in MBAL tool that the total gas production is reduced to 0.6 GSm^3as shown in Table 5.7.

5.4 Material Balance vs. Simulation Average Pressure

This subsection compares the average reservoir pressure versus time profile computed from ECLIPSE and MBAL models against the measured pressure at datum depth (2701 m) calculated from DHPG surveys during the turn-around (T/A). The turn-around pressure points

(T/A) reflect the average reservoir pressure because the wells are closed for longer period. The average pressure calculations for both models (MBAL_2030 and MBAL_2020) were based on the target fluid rates retrieved from ECLIPSE simulation model as mentioned in subsection 5.3.

Fig. 5.12 reveals the predicted pressure behavior, but SF_UP_N and SF_LOW_N tanks have been included also the history to show the representativeness of the models against datum pressure during turn-around.

The MBAL results reflect the theory underlined this model, such as, for example. any pressure change is instantaneous and uniform throughout the tank. This implies that the MBAL reservoir pressure depletion associated with fluid production dropped slightly faster compared to ECLIPSE one. Fig. 5.12 compares the future pressure depletion from ECLIPSE and MBAL. The most noticeable features are:

1. The prognosis (MBAL and ECLIPSE simulator results) for SF_UP_S tank matched perfectly until 01/2014 and then the discrepancy has started between the data. It is interesting that pressure trend almost levels off between 2013 and 2015 in ECLIPSE simulator data;
2. Comparably, slightly large change has happened in results with SF_LOW_N tank while for both SF_UP_N and SF_LOW_S MBAL pressure prognosis looked alike to ECLIPSE simulator.

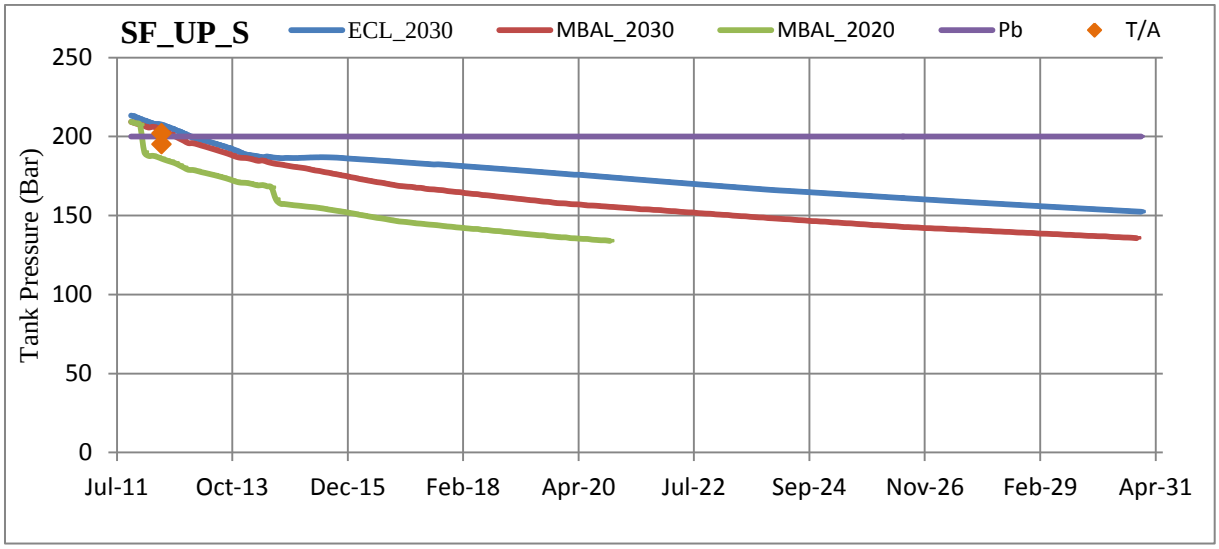

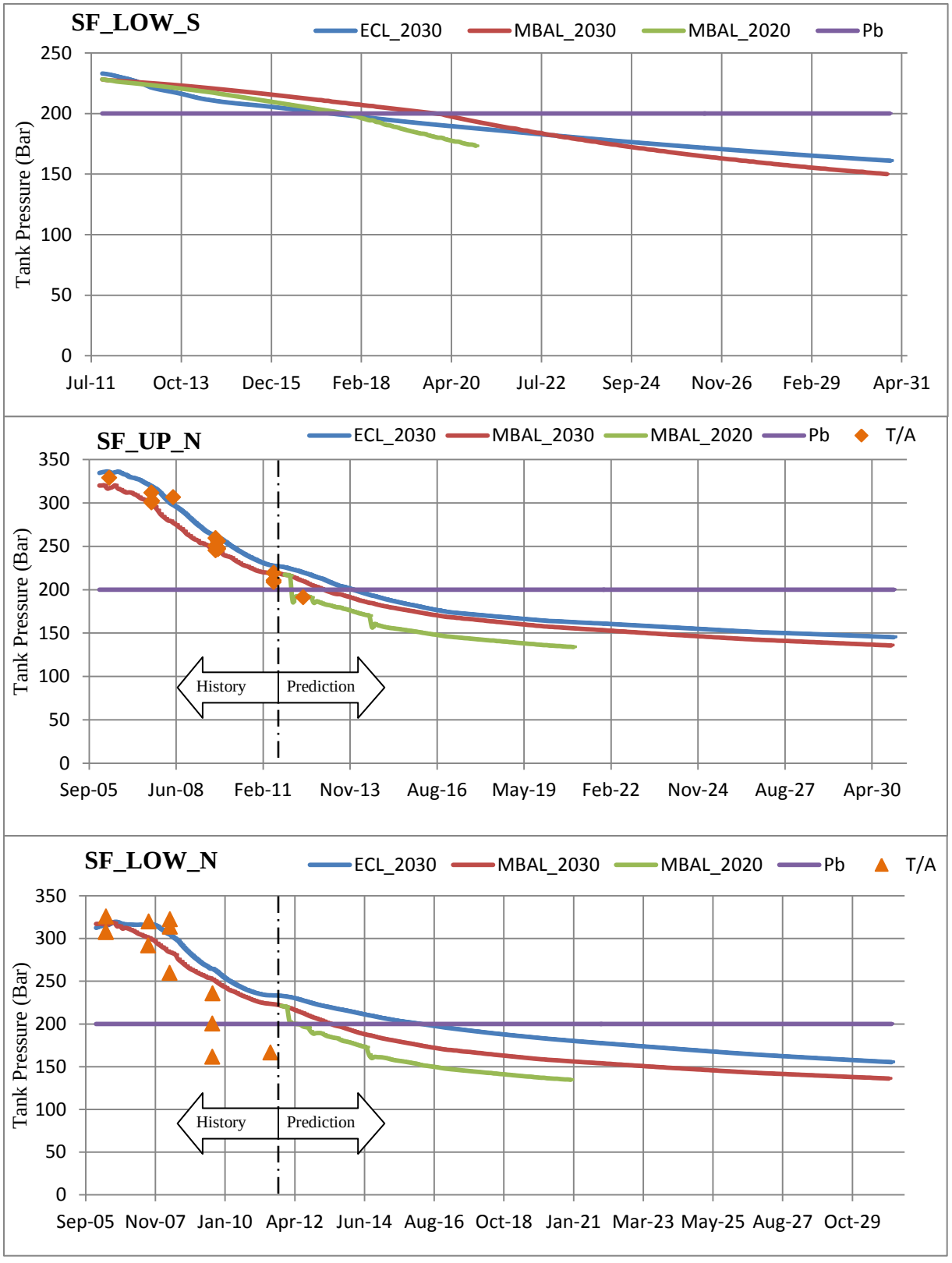

Figure 5.12 – Reservoir pressure prognosis.

It has been always a challenge to get a representative average reservoir pressure depletion behavior for the lower Statfjord as it is shown in Fig. 5.12.The measured average pressure

data in the lower part of the formation is erratic due to the complex geology, so that the well location affects it substantially. The last turn-around was done June 2011 for the lower part, unfortunately there was not any DHPG for the southern lower part. For the upper part the recent (June 2012) measurements included, however the measured pressure has to be updated at the end of turn-around because the pressure has not stabilized yet, there is still a slight increase for the SF_UP_N. Overall, MBAL pressure trend seems to be in agreement with measured pressure point, except SF_LOW_N.

Since there is no future prognosis for the lower part the priority is given to the upper part. As Fig. 5.12 reveals the upper part prediction is within acceptable range. However, the attempt is done to explain what can cause the disagreement between ECLIPSE and MBAL in SF_LOW_N tank.

The first remarkable aspect that the starting point of prediction procedure is different, despite the input pressure points were used the same for both ECLIPSE and MBAL tools, in other word the average reservoir pressures for the MBAL are not from ECLIPSE model. Consequently, in MBAL the rate of pressure depletion is faster. Besides ECLIPSE model is not fully matched for the lower part, therefore it is questionable whether the result reliable or not.

It is worthwhile noting that the gas liberation has occurred approximately at the same period of time in 2013 for the three tanks, except SF_LOW_S tank because of bad connection. Whereas in ECLIPSE the upper part of Statfjord formation gas starts to liberate approximately in 2013 the same as for the MBAL, but for lower part of Statfjord is 2018.

CONCLUSIONS

Multi- and single-tank MBAL models were constructed for the Statfjord formation, based on the same reservoir input parameters data used in the ECLIPSE full-field simulation model. The only exception is the production/injection rates which were extracted from the Prosty production data-base and the average reservoir pressures obtained from RFT measurements.

The quality assurance of STOIIP and aquifer influx is analyzed and concluded that there is no significant variation in the results between the ECLIPSE and MBAL models.

As the future gas production performance is the main target of the work, the history matching procedure is crucial. Therefore, the workflow for the history matching procedure was established to minimize the errors and pitfalls. It is important to note that geological variations in the Statfjord formation were considered when choosing the values for the uncertain parameters used in the history matching and non-linear regression method was applied after each realization. The main advantage of using the MBAL model instead of the ECLIPSE model was that historical gas production volume from the former does not have discrepancy between simulated and observed volumes while the later has a difference of ca. 0.4 GSm^3 (Fig. A.1.1).

The single-tank MBAL model cannot project reservoir behavior as accurate as the multi-tank model; however, it is able to provide rough estimates of the aquifer size.

The sensitivity analysis suggests that the MBAL model results are not influenced by increasing all transmissibility constants to the same magnitude at once. Generally speaking, the transmissibility affects the pressure response of each tank in the model. The aquifer permeability parameter is the least sensitive parameter; the reason is that the aquifer size connected to the Statfjord formation is around 13.1 times larger than the HCPV of the Statfjord formation reservoir.

The material balance model is effective at history matching the production performance but has substantial drawbacks when it comes to field predictions. As an illustration, in relative permeability matching procedure, conditioning the relative permeability curves only to production data is not the best approach. This is because production data might be influenced by the applied EOR methods and other factors such as field geology, reservoir heterogeneities, well completion, etc.

The prediction results from the MBAL model show that the future cumulative gas production is reduced compared to ECLIPSE and the potential of remaining gas is assessed to be in the south part of the upper Statfjord, which is similar to the ECLIPSE predictions. The

pressure depletion behavior is more or less similar without marginal differences except for the SF_LOW_N tank.

One of the limitations of the MBAL tool is that it cannot be used for the estimation of trapped gas. The reason is that the MBAL tool is not able to deal with the task, in other words, it is out of the MBAL's scope, and the work (issue) was analyzed from ECLIPSE simulator's results. Another limitation concerns the allocation data because it might be one of the reasons of ECLIPSE simulator mismatch.

Taken together the MBAL tool would seem to bring insights into reservoir characterization and practical in running different scenarios in spite of its simplicity it is able to predict similar pressure depletion trends as the ECLIPSE simulator. Moreover, it will allow us to spend less time on each realization, for example, we might run the MBAL model with different PVT data, to see the changes in the model.

Recommendations for Further Work

Further studies are required to account for the fluid misallocation on the reservoir future performance. As the claim concerned about the allocated rates being wrong due to wells that were perforated in several formations, for example, the wells were perforated in the Brent and Statfjord or the lower and upper part of the Statfjord formation. The reservoir allocation tool (part of IPM software) can be used to solve the issue.

As it is known from the history of production performance, the gas was injected as soon as the fluid production started. Due to miscibility process between two different phase contact the original fluid composition was changed. However, the ECLIPSE simulator uses the initial PVT data throughout the simulated field history and future performance. Therefore, further work is needed to be done to enhance the simulation quality.

The current study's result can be enhanced by generating integrated system model in GAP, i.e. MBAL can be initialized in GAP. So that, material balance production prediction computation can be performed by GAP where the model is already have been built with all the Statfjord wells.

REFERENCES

1. Aadland A., Dyrnes O., Olsen S.R., and Drønen O.M.,1994. Statfjord Field: Field and Reservoir Management Perspectives. SPE 25027 was presented at the European Petroleum Conference, Cannes, November 16-18.
2. Amudo C., Walters M.S., O'Reilly D.I., Clough M.D., Beinke J.P., and Sawiris R:S:T., 2011. Best Practices and Lessons Learned in the Contraction and Maintenance of a Complex Gas Asset Integrated Production Model. SPE 146968 was presented at the SPE Asia and pacific Oil and Gas Conference and Exhibition. Indonesia, Jakarta, September 20-22.
3. Baker R.O., Chugh S., Mcburney C., and Mckishnie, 2006. History Matching Standards; Quality Control and Risk Analysis for Simulation. The paper was presented at the Petroleum Society's 7th Canadian International Petroleum Conference. Canada, Alberta, Calgary, June 13-15.
4. Boge R., Lien A., Gjesdal A.,and Hansen A.G., 2005. Turning a North Sea Oil Giant Into a Gas Field – Depressurization of the Statfjord Field. SPE 96403 was presented at Offshore Europe. U.K., Scotland, Aberdeen, September 6-9.
5. Bui T., Bandal M., Hutamin N., and Gajraj A., 2006. Material Balance analysis in Complex Mature reservoirs – Experience in Samarang Field, Malaysia. SPE 101138waspresented at SPE Asia Pacific Oil & Gas Conference and Exhibition. Australia, Adelaide, September 11-13.
6. Dake L.P., 2001. The practice of reservoir engineering. Revised ed. Netherlands: ElsevierScience B.V.
7. DeSorcy G.J., 1979. Estimation methods for proved recoverable reserves of oil and gas. Canada, Alberta.
8. Esor E., Stefano D., and Carlo M., 2004. Use of Material Balance to Enhance 3D Reservoir Simulation: A Case Study. SPE 90362 was presented at the SPE annual Technical Conference and Exhibition. U.S.A., Texas Huston, September 26-29.
9. Galas C., 1994. Confidence Limits of Reservoir Parameters by Material Balance. SPE 94-035 was presented at the 45th annual technical meeting of the Petroleum Society of CIM, Canada, Calgary, June 12-15.
10. Garcia C. A., and Villa J. R., 2007. Pressure and PVT Uncertainty in Material balance Calculations. SPE 107907 was presented at the 2007 Latin American and Caribbean Petroleum Engineering Conference. Argentina, Buenos Aires, April 15-18.

11. Hegre E., Dalen V., and Strandenaes H.O., 1994. IOR Potential With Updip Water Injection in the Statfjord Fm. at the Statfjord Field. SPE 28841 was presented at the European Petroleum Conference. U.K., London, October 25-27.
12. John R. F., 2001. Principles of applied reservoir simulation. 2nd ed. U.S.A.: Butterworth-Heinemann.
13. Marquardt D. W., 1963. An Algorithm for Least-Squares Estimation of Nonlinear Parameters. J. Soc. Ind. Appl. Math., June.
14. Marques J. B., Trevisan O. V., and Suslick S. B., 2007. Classic Models of Calculation of Influx: A Comparative Study. SPE 107265 was presented at the 2007 Latin American and Caribbean Petroleum Engineering Conference. Argentina, Buenos Aires, April 15-18.
15. Mazloom J., Tosdevin M., Frizzell D., Foley B., and Sibley M., 2007. Capturing Complex Dynamic Behavior in a Material Balance Model. IPTC 11489 was presented at the International Petroleum Technology Conference. U.A.E., Dubai, December 4-6.
16. MBAL User Manual, ver. 10.5, Petroleum Experts 2011.
17. Miranda A., and Raghavan R., 1975. Optimization of The Material Balance Equations. Montreal, October-December.
18. Onyeizu C., Collins J., and Eric T., 2010. Using an Automated Approach To Reservoir History Matching and Property Selection in Material Balance Modeling. SPE 136976 was presented at the 34th Annual SPE International Conference and Exhibition. Nigeria, Calabar, 31 July-7 August.
19. Schilthuis R.J., 1936. Active Oil and Reservoir Energy.Trans. AIME.
20. StatoilHydro, 2001/02. Upper Statfjord reservoir drainage strategy review. Stavanger: StatoilHydro.
21. StatoilHydro, 2005. Statfjord reservoir development plan. Stavanger: StatoilHydro.
22. StatoilHydro,2005. The Statfjord field FFM2005 study. Draft version.Stavanger: StatoilHydro.
23. StatoilHydro, 2007. Reservoir Engineering Dynamic Model and Forecast.Stavanger: StatoilHydro.
24. StatoilHydro, 2007. Statfjord reservoir development plan. Stavanger: StatoilHydro.
25. StatoilHydro,2011. Statfjord Fm: Trapped gas. Stavanger: StatoilHydro.
26. StatoilHydro, 2011. Statfjord reservoir development plan. Stavanger: StatoilHydro.
27. StatoilHydro, 2011. Well comments. Draft version.Stavanger: StatoilHydro.
28. Tavassoli Z., Carter J., and King P., 2004. Errors in History Matching. U.K., London.

29. Tehrani D. H., 1985. An Analysis of Volumetric Balance Equation for Calculation of Oil in Place and Water Influx. U. K., Scotland.
30. Torony M., and Saleri G., 1988. Engineering Control in Reservoir Simulation. SPE 17937 was presented at the Society of Petroleum Engineering Fall Conference, October 2-5.
31. Vera L. B., Ariffin T., Trabelsi A., and Al-Ansi H., 2008. Assessing Fluid Migration and Quantifying Remaining Oil Saturation in a Mature Carbonate Reservoir: Durkhan Arab D. IPTC 13503 was presented at the International Petroleum Technology Conference, Doha, Qatar, December 7-9.

NOMENCLATURE

χ^2: Chi Square

ΔP: Pressure difference between two tanks [bar]

μ_i: Viscosity of phase i [cp]

B_g: Gas formation Volume Factor [m^3/Sm^3]

B_o: Oil formation Volume Factor [m^3/Sm^3]

B_w: Water formation Volume Factor [m^3/Sm^3]

ca: Circa

c_f: Pore Compressibility [1/bar]

c_w: Water Compressibility [1/bar]

DHPG: Downhole Pressure Gauge

EOR: Enhanced Oil Recovery

F&F: Fuel and Flare

FFM2005: Full Field Model 2005

$f_{g:}$ Gas Fractional Flow [-]

FVF: Formation Volume Factor [m^3/Sm^3]

f_w: Water Fractional Flow [-]

GIIP: Gas Initial In Place [MSm^3]

GOC: Gas Oil Contact [m]

GWC: Gas Water Contact [m]

HCPV: Hydrocarbon Pore Volume

IOR: Improved Oil Recovery

K: Land's Constant [-]

k_{aq}: Aquifer Permeability [mD]

k_{ri}: Relative Permeability [-]

m: Gas Cap Fraction.

MBAL: Material Balance

MT-MBAL: Multi-tank MBAL

N: Stock Tank Oil In Place [MSm^3]

N_p: Cumulative Oil Recovery [MSm^3]

OOIP: Original Oil In Place [MSm^3]

OWIP: Original Water In Place [MSm^3]

PETEX: Petroleum Expert

PVT: Pressure, volume, temperature

Q_T: Total Downhole flow rate [m^3/day]

R_d: Reservoir radius/aquifer outer radius [-]

RFT: Repeat Formation Tester

RMS: Reservoir Management Software

R_p: Cumulative Gas-Oil Ratio [Sm3/Sm3]

R_s: Solution Gas-Oil Ratio [Sm3/Sm3]

S_{cw}: Connate Water Saturation [-]

SF_LOW_N: North area of the lower Statfjord from F11 fault

SF_LOW_S: South area of the lower Statfjord from F11 fault

SF_UP_N: North area of the upper Statfjord from F11 fault

SF_UP_S: South area of the upper Statfjord from F11 fault

SFA: Statfjord A Platform

SFB: Statfjord B Platform

SFC: Statfjord C Platform

SFLL: Statfjord Late Life

S_{gi}: Initial Gas Saturation [-]

ST-MBAL: Single-tank MBAL

STOIIP: Stock Tank Oil Initially In Place [MSm^3]

STRDP: Statfjord Reservoir Development Plan

T/A: Turn-Around

T: Transmissibility Constant [cP*m^3/day/bar]

t_D: Dimensionless Time

V_a: Aquifer Volume [MSm^3]

WC: Water Cut [%]

W_e: Cumulative Water Influx [MSm^3]

W_p: Cumulative Water Produced [MSm^3]

σ: Standard error

APPENDIX

Appendix 1

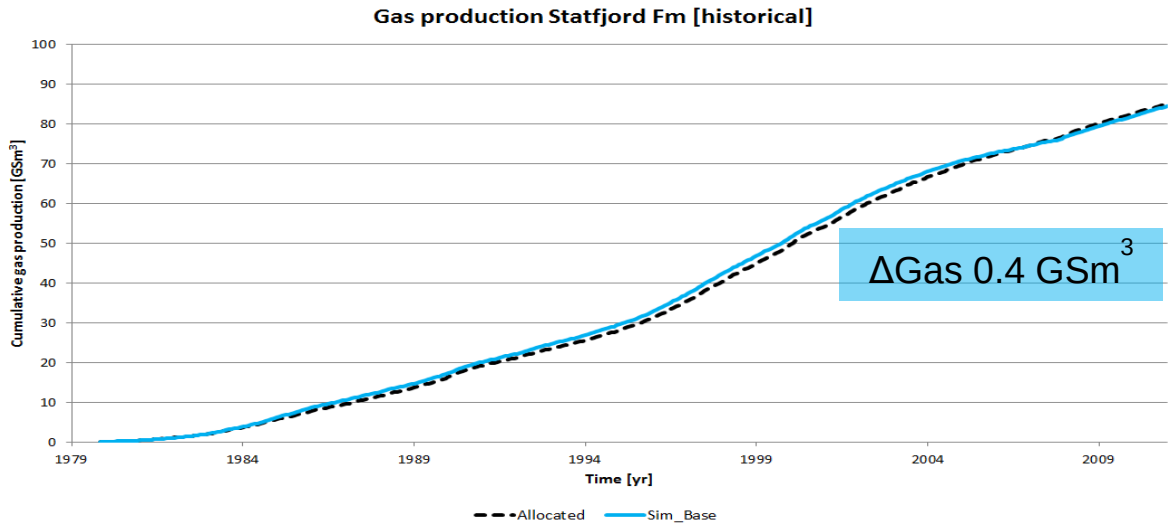

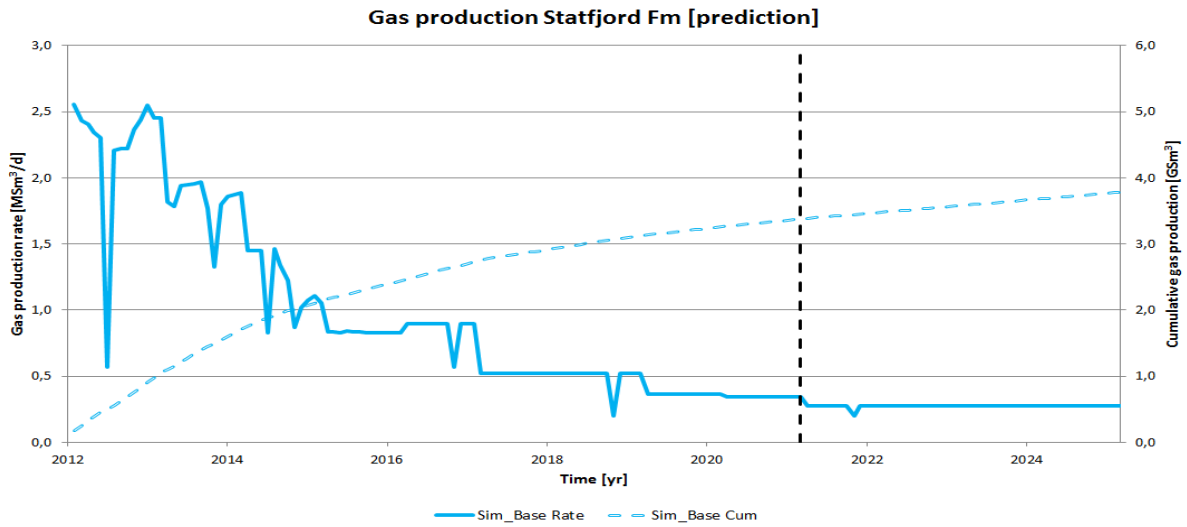

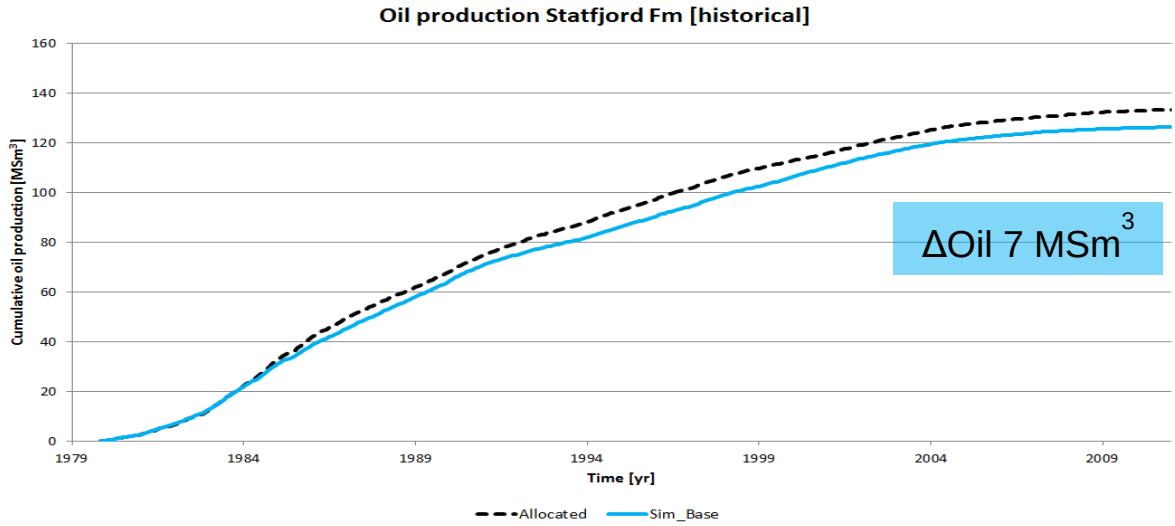

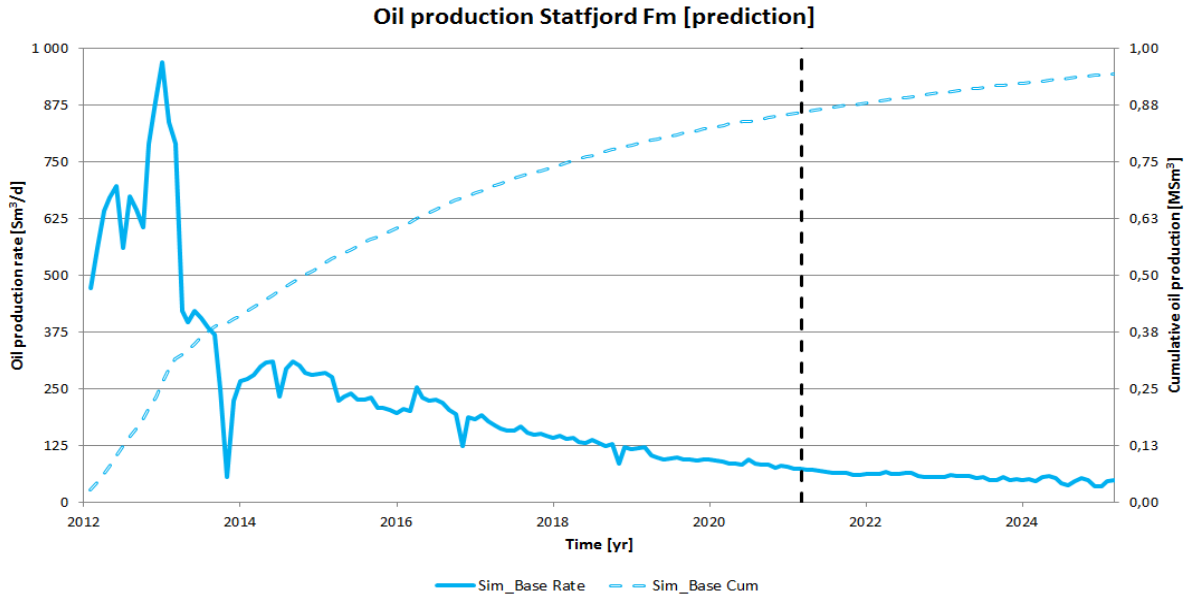
Oil production Statfjord Fm [prediction]
Oil production rate [Sm³/d]
Cumulative oil production [MSm³]
Time [yr]
Sim_Base Rate
Sim_Base Cum

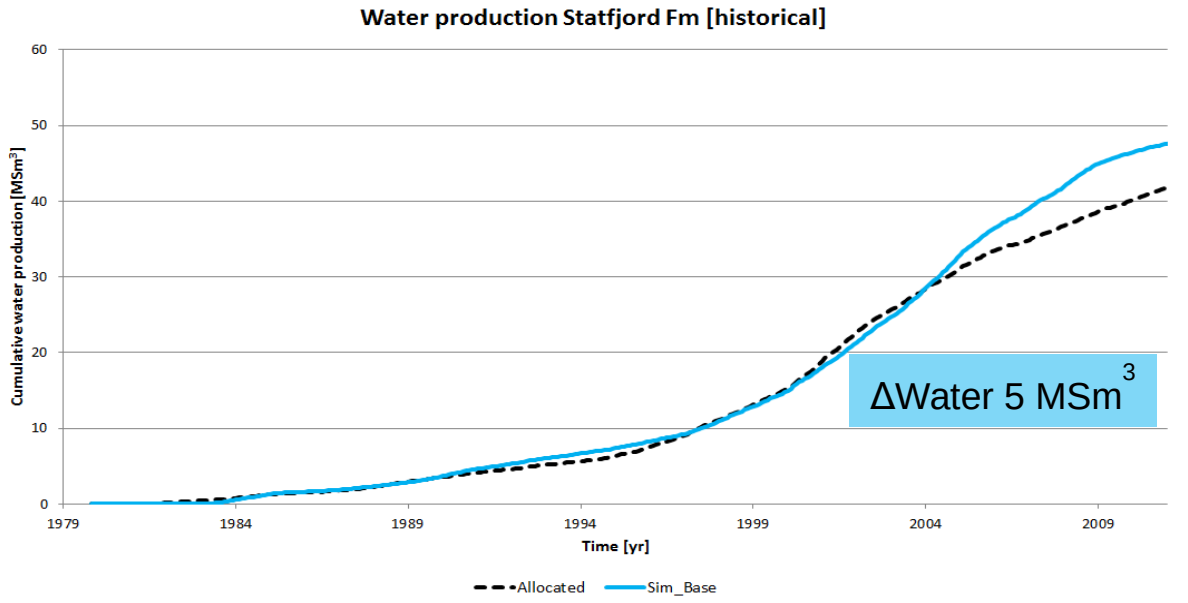
Water production Statfjord Fm [historical]
Cumulative water production [MSm³]
ΔWater 5 MSm³
Time [yr]
Allocated
Sim_Base

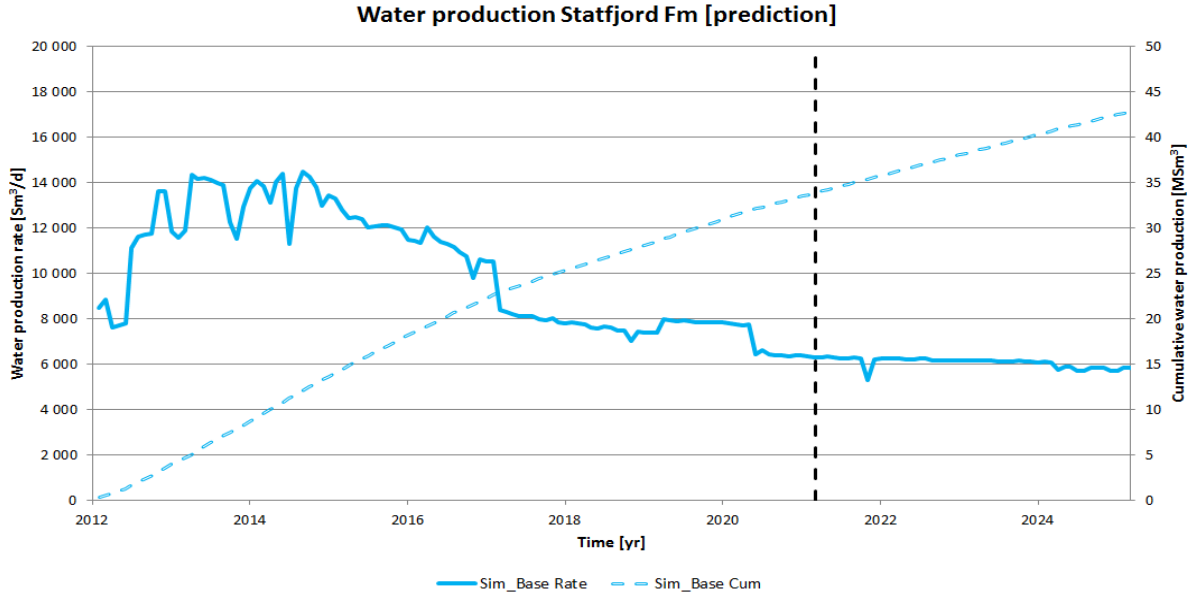
Water production Statfjord Fm [prediction]
Water production rate [Sm³/d]
Cumulative water production [MSm³]
Time [yr]
Sim_Base Rate
Sim_Base Cum

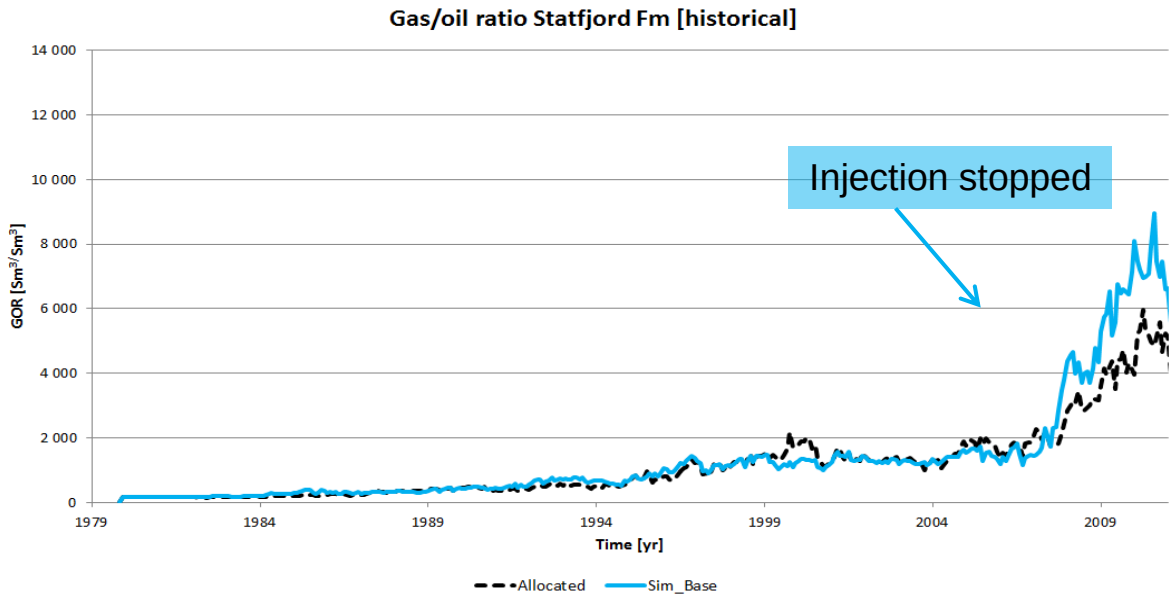
Gas/oil ratio Statfjord Fm [historical]
Injection stopped
GOR [Sm³/Sm³]
Time [yr]
Allocated
Sim_Base

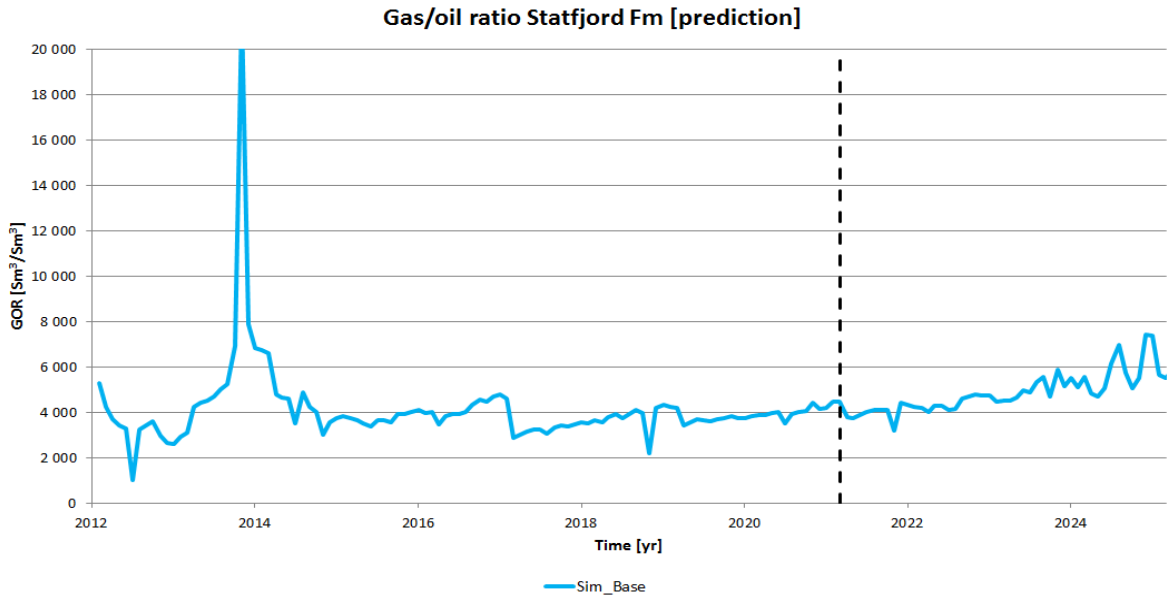
Gas/oil ratio Statfjord Fm [prediction]
GOR [Sm³/Sm³]
Time [yr]
Sim_Base

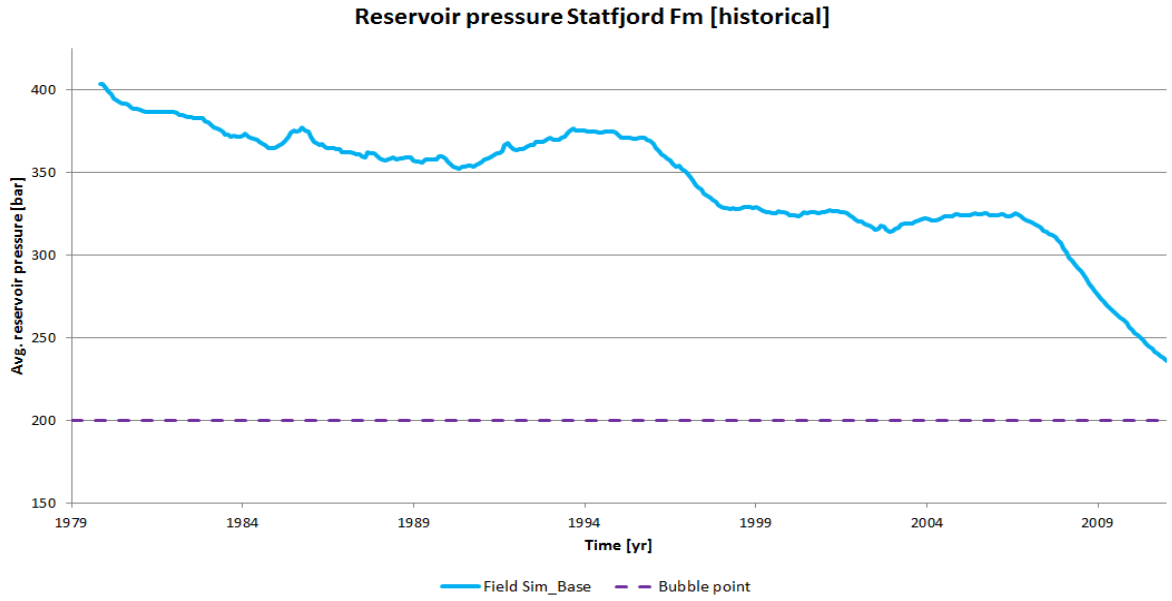
Reservoir pressure Statfjord Fm [historical]
Avg. reservoir pressure [bar]
Time [yr]
Field Sim_Base
Bubble point

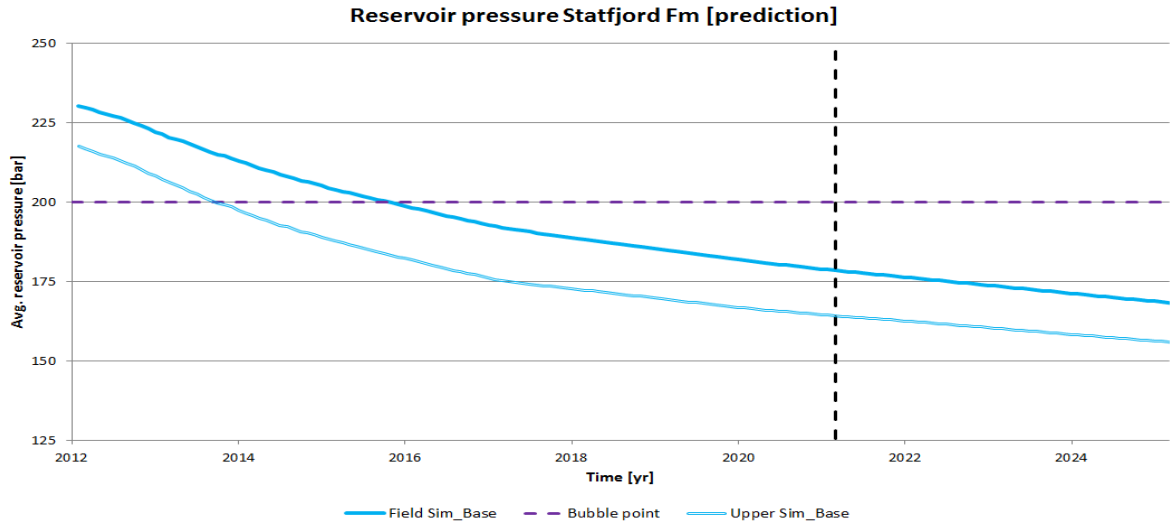

Figure A.1.1 – ECLIPSE historical and prediction simulator data.

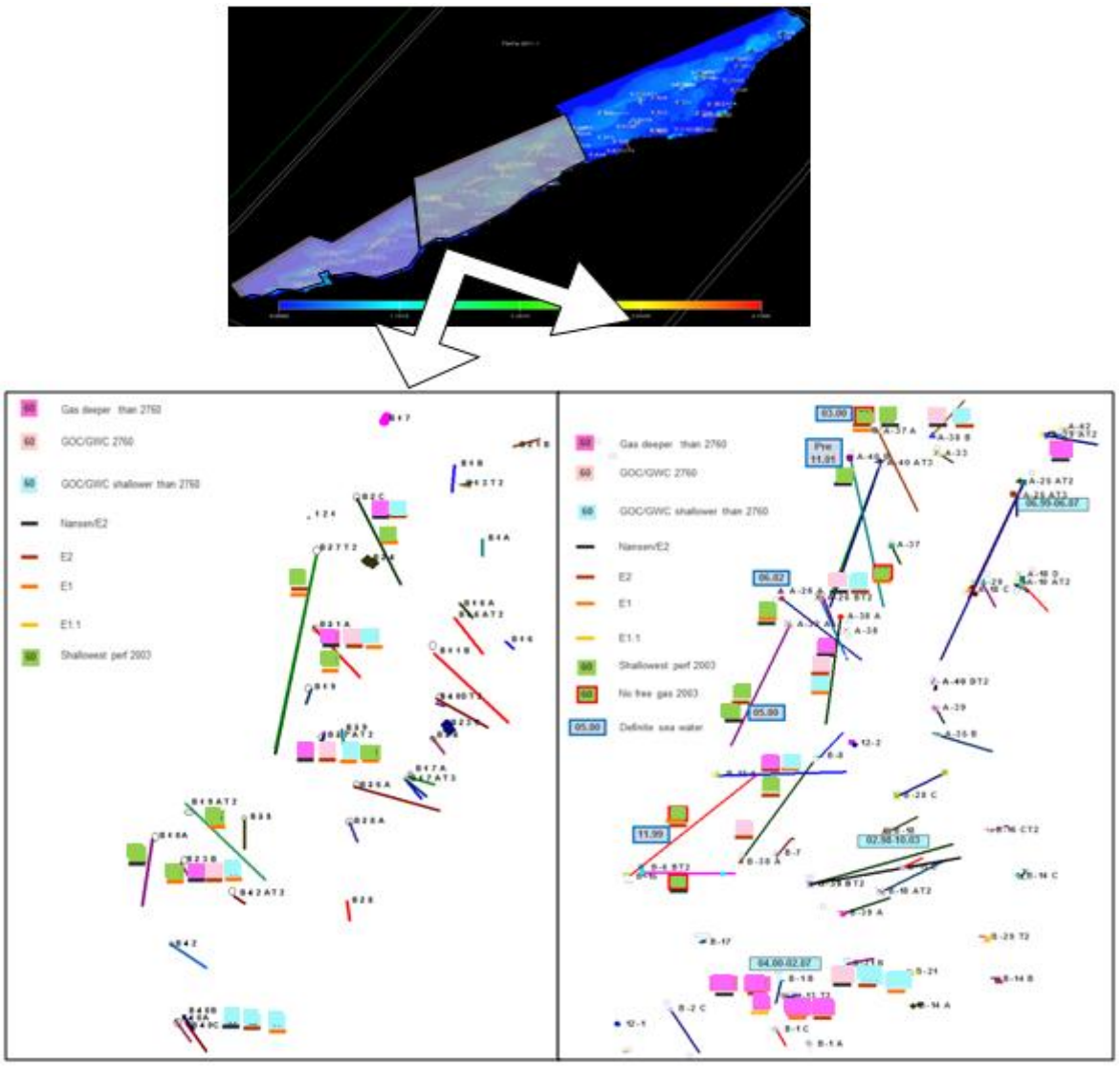

Figure A.1.2 - Fluid contact and production information in 2003 (Well comments, 2011).

Injection well	Tracer inj. date	Formation	Tracer	Obs. well	Formation	Breakthrough date	# days	Distance from inj. (m)	Velocity (m/d)
A08C	27/11/2002	Eiriksson	HTO	A02A	Dunlin/LB	Not detected		1317	
				A12	Raude/Eiriksson	20/09/2003	297	1561	5.26
				A17A	Eiriksson/Raude	7/7/2003	222	471	2.12
				C8A	Eiriksson/Nansen/Ness	Not detected			
B01B	4/11/2003	Nansen/Eiriksson	2.4.5-TFBA	B15A	Ra1/Ei MF	Not detected		1770	
				B17	Et EFB	10/5/2006	918	620	0.68
				B2C	Eiriksson	Not detected		876	
				B21B	Raude/Eiriksson	Not detected		544	
				B38A	Raude/Eiriksson/Cook	5/1/2007	1158	1030	
B18	7/3/2003	Eiriksson	3.4 DFBA	A26BT2	Eiriksson/Nansen/Cook/Rannoch	12.04.2005	767	1950	2.54
				B15A	Ra1/Ei MF	5/10/2005	943	940	1
				B17	Et EFB	Not detected		1545	
				B21B	Raude/Eiriksson	18/03/2007	1472	1099	
				B38A	Raude/Eiriksson/Cook	Not detected			
C04A	23/09/2002	US	2.6 DFBA	C15A	Eiriksson	11/6/2003	261	1870	7.16
				C19C	Raude/Eiriksson	Not detected		32840	
				C29	Eiriksson	Not detected		2740	
C04B	4/4/2003	US	4-FBA	C15A	Eiriksson	19/08/2004	503	1365	2.71
				C29	Eiriksson	16/06/2004	439	1120	2.55
				C31A	Eiriksson	13/03/2005	2313	1060	0.46
				C8A	Eiriksson/Nansen/Ness	Not detected		1560	
A38B	11/10/2003	Raude	2.6DFBA	A13B	Raude	Not detected		2159	
				A15CT4	Raude/Eiriksson/Rannoch	Not detected		1738	
				A29AT2	Raude	Not detected		822	
C14A	4/4/2003	Raude	3.4DFBA	C11B	Raude	Not detected		1525	
				C19C	Raude/Eiriksson	Not detected		875	
				C29	Eiriksson	15/12/2004	621	205	

Table A.1.1 - Statfjord – water tracer detection and flow velocities (SFRDP, 2007).

Injection well	Tracer inj. date	Formation	Tracer	Obs. well	Breakthrough date	# days	Distance from inj. (m)	Velocity (m/d)
C04A	3/3/2003	Eiriksson	PFD/PDEC	C15AT2	21/06/2003	110	1870	17
				C29T4	Not detected		2740	
				C31A	Not detected		4386	
C04B	1/4/2005	RwB7Ra/Ei	PDMCB	C8AT2	Background		1560	
				C15AT2	14/01/2006	288	1365	4.7
				C17	Not detected		570	
				C31A	Background		1060	
				C32A	19/09/2005	171	770	4.5
				C37A	15/07/2005	105	1230	11.7
C13	23.09.2002	Eiriksson	1.3-PDMCH	C15AT2	14/08/2003	325	2070	6.4
				C29T4	9/9/2003	350	1350	
				C8AT2	10/10/2003	380	1035	2.7
				C31A	12/6/2005	993	1240	1.2
				C19C	Background		950	
				C11B	17/07/2004	663	566	0.9
				C12BT2	Not detected		475	
				C41A	Background		435	
				C38CT2	Background			
C14A	20/12/2003	Raude	PMCH	C19C	Background		875	
				C11B	Background		1525	
				C29T4	Not detected			
				C29AT2	Background		1900	
				C38CT2	Background		2950	
				C41A	Background		1790	

Table A.1.2 - Statfjord – gas tracer detection and flow velocities (SFRDP, 2007).

Appendix 2

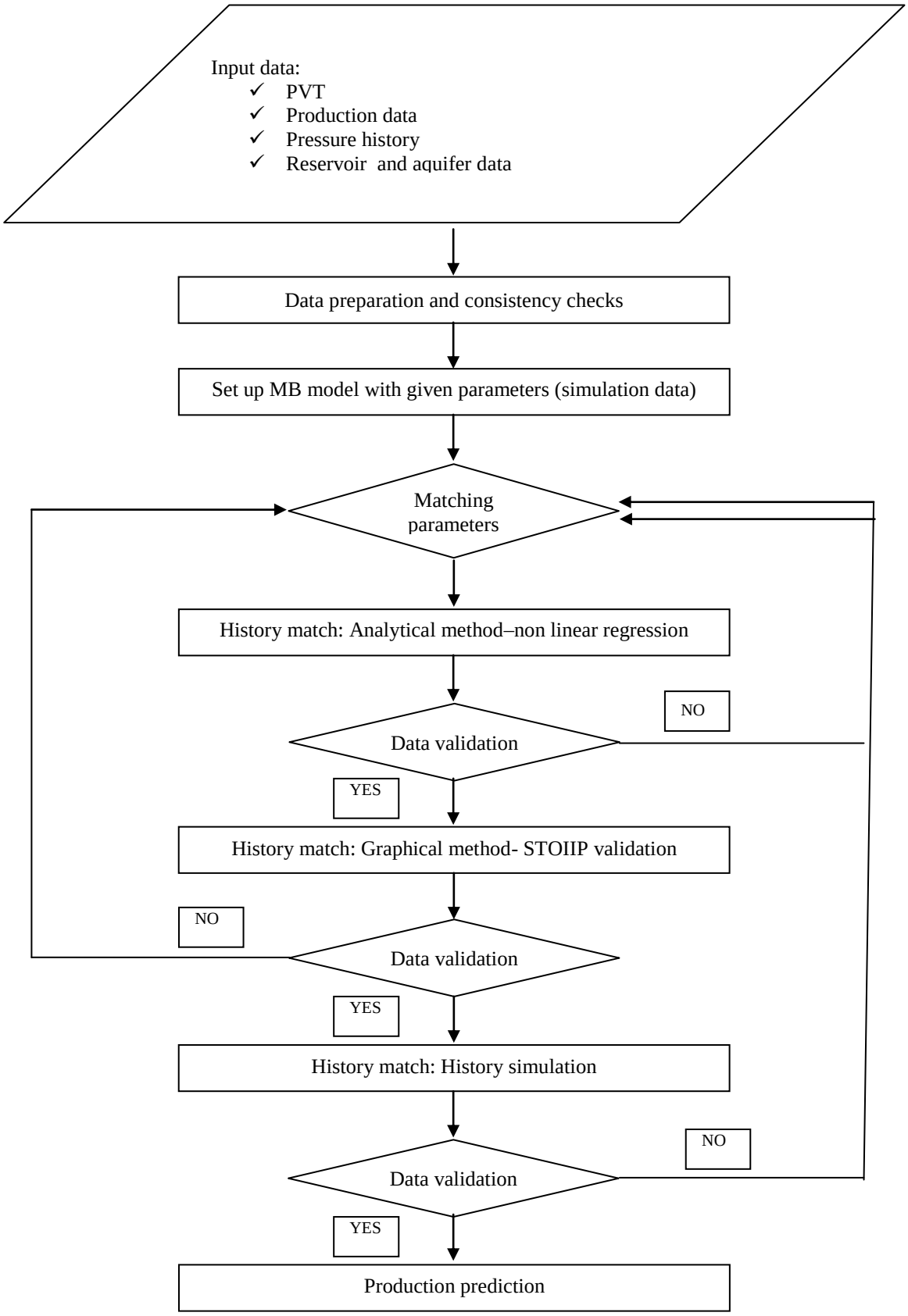

Figure A.2.1 - Workflow diagram for MBAL.

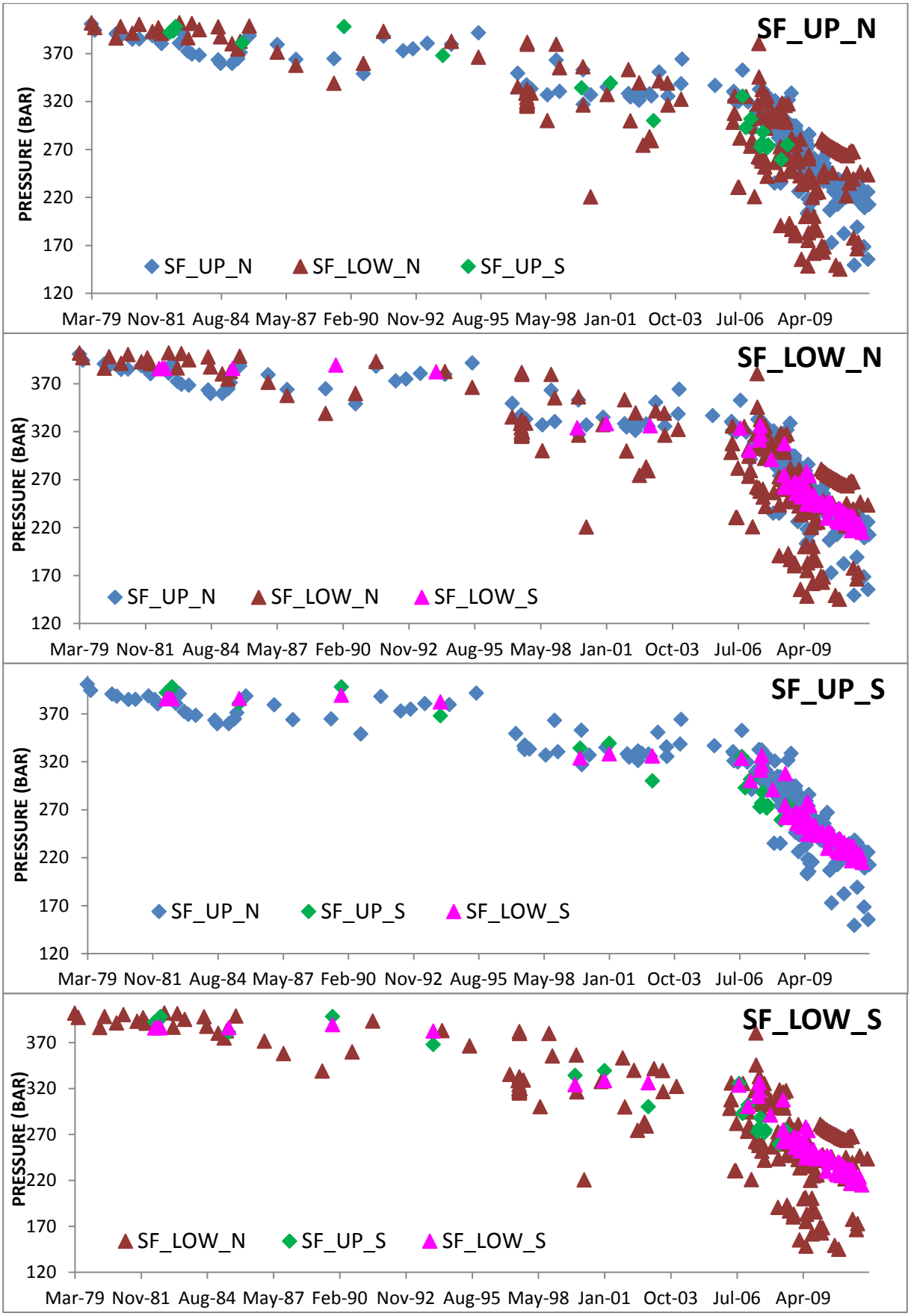

Figure A.2.2 - Pressure data for each tank together with connecting tanks (RFT measurement spreadsheet).

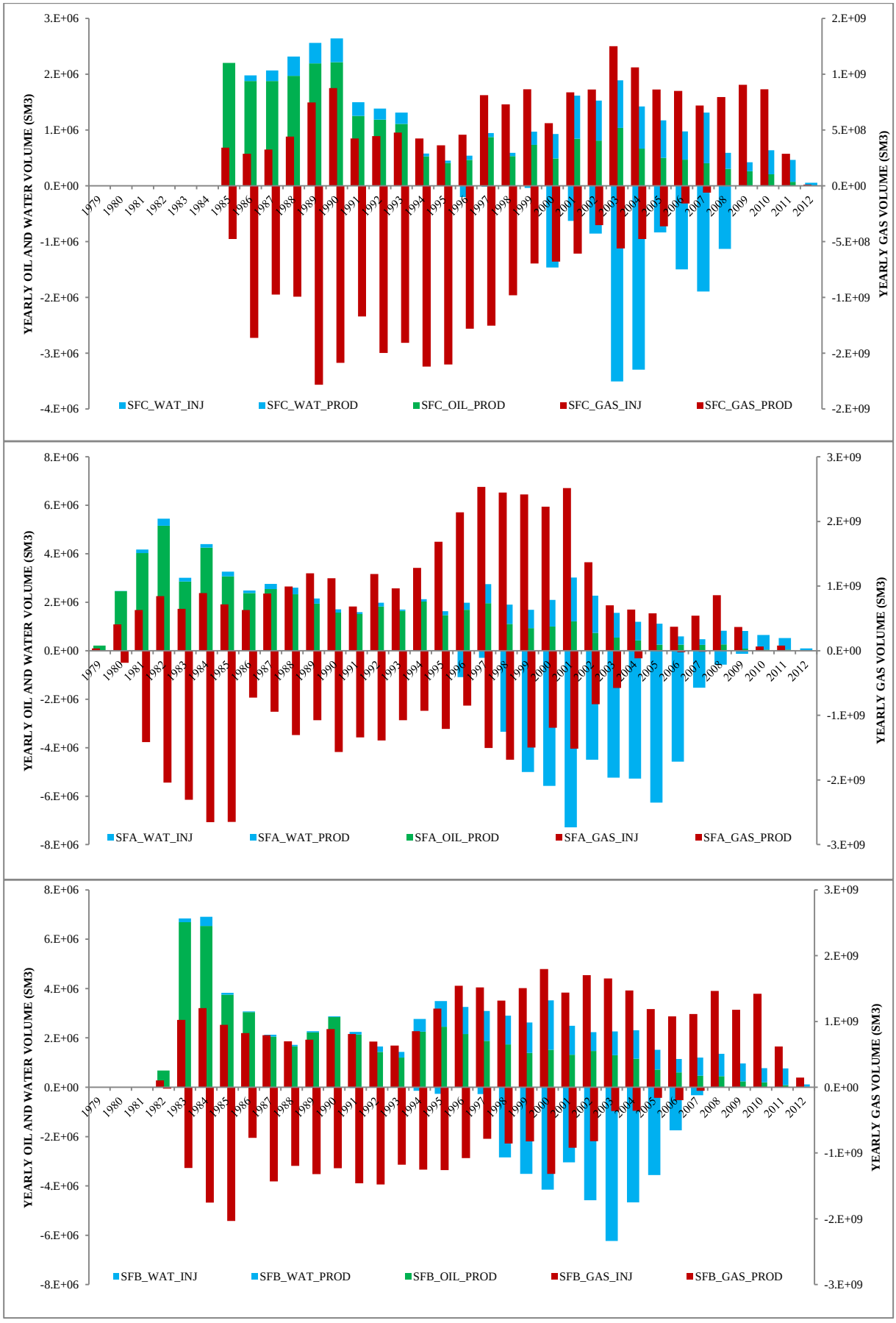

Figure A.2.3 - History production/injection performance (Prosty, 2010).

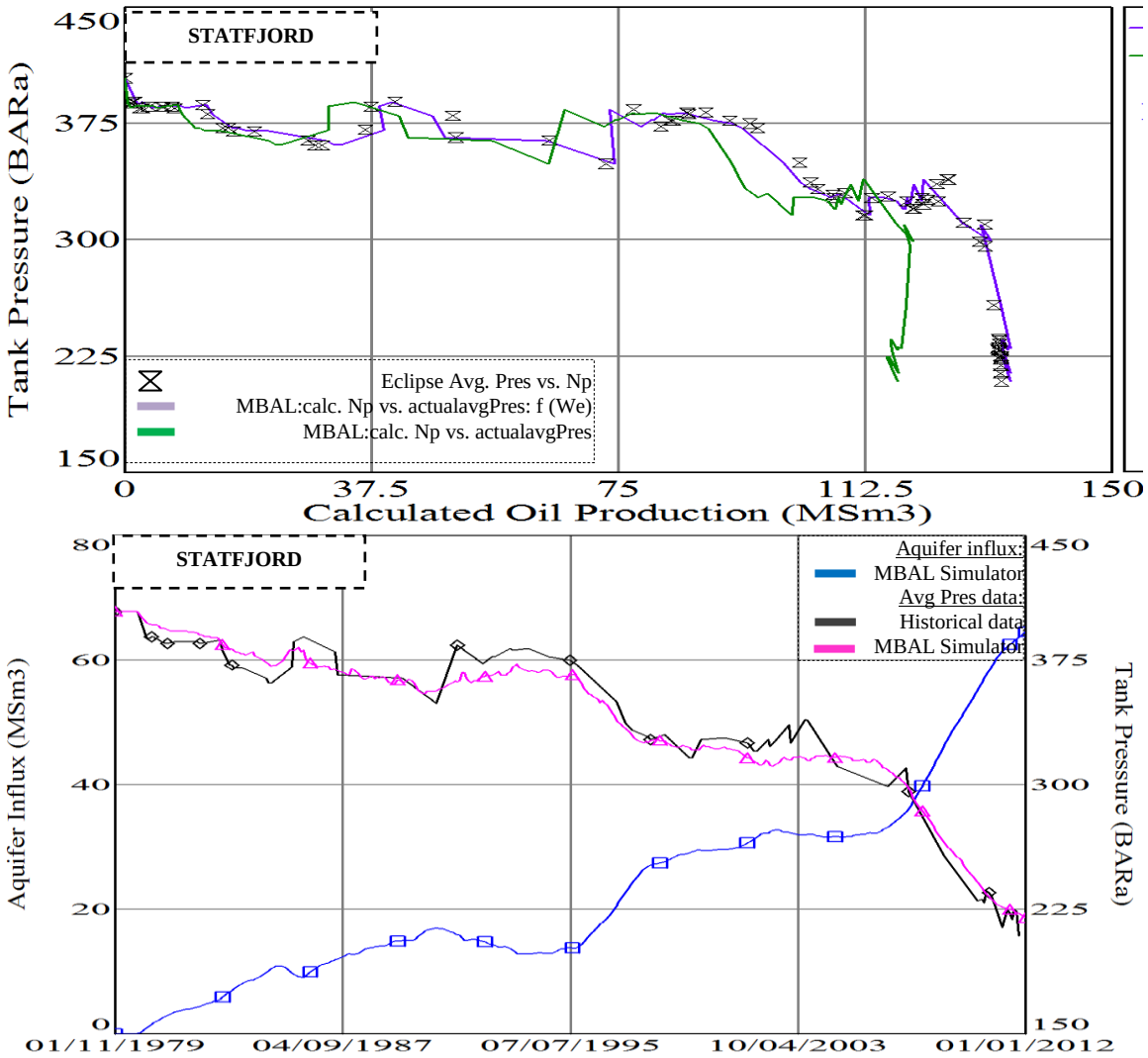

Figure A.2.4 – Single-tank model results.

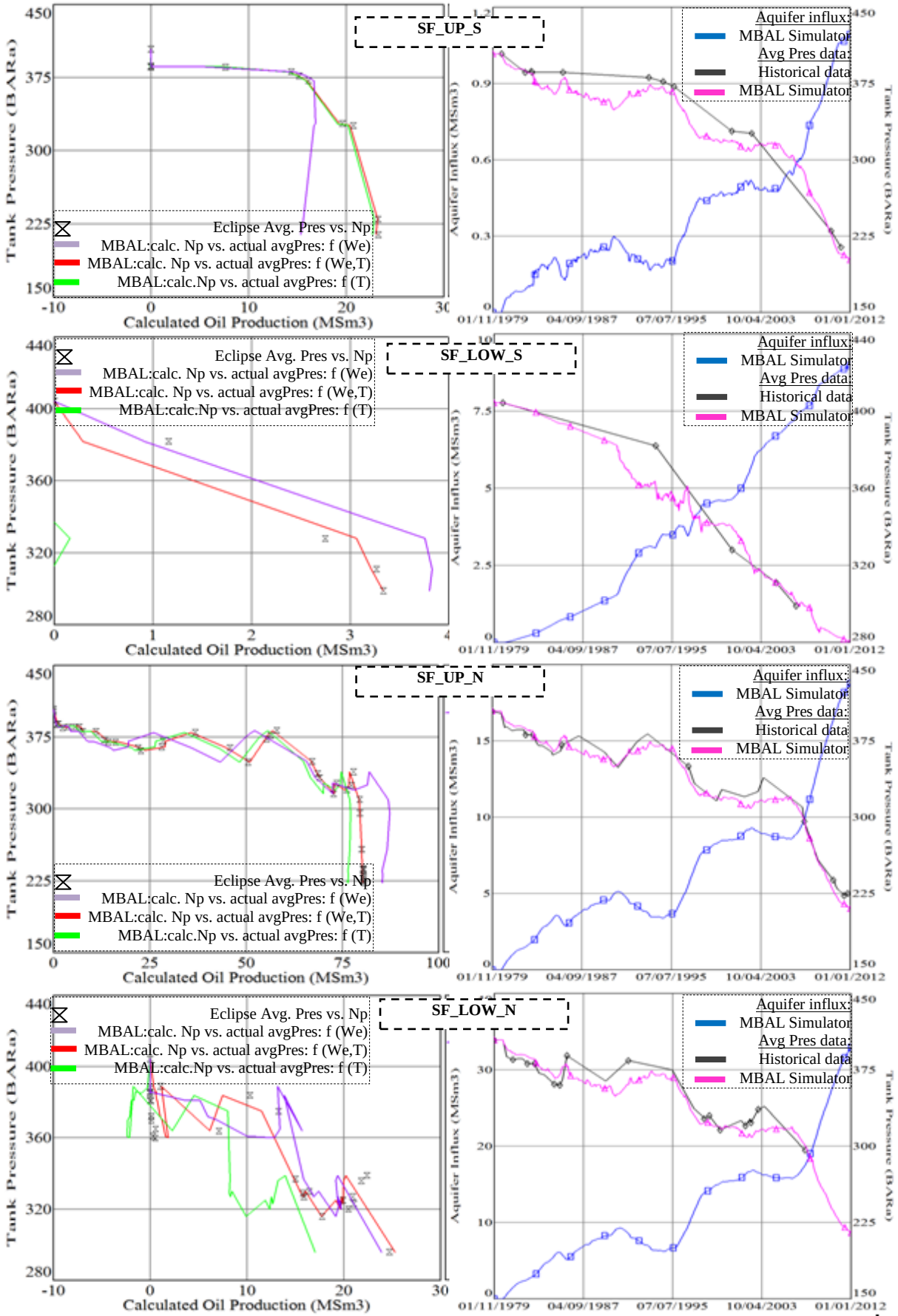

Figure A.2.5 – Pure non-linear regression (exc. perm.) based history matched MBAL model.

Parameters	Model	STATFJORD	SF_UP_S	SF_LOW_S	SF_UP_N	SF_LOW_N
Aquifer volume (MSm^3)	ECLIPSE		132	374	1359	1887
	ST-MBAL	3750				
	MT-MBAL (regression)		452.36	38.3	3337.4	1042.7
	MT-MBAL (reg. exc. perm)		56.45	760.342	1038.4	1887
	MT-MBAL		133.5	387	1359	1886
Aquifer perm. (mD)	ECLIPSE		100	100	100	100
	ST-MBAL	95				
	MT-MBAL (regression)		7.8	0.07	115.6	8.7
	MT-MBAL (reg. exc. perm)		95	120	100	120
	MT-MBAL		118	110	90	70
STOIIP (MSm^3)	ECLIPSE		27.8	10.33	103.52	52.25
	ST-MBAL	193.9				
	MT-MBAL (regression)		27.75	10.3125	103.5	52.5
	MT-MBAL (reg. exc. perm)		27.8	10.33	103.52	52.25
	MT-MBAL		27.75	10.3125	103.52	52

Table A.2.1 - Different MBAL model input data. Note: Other reservoir parameters are presented in 'Statfjord reservoir description' part.

	Model	SF_UP_S^SF_LOW_S	SF_UP_N^SF_LOW_N	SF_UP_S^SF_UP_N	SF_LOW_S^SF_LOW_N
Transmissibility ($CPM^3/D/B$)	ECLIPSE	136	260	14	4
	MT-MBAL (regression)	120.2	2527.6	567.5	62.5
	MT-MBAL (exc. perm)	2.44	4771	1539	10.9
	MT-MBAL	33.56	5607.89	1396.72	34.86

Table A.2.2 – Different MBAL model input data.

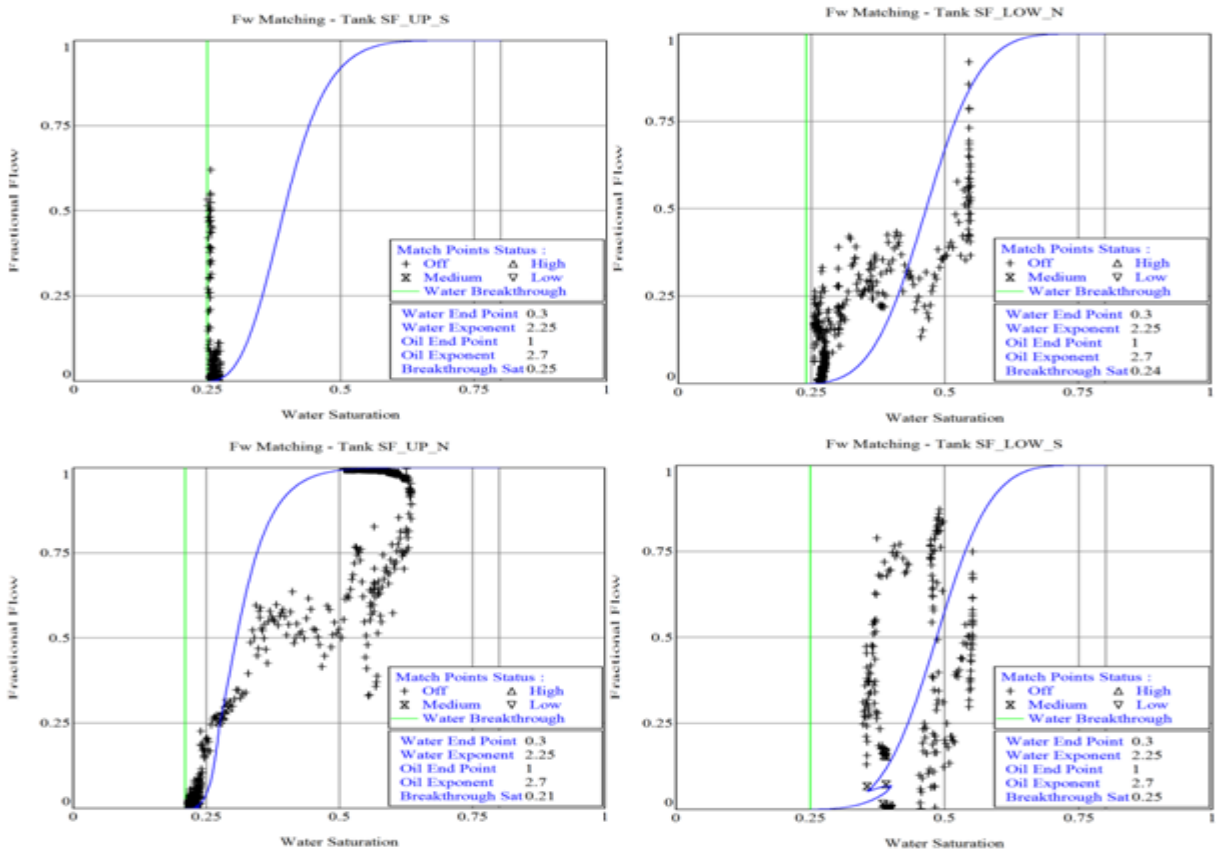

Figure A.2.6 - Fractional flow vs. saturation.

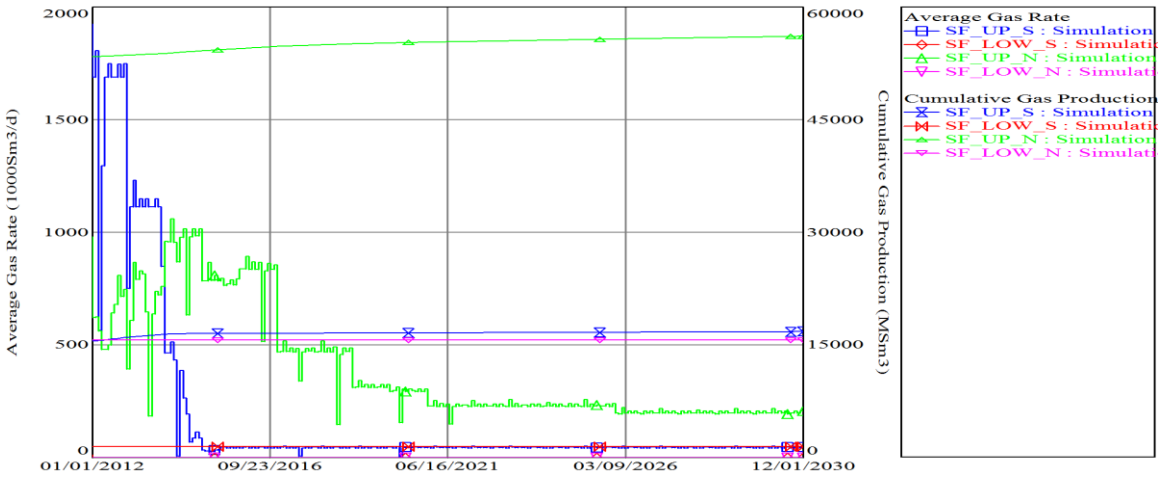

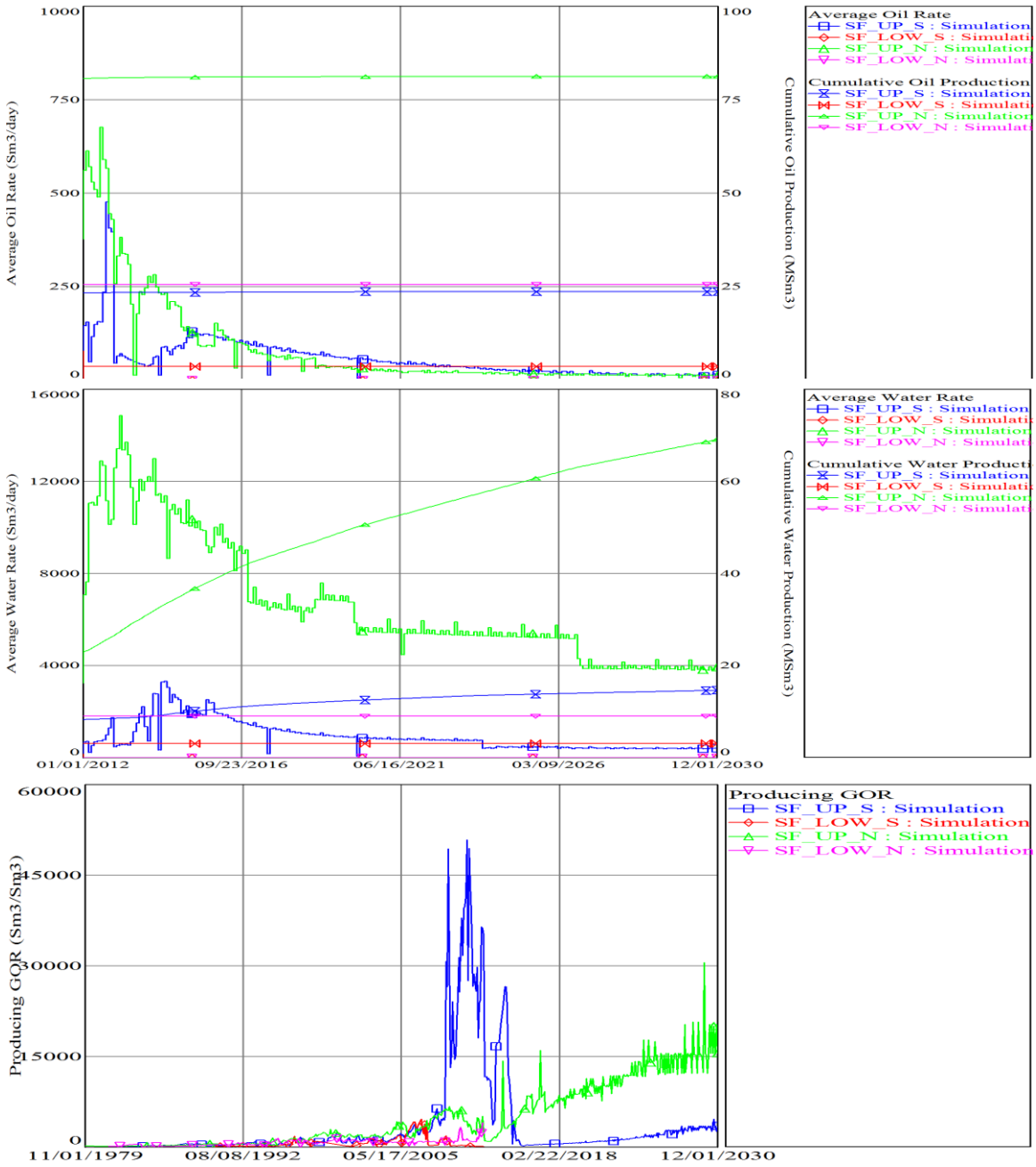

Figure A.2.7 – MBAL prediction results.